

May 2023

# The Use of Portland Cement in Reactive Powder Hybrid Asphalt Concrete

Behrouz Farahi  
*University of Wisconsin-Milwaukee*

Follow this and additional works at: <https://dc.uwm.edu/etd>



Part of the [Civil Engineering Commons](#)

---

## Recommended Citation

Farahi, Behrouz, "The Use of Portland Cement in Reactive Powder Hybrid Asphalt Concrete" (2023).  
*Theses and Dissertations*. 3142.  
<https://dc.uwm.edu/etd/3142>

This Dissertation is brought to you for free and open access by UWM Digital Commons. It has been accepted for inclusion in Theses and Dissertations by an authorized administrator of UWM Digital Commons. For more information, please contact [scholarlycommunicationteam-group@uwm.edu](mailto:scholarlycommunicationteam-group@uwm.edu).

THE USE OF PORTLAND CEMENT IN REACTIVE POWDER HYBRID ASPHALT  
CONCRETE

by

Behrouz Farahi

A Dissertation Submitted in  
Partial Fulfillment of the  
Requirements for the Degree of

Doctor of Philosophy  
in Engineering

at

The University of Wisconsin-Milwaukee

May 2023

## ABSTRACT

### THE USE OF PORTLAND CEMENT IN REACTIVE POWDER HYBRID ASPHALT CONCRETE

by

Behrouz Farahi

The University of Wisconsin-Milwaukee, 2023  
Under the Supervision of Professor Konstantin Sobolev

In order to establish a cost-effective and enduring road infrastructure, it is imperative to employ inventive methodologies that prioritize environmental sustainability. The current climate necessitates the development of a sustainable, enduring, and effective road infrastructure that requires minimal maintenance, however, achieving this goal is an effortful undertaking, and necessitates urgent and groundbreaking technological advancements. The use of fillers (aggregates with a diameter smaller than 75  $\mu\text{m}$ ) in asphalt mix design is a common practice in the pavement industry. They can occupy up to 12% by weight in asphalt mixes. The inclusion of fillers in asphalt mix, even in limited concentrations, has a significant impact on the properties of the mix. Limited studies have been conducted on using Portland Cement (PC) as a filler in asphalt pavement. Portland cement has the potential to improve the rheological, mechanical and durability properties of asphalt concrete. The incorporation of polymers in asphalt has been found to enhance its performance by increasing resistance to cracking, rutting, fatigue damage, and temperature susceptibility. Polymer-modified binders have been successfully applied in high-stress areas, such as airports and busy roads. Various types of polymers have been utilized to modify asphalt for improved properties. The use of Hot Mix Asphalt (HMA) in pavements causes environmental harm due to high CO<sub>2</sub> emissions and energy consumption. Warm Mix Asphalt (WMA) is gaining popularity because it offers numerous technical, environmental, and economic benefits such as

improved workability, reduced emissions and energy consumption, better working conditions, less binder aging, and extended construction time.

The objective of the current study is to investigate the effect of PC incorporation, warm-mix addition, and polymer modification on the properties of asphalt materials. The study was divided into two phases: phase one was mastic level, in which the rheological properties of asphalt binders and asphalt mastics (binder + filler) were discussed, while phase 2 was focused on the mechanical response of asphalt concrete (binder + filler + aggregates). In phase 1, first, PC reactive powder and Limestone (LS) as a reference filler were physically, chemically, and morphologically characterized. Thereafter, the filler/ powder was incorporated into HMA and WMA plain and polymer-modified asphalt binders at filler volume concentrations of 0, 10, and 25% as a partial replacement of asphalt binder, using a blade speed mixer. The binders used in this study were PG58-28, polymer modified PG58-28, PG64-10, and polymer modified PG64-10. The first two binders are commonly used in northern states of the U.S., while the second two binders are widely utilized in the U.S. southern states. Totally 40 mastics were made and tested. The high-temperature investigated rheological properties included viscosity, complex modulus ( $G^*$ ), phase angle ( $\delta$ ), rutting resistance ( $G^*/\sin(\delta)$ ) and multiple stress and creep and recovery. The research results demonstrated that filler/powder incorporation and polymer modification leads to an increase in the viscosity of the mastics, while warm-mix addition reduces the viscosity. Further, it was noted that filler incorporation and polymer-modification improved the complex modulus and rutting resistance of the mastics. While phase angle remained unaffected from filler incorporation, warm-mix addition, polymer modification resulted in a reduction in the phase angle, making the mastics have a more elastic response

With regards to multiple stress and creep and recovery test results, it was observed that filler incorporation and polymer modification resulted in an enhancement in J value and recovery percentage of the mastics. Moreover, the mastics containing PC reactive powder and based on PG64-10 and polymer-modified PG64-10 asphalt binders outperformed the mastics containing LS filler at different filler volume concentrations and different temperatures. The intermediate rheological performance of the mastics was evaluated by performing a fatigue test. The research results demonstrated that warm-mix additives, due to the softening effect improved the fatigue response of the mastics. Further, PC-based mastics had a better fatigue performance in most of the cases, when compared with LS-based mastics. Low-temperature performance of the mastics was assessed by conducting Bending Beam Rheometer (BBR) and Dynamic Mechanical Analysis (DMA) tests. It was noted that filler incorporation led to more brittle behavior of the mastics, polymer modification led to a relatively similar rheological response, while warm-mix additives reduced the stiffness of the investigated mastics at low temperatures.

In phase 2 of the study, eight (8) WMA mixtures based on PG58-28, polymer-modified PG58-28, and polymer-modified PG64-10, and with filler volume concentrations of 0 and 40% were made and tested. The evaluated parameters included constructability, moisture susceptibility, and fatigue resistance. In terms of constructability, PG58-28 and polymer-modified PG58-28 mixtures containing PC reactive powder needed less compaction effort to reach desired density. Moreover, such mixtures showed higher strengths under indirect tensile test and had a similar or better resistance against moisture damage. The reported results from the fatigue test demonstrated that the mixtures containing PC reactive powder can undergo larger fatigue loads with a lower deformation rate, which helps them to be more durable under traffic loading in the roads. Overall,

it can be concluded that the use of PC reactive powder in a hybrid WMA asphalt system can be a sustainable alternative from economic, environmental, and durability points of view.

© Copyright by Behrouz Farahi, 2023  
All Rights Reserved

I would like to dedicate this thesis to my parents for their endless love, support, and encouragement. I am so proud to be your son.

## TABLE OF CONTENTS

LIST OF FIGURES .....	x
LIST OF TABLES .....	xiv
LIST OF ABBREVIATIONS.....	xvi
<b>CHAPTER 1: INTRODUCTION</b> .....	1
1.1. BACKGROUND AND PROBLEM STATEMENT .....	1
1.2. HYPOTHESIS .....	6
1.3. OBJECTIVES .....	6
<b>CHAPTER 2: LITERATURE REVIEW</b> .....	9
2.1 Asphalt Binder .....	9
2.2 Polymer-modified Asphalt Binder .....	13
2.3 Warm Mix Asphalt .....	21
2.4 Fillers .....	25
<b>CHAPTER 3: MATERIALS AND METHODS</b> .....	27
3.1 Materials Characterization .....	27
3.1.1 Chemical Properties .....	27
3.1.2 Physical Properties.....	32
3.2 Test Methods for Superpave® Asphalt Mastic Testing Protocol .....	38
3.2.1 Mastic Preparation .....	40
3.2.2 Aging Procedures.....	41
3.2.3 Brookfield Rotational Viscometer (RV).....	43
3.2.4 Dynamic Shear Rheometer (DSR).....	46
3.2.5 Bending Beam Rheometer (BBR) .....	53
3.2.6 Dynamic Mechanical Analysis (DMA) .....	55
3.3 SUPERPAVE® ASPHALT MIXTURE TESTING PROTOCOL.....	59
3.3.1 Mixture Preparation .....	60
3.3.2 Aging Procedures.....	61
3.3.3 Asphalt Mixture Volumetric .....	62
3.3.4 Workability .....	65
3.3.5 Aggregate Coating .....	71
3.3.6 Moisture Damage.....	74
3.3.7 Indirect Tensile (IDT) Test .....	77

3.3.8 Fatigue-Cracking Resistance .....	79
<b>CHAPTER 4: PERFORMANCE OF MASTICS .....</b>	<b>85</b>
4.1 Self-Healing Characteristic .....	85
4.2 Constructability .....	87
4.3 Complex Shear Modulus ( $G^*$ ) .....	92
4.4 Rutting Resistance .....	102
4.5 Fatigue Resistance .....	116
4.6 Thermal-Cracking Resistance .....	120
<b>CHAPTER 5: PERFORMANCE OF MIXTURES .....</b>	<b>135</b>
5.1 Asphalt Mixtures .....	136
5.2 Aggregate Blends .....	136
5.3 Aggregate Coating .....	139
5.4 Constructability .....	141
5.5 Moisture Susceptibility .....	146
5.6 Fatigue Resistance .....	157
<b>CHAPTER 6: CONCLUSIONS .....</b>	<b>165</b>
6.1 MASTIC STUDY .....	165
6.2 MIXTURE STUDY .....	169
<b>REFERENCES .....</b>	<b>172</b>

## LIST OF FIGURES

Figure 3.1: Chemical Oxide Content for Investigated Fillers .....	28
Figure 3.2: Ternary Diagram of Filler/ Reactive Powders .....	29
Figure 3.3: LOI content of Investigated Fillers .....	30
Figure 3.4: XRD Spectrum for Control Limestone .....	31
Figure 3.5: XRD Spectrum for Portland Cement Reactive Powder .....	32
Figure 3.6: Specific Gravity of Investigated Powders .....	33
Figure 3.7: Particle Size Distribution of Investigated Powders .....	34
Figure 3.8: D <sub>10</sub> Values of Investigated Powders .....	34
Figure 3.9: D <sub>50</sub> Values of Investigated Powders .....	35
Figure 3.10: D <sub>90</sub> Values of Investigated Powders.....	35
Figure 3.11: SEM Images of (a) LS Filler and (b) PC Reactive Powder.....	36
Figure 3.12: Rigden Void Values for Investigated Powders .....	38
Figure 3.13: Rolling Thin Film Oven (RTFO) .....	42
Figure 3.14: Pressure Aging Vessel (PAV) .....	43
Figure 3.15: Rotational Viscometer (RV).....	45
Figure 3.16: Schematic of Spindle #27 in Viscosity Test (Dimensions are in mm) (Presti, Giancontieri et al. 2017) .....	45
Figure 3.17: Stress-Strain Response of Viscoelastic Materials .....	46
Figure 3.18: : Complex Shear Modulus Representation.....	49
Figure 3.19: Multiple Stress Creep and Recovery Test Principle.....	51
Figure 3.20: Plot Showing Determination of J <sub>nr</sub> from MSCR Test (D'Angelo 2009).....	52
Figure 3.21: Plot Showing Determination of %Recovery from MSCR Test (D'Angelo 2009)...	52
Figure 3.22: Creep and Recovery Stress ( $\sigma$ ) and Strain ( $\epsilon$ ) Versus Time (t).....	53
Figure 3.23: Bending Beam Rheometer.....	55
Figure 3.24: DMA Machine and Cantilever Clamp (Wang, Wang et al. 2022).....	57
Figure 3.25: Behavior of Different Materials Under Creep Testing.....	58
Figure 3.26: Component Diagram of Compacted HMA Specimen (Asphalt Institute 2001) .....	63
Figure 3.27: Superpave® Gyrotory Compactor .....	67
Figure 3.28: Superpave® Gyrotory Compactor Mold .....	68
Figure 3.29: Maximum Theoretical Specific Gravity vs. Number of Gyration (Faheem, Hanz et al. 2008) .....	70
Figure 3.30: Indirect Tension Test at Failure.....	77

Figure 3.31: Typical Fatigue Curve .....	80
Figure 3.32: 10 Hz Sine Wave Representation of Fatigue Test.....	82
Figure 3.33: MTS Environmental Chamber with IDT Testing Frame .....	83
Figure 4.1: SEM image of cement-based mastic after self-healing .....	86
Figure 4.2: Thermally-induced cracks in limestone-based mastics .....	87
Figure 4.3: Viscosity for Unaged PG58-28 Mastics at 135°C .....	90
Figure 4.4: Viscosity for Unaged Polymer-modified PG58-28 Mastics at 135°C.....	90
Figure 4.5: Viscosity for Unaged PG64-10 Mastics at 135°C .....	91
Figure 4.6: Viscosity for Unaged Polymer-modified PG64-10 Mastics at 135°C.....	92
Figure 4.7: Complex Modulus ( $G^*$ ) for Unaged HMA and WMA PG58-28 Mastics at 58°C ....	95
Figure 4.8: Complex Modulus ( $G^*$ ) for Unaged HMA and WMA Polymer-modified PG58-28 Mastics at 58°C .....	96
Figure 4.9: Complex Modulus ( $G^*$ ) for Unaged HMA and WMA PG64-10 Mastics at 64°C ....	97
Figure 4.10: Complex Modulus ( $G^*$ ) for Unaged HMA and WMA Polymer-modified PG64-10 Mastics at 64°C.....	98
Figure 4.11: Relative Complex Modulus ( $G^*$ ) for Unaged PG58-28 Mastics .....	99
Figure 4.12: Relative Complex Modulus ( $G^*$ ) for Unaged PG64-10 Mastics .....	100
Figure 4.13: $G^*/\sin(\delta)$ for RTFO Aged PG58-28 Mastics at 58°C .....	105
Figure 4.14: $G^*/\sin(\delta)$ for RTFO Aged Polymer-modified PG58-28 Mastics at 58°C .....	106
Figure 4.15: $G^*/\sin(\delta)$ for RTFO Aged PG64-10 Mastics at 64°C .....	106
Figure 4.16: $G^*/\sin(\delta)$ for RTFO Aged Polymer-modified PG64-10 Mastics at 64°C .....	107
Figure 4.17: $J_{nr}$ for RTFO Aged HMA and WMA PG58-28 Mastics at 58°C.....	109
Figure 4.18: $J_{nr}$ for RTFO Aged HMA and WMA Polymer-modified PG58-28 Mastics at 58°C .....	110
Figure 4.19: $J_{nr}$ for RTFO Aged HMA PG64-10 Mastics at 58°C, 64°C, and 70°C.....	111
Figure 4.20: $J_{nr}$ for RTFO Aged WMA PG64-10 Mastics at 58°C, 64°C, and 70°C.....	111
Figure 4.21: $J_{nr}$ for RTFO Aged HMA Polymer-modified PG64-10 Mastics at 58°C, 64°C, and 70°C.....	112
Figure 4.22: $J_{nr}$ for RTFO Aged WMA Polymer-modified PG64-10 Mastics at 58°C, 64°C, and 70°C.....	112
Figure 4.23: Percent Recovery for RTFO Aged HMA and WMA PG58-28 Mastics at 58° .....	114
Figure 4.24: Percent Recovery for RTFO Aged HMA and WMA Polymer-modified PG58-28 Mastics at 58°C .....	115
Figure 4.25: Percent Recovery for RTFO Aged HMA and WMA PG64-10Mastics at 64°C ....	115

Figure 4.26: Percent Recovery for RTFO Aged HMA and WMA Polymer-modified PG64-10 Mastics at 64oC.....	116
Figure 4.27: Fatigue Performance for PAV-Aged HMA and WMA PG58-28 Mastics at 19°C	118
Figure 4.28: Fatigue Performance for PAV-Aged HMA and WMA Polymer-modified PG58-28 Mastics at 19°C .....	119
Figure 4.29: Fatigue Performance for PAV-Aged HMA and WMA PG64-10 Mastics at 31°C	119
Figure 4.30: Fatigue Performance for PAV-Aged HMA and WMA Polymer-modified PG64-10 Mastics at 31°C .....	120
Figure 4.31: Stiffness of PAV-Aged HMA and WMA PG58-28 Mastics at -18°C .....	122
Figure 4.32: Stiffness of PAV-Aged HMA and WMA Polymer-modified PG58-28 Mastics at -18°C.....	122
Figure 4.33: Stiffness of PAV-Aged HMA and WMA PG64-10 Mastics at 0°C.....	123
Figure 4.34: Stiffness of PAV-Aged HMA and WMA Polymer-modified PG64-10 Mastics at 0°C.....	124
Figure 4.35: m-value of PAV-Aged HMA and WMA PG58-28 Mastics at -18°C .....	125
Figure 4.36: m-value of PAV-Aged HMA and WMA HMA and WMA Polymer-modified PG58-28 Mastics at -18°C.....	125
Figure 4.37: m-value of PAV-Aged HMA and WMA PG64-10 Mastics at 0°C .....	126
Figure 4.38: m-value of PAV-Aged HMA and WMA Polymer-modified PG64-10 Mastics at 0°C .....	126
Figure 4.39: Creep Compliance of PAV-Aged HMA and WMA PG58-28 Mastics at -18°C ...	127
Figure 4.40: Creep Compliance of PAV-Aged HMA and WMA Polymer-modified PG58-28 Mastics at -18°C.....	127
Figure 4.41: Creep Compliance of PAV-Aged HMA and WMA PG64-10 Mastics at 0°C.....	128
Figure 4.42: Creep Compliance of PAV-Aged HMA and WMA Polymer-modified PG64-10 Mastics at 0°C .....	129
Figure 4.43: Creep Compliance vs Stiffness of PAV-Aged HMA and WMA mastics Based on Plain and Polymer-modified PG58-28 Mastics at -18°C .....	130
Figure 4.44: Creep Compliance vs Stiffness of PAV-Aged HMA and WMA mastics Based on Plain and Polymer-modified PG64-10 Mastics at 0°C .....	130
Figure 4.45: Relaxation Modulus of PAV-Aged HMA and WMA PG58-28 Mastics at -18°C.	131
Figure 4.46: Relaxation Modulus of PAV-Aged HMA and WMA Polymer-modified PG58-28 Mastics at -18°C.....	132
Figure 4.47: Relaxation Modulus of PAV-Aged HMA and WMA.....	132
Figure 4.48: Relaxation Modulus of PAV-Aged HMA and WMA Polymer-modified .....	133
Figure 5.1: Aggregate Particle Size Distribution Graphs .....	138

Figure 5.2: JMF vs. 0.45 Power Curve Particle Size Distribution Graph.....	138
Figure 5.3: Superpave® Gradation Limitations.....	139
Figure 5.4: Densification Curves for WMA PG58-28 Mixtures .....	143
Figure 5.5: Densification Curves for Polymer-modified WMA PG58-28 Mixtures .....	143
Figure 5.6: Densification Curves for Polymer-modified WMA PG64-10 Mixtures .....	144
Figure 5.7: Horizontal Tensile Stress at Center of Samples for WMA PG58-28 Mixtures .....	150
Figure 5.8: Horizontal Tensile Stress at Center of Samples for Polymer-modified WMA PG58-28 Mixtures .....	150
Figure 5.9: Horizontal Tensile Stress at Center of Samples for Polymer-modified WMA PG64-10 Mixtures .....	151
Figure 5.10: Vertical Compressive Stress at Center of Specimen for WMA PG58-28 Mixtures .....	152
Figure 5.11: Vertical Compressive Stress at Center of Specimen for Polymer-modified WMA PG58-28 Mixtures .....	152
Figure 5.12: Vertical Compressive Stress at Center of Specimen for Polymer-modified WMA PG64-10 Mixtures.....	153
Figure 5.13: Tensile Strain at Failure for WMA PG58-28 Mixtures.....	154
Figure 5.14: Tensile Strain at Failure for Polymer-modified WMA PG58-28 Mixtures .....	154
Figure 5.15: Tensile Strain at Failure for Polymer-modified WMA PG64-10 Mixtures .....	155
Figure 5.16: TSR for WMA PG58-28 Mixtures.....	156
Figure 5.17: TSR for Polymer-modified WMA PG58-28 Mixtures.....	156
Figure 5.18: TSR for Polymer-modified WMA PG64-10 Mixtures.....	157
Figure 5.19: Number of Cycles Drop in E* for WMA PG58-28 Mixtures .....	159
Figure 5.20: Number of Cycles Drop in E* for Polymer-modified WMA PG58-28 Mixtures..	159
Figure 5.21: Number of Cycles Drop in E* for Polymer-modified WMA PG64-10 Mixtures..	160
Figure 5.22: Vertical Deformation Fatigue Slope for WMA PG58-28 Mixtures.....	161
Figure 5.23: Vertical Deformation Fatigue Slope for Polymer-modified WMA PG58-28 Mixtures .....	161
Figure 5.24: Vertical Deformation Fatigue Slope for Polymer-modified WMA PG64-10 Mixtures .....	162
Figure 5.25: Dispersion of Fatigue Life Data Points in Fatigue Life vs. Tensile Stress Graph Developed by (Porter and Kennedy 1975).....	163
Figure 5.26: Dispersion of Fatigue Life Data Points in Fatigue Life vs. Stress/Strength Ratio Graph Developed by (Adedimila and Kennedy 1975) .....	164

## LIST OF TABLES

Table 3.1: Used Fillers in the Study.....	27
Table 3.2: Chemical Composition of Powder Components.....	29
Table 3.3: Characteristics of Investigated Mastics .....	39
Table 3.4: Experimental Matrix for Asphalt Mastic Tests .....	39
Table 3.5: Experimental Matrix for Asphalt Concrete Tests .....	59
Table 3.6: Superpave® Gyrotory Compaction Parameters for Different Roadway Applications	70
Table 3.7: Surface Area Factors for Different Aggregate Sizes .....	72
Table 4.1: Viscosity for Unaged HMA and WMA PG58-28 Binders at 135°C.....	88
Table 4.2: Viscosity for Unaged HMA and WMA Polymer-modified PG58-28 Binders at 135°C .....	88
Table 4.3: Viscosity for Unaged HMA and WMA PG64-10 Binders at 135oC .....	88
Table 4.4: Viscosity for Unaged HMA and WMA Polymer-modified PG64-10 Binders at 135oC .....	89
Table 4.5: Complex Modulus and Phase Angle Results for Unaged PG58-28-based samples of HMA and WMA at 58°C .....	93
Table 4.6: Complex Modulus and Phase Angle Results for Unaged Polymer-modified PG58-28- based samples of HMA and WMA at 58°C.....	93
Table 4.7: Complex Modulus and Phase Angle Results for Unaged PG64-10-based samples of HMA and WMA at 64°C .....	93
Table 4.8: Complex Modulus and Phase Angle Results for Unaged Polymer-modified PG64-10- based samples of HMA and WMA at 64°C.....	94
Table 4.9: Relative Phase Angle ( $\delta_r$ ) for Unaged PG58-28 based Mastics at 58°C.....	101
Table 4.10: Relative Phase Angle ( $\delta_r$ ) for Unaged PG64-10-based Mastics at 64°C.....	101
Table 4.11: $G^*/\sin(\delta)$ for Unaged HMA and WMA PG58-28 .....	103
Table 4.12: $G^*/\sin(\delta)$ for Unaged HMA and WMA Polymer-modified PG58-28.....	103
Table 4.13: $G^*/\sin(\delta)$ for Unaged HMA and WMA PG64-10 .....	103
Table 4.14: $G^*/\sin(\delta)$ for Unaged HMA and WMA Polymer-modified PG64-10.....	103
Table 4.15: $G^*/\sin(\delta)$ for RTFO Aged HMA and WMA PG58-28.....	104
Table 4.16: $G^*/\sin(\delta)$ for RTFO Aged HMA and WMA Polymer-modified PG58-28 .....	104
Table 4.17: $G^*/\sin(\delta)$ for RTFO Aged HMA and WMA PG64-10.....	104

Table 4.18: $G^*/\sin(\delta)$ for RTFO Aged HMA and WMA Polymer-modified PG64-10 .....	105
Table 4.19: $J_{nr}$ for RTFO Aged HMA and WMA PG58-28 at 58°C at 3.2 kPa loading level ..	108
Table 4.20: $J_{nr}$ for RTFO Aged HMA and WMA Polymer-modified PG58-28 at 58°C at 3.2 kPa loading level.....	108
Table 4.21: $J_{nr}$ for RTFO Aged HMA and WMA PG64-10 at 64°C at 3.2 kPa loading level ...	108
Table 4.22: $J_{nr}$ for RTFO Aged HMA and WMA PG64-10 at 64°C at 3.2 kPa loading level ...	108
Table 4.23 Recovery percentage for RTFO Aged HMA and WMA PG58-28 at 58°C at 3.2 kPa loading level.....	113
Table 4.24: Recovery percentage for RTFO Aged HMA and WMA Polymer-modified PG58-28 at 58°C at 3.2 kPa loading level .....	113
Table 4.25: Recovery percentage for RTFO Aged HMA and WMA PG64-10 at 64°C at 3.2 kPa loading level.....	113
Table 4.26: Recovery percentage for RTFO Aged HMA and WMA Polymer-modified PG64-10 at 64°C at 3.2 kPa loading level.....	114
Table 4.27 $G^*\sin(\delta)$ for PAV Aged HMA and WMAPG58-28 at 19°C .....	117
Table 4.28: $G^*\sin(\delta)$ for PAV Aged HMA and WMA Polymer-modified PG58-28 at 19°C....	117
Table 4.29: $G^*\sin(\delta)$ for PAV Aged HMA and WMA PG64-10 at 31°C .....	117
Table 4.30: $G^*\sin(\delta)$ for PAV Aged HMA and WMA Polymer-modified PG64-10 at 31°C....	117
Table 5.1: The 4-MT Job Mix Formula Determining Combination of Aggregates (by WisDOT) .....	137
Table 5.2: Particle Size Distribution (PSD) for All Aggregate Types.....	137
Table 5.3: Calculated Surface Area of Aggregates.....	140
Table 5.4: Asphalt Film Thickness for Investigated Mixtures .....	141
Table 5.5: The Volumetrics of WMA PG58-28 Asphalt Mixture .....	145
Table 5.6: The Volumetrics of Polymer-modified WMA PG58-28 Asphalt Mixture.....	146
Table 5.7: The Volumetrics of Polymer-modified WMA PG64-10 Asphalt Mixture.....	146
Table 5.8: Moisture Damage Load and Flow Results for WMA PG58-28 Mixtures.....	148
Table 5.9: Moisture Damage Load and Flow Results for WMA Polymer-modified PG58-28 Mixtures .....	148
Table 5.10: Moisture Damage Load and Flow Results for WMA Polymer-modified PG64-10 Mixtures .....	149

## LIST OF ABBREVIATIONS

AASHTO	American Society of State Highway and Transportation Officials
ASTM	American Society for Testing Materials
BBR	Bending Beam Rheometer
DSR	Dynamic Shear Rheometer
$\delta$	Phase Angle
$E^*$	Complex Fatigue Modulus
$G^*$	Complex Shear Modulus
$G_f$	Fracture Energy
$G_{mb}$	Bulk Specific Gravity
$G_{mm}$	Maximum Specific Gravity
IDT	Indirect Tensile Test
MSCR	Multiple Stress Creep and Recovery
PAV	Pressure Aging Vessel
RTFO	Rolling Thin Film Oven
$S(t)$	Stiffness
SEM	Scanning Electron Microscope
SGC	Superpave® Gyrotory Compactor
VFA	Voids Filled with Asphalt
VMA	Voids in Mineral Aggregate

## ACKNOWLEDGMENTS

I would like to express my sincere gratitude to Dr. Konstantin Sobolev for his knowledge and expertise during the project developmental stages. He has become one of the biggest influences in my life and his help and recommendations have been vital to this research. Without his guidance I would not be where I am today.

I would also like to give special thanks to my parents as a whole for their continuous support and understanding when overcoming immigration challenges and undertaking my research. Your prayer for me was what sustained me this far.

I would like to thank Portland Cement Association, Payne and Dolan Inc., Lafarge, and all other sponsors of this research who made this work possible. A special thanks to Steve Kosmatka, Emil Bautista, Andrew Hanz, and Ahmed Faheem for their continuous help and support.

# 1. CHAPTER 1: INTRODUCTION

## 1.1. BACKGROUND AND PROBLEM STATEMENT

Today, building a Building a durable and cost-efficient infrastructure while minimizing future repairs is challenging (Farahi, Esfahani et al. 2019, Muzenski, Flores-Vivian et al. 2020, Sabzi, Esfahani et al. 2020). Asphalt is a substantial material that has been utilized in construction of more than 93% of the roadways in the U.S. Asphalt has a long-standing history as a construction material, dating back to ancient civilizations. One of the earliest references to the use of asphalt can be found in the Book of Genesis 6:14, in which the Lord instructed Noah, ‘So make yourself an ark of cypress wood; make rooms in it and coat it with pitch inside and out.’ Pitch refers to a type of asphalt that rises to the surface of bodies of water from fissures in the Earth's crust, where crude oil leaks out. Upon exposure to air, volatile compounds in crude oil evaporate, leaving behind the heavier molecules that coalesce to form a viscous, adhesive brown substance. Pitch possesses a similar unit weight as water, allowing it to float on the surface of water bodies. The use of asphalt continued throughout history, with various civilizations utilizing it for construction purposes, including the ancient Egyptians, Babylonians, and Persians. The ancient Egyptians incorporated asphalt into their process of mummification, while the Romans utilized this material for practical purposes such as sealing their baths and constructing waterproof hydraulic connections for water distribution systems. According to rumor, the success of Columbus's return trip from the Americas was made possible by the discovery of asphalt deposits, which enabled his crew to repair their leaking ships. It should be

noted that the use of asphalt in road construction is a comparatively recent development, and was preceded by its use in shipbuilding and hydraulics.

The design of hot mix asphalt (HMA) has been a necessity since the placement of the first asphalt mixes in the late 19th century. In the 1880s, asphalt road mixes were introduced in the United States as patented products, primarily composed of natural asphalt sourced from the lake deposits of Trinidad near the village of La Brea, British West Indies. To construct projects, this asphalt was transported in barrels to the construction site, blended with local petroleum fluxes, and mixed with local aggregates using proportions that were determined through a trial-and-error approach by the patent holder. The first asphalt paving project in the United States was possibly constructed in New York City by DeSmedt before 1875, as noted by the New York Section of the Society of the Chemical Industry in 1907. Evidence suggests that S.H. Robertson of the District of Columbia may have built a hot mix asphalt pavement in 1874. The most significant early project was laid on Pennsylvania Avenue in Washington, D.C., in 1876, which utilized a blend of 50% Trinidad asphalt and 50% heavy petroleum oil mixed with local aggregate as the asphalt binder. Prior to 1900, the refining tools available could not convert crude oils produced east of the Rocky Mountains to a paving grade asphalt, which resulted in Trinidad asphalt becoming the standard against which all other asphalts were measured. There was no competition for Trinidad asphalt at that time. However, on the West Coast, California crude oils were easily converted to asphalt using shell stills available at that time. California-produced asphalt was first used in a job in Los Angeles in 1895 and by 1904, 38 California refineries were producing asphalt, exceeding market requirements. As a result, asphalt was transported by ship and arrived at East Coast ports at a cost 10% lower than Trinidad asphalt. Rail transportation facilitated the delivery of California asphalt to the East Coast at a cost only marginally higher than that of Trinidad asphalt, thereby

stimulating competition between the two. The California producers claimed that their asphalt was of superior quality, being composed entirely of asphalt, while Trinidad asphalt was allegedly comprised of 35-50% filler. In contrast, Trinidad asphalt manufacturers argued that their product was naturally sourced, and the filler was unique, distinguishing it from other materials. This competition exerted downward pressure on the price of paving in New York, which fell from \$3.36 per square yard in 1901 to \$1.52 per square yard by around 1910. The emergence of air blowing technology in 1903 enabled the production of asphalt from Texas crude oils, which was otherwise unsuitable for refining using the shell stills available at the time. This innovation provided a means of increasing the viscosity of Texas crude to yield a paving-grade asphalt equivalent in quality to that of California crude. Although Mexican crude, which could be refined using shell stills, became available for processing in 1912, most refiners continued to produce solid asphalt that required fluxing before use in paving. The solid asphalt was then transported in barrels to job sites, where local flux materials were used to adjust viscosity. However, by the onset of World War I, direct refining to grade had become a widespread practice, even after the development of pumps that allowed the storage and blending of various materials.

The asphalt-concrete mixture is a composite material composed of aggregates and asphalt that is commonly used as a surface layer for flexible-pavement roads. The function of the aggregates is to provide a framework that can resist the repeated application of traffic loads, while the asphalt acts as an adhesive, bonding the aggregate particles together and contributing viscoelastic properties to the mixture (Read and Whiteoak, 2003). During the blending of aggregate proportions in the mixture, the aggregates are typically classified according to their size. Aggregates that are larger than 4.75 mm are referred to as coarse, while those smaller than 4.75 mm are known as fine aggregates. This classification based on size aids in the proper

proportioning of aggregates in the mixture. Filler refers to aggregate particles that are finer than 75  $\mu\text{m}$  in size. Despite the small size of filler particles, it has been widely acknowledged that they play a significant role in shaping the characteristics and performance of asphalt-concrete mixture. The efficient packing of coarse, fine, and filler aggregates creates a robust framework for the mixture (Vavrik et al., 2002; Qiu, 2006). The use of filler in the mixture is linked to a lower optimal asphalt content (Brown et al., 1989; Kandhal et al., 1998; Tayebali et al., 1998), and higher filler concentrations contribute to stronger pavement, resulting from better asphalt cohesiveness and improved internal stability caused by the filler's efficient packing (Brown et al., 1989). The inclusion of mineral filler increases the resilient modulus of the asphalt-concrete mixture (Anderson, 1987; Tayebali et al., 1998). However, excessive use of filler may weaken the mixture by increasing the amount of asphalt needed to coat the aggregates (Elliot et al., 1991; Kandhal et al., 1998) or by making the asphalt stiff, which can negatively impact the workability of the mixture.

The conventional method of producing asphalt mixtures involves the use of mineral aggregates and bitumen, and is typically carried out at high temperatures exceeding 150 °C. This is done to ensure that the binder's low viscosity allows for proper coating of the aggregates, resulting in the formation of what is known as hot-mix asphalt technology (HMA). However, growing concerns over global warming and environmental pollution, rising energy costs, and limited financial resources have compelled pavement engineers to explore alternative technologies, including warm mix asphalt (WMA) technology [see Formulation and processing of recycled-low-density-polyethylene-modified bitumen emulsions for reduced-temperature asphalt technologies for reference]. Use of WMA has attracted a lot of attention in pavement industry due providing several technical, economic, and environmental advantages, including (a) reduced energy

consumption required for material heating, (b) approximately 24% reduction in air pollution, (c) lower aging of asphalt binder, (d) extended construction season by allowing paving during cooler weather, (e) extended mix haul distance and construction time due to smaller temperature difference between the ambient temperature and mix temperature as compared with HMA, and (f), reduced production cost [ see Performance evaluation of asphalt mixtures containing warm mix

asphalt (WMA) additives and reclaimed asphalt pavement (RAP) for references].

The incorporation of polymers, which are composed of repeating small molecules, into asphalt has been demonstrated to enhance its performance. The application of polymer-modified asphalt results in increased resistance to rutting and thermal cracking, as well as reduced fatigue damage, stripping, and temperature sensitivity. Polymer-modified binders have been effectively implemented in high-stress areas, such as busy intersections, airports, vehicle weigh stations, and race tracks. A range of polymers, such as styrene-butadiene-styrene (SBS), styrene-butadiene rubber (SBR), Elvaloy, rubber, ethylene vinyl acetate (EVA), and polyethylene, have been utilized to modify asphalt. The desirable properties of polymer-modified binders include enhanced elastic recovery, higher softening point, greater viscosity, stronger cohesive strength, and increased ductility.

It is envisioned that using reactive powder like cement particles as fillers as partial replacement of asphalt binder with polymer-modified asphalt binder and incorporation of warm-mix modifier in the production of a of asphalt concrete can be advantageous in different aspects: it can reduce the asphalt binder content, which in turn, can reduce the carbon footprint and associated production cost, reduce the mixing and placement temperature which is environmentally and

economically advantageous, and it enables the asphalt mixture to possess higher strength, longer life cycle, moisture- induced self-healing property, and higher durability in extreme environmental conditions. Within this context, it is necessary to undertake a renewed examination of cement reactive-powder incorporation, polymer modification, and warm-mix addition to conduct a comprehensive investigation utilizing Superpave® testing methodology to evaluate the performance of asphalt in mastic (binder + filler) and concrete mixture (binder + filler + aggregates) levels. This study aims to explore the interactions between cement reactive powder, warm-mix additive and different types of plain and polymer-modified asphalt binders and to provide insights into the influence of cement modification on the mechanical and functional properties of asphalt concrete and will identify the potential improvement of performance in WMA-portland cement hybrid systems.

## **1.2. HYPOTHESIS**

The incorporation of engineered amount of portland cement as a partial replacement of asphalt binder can have beneficial interactions with different performance grade (PG) plain and polymer-modified asphalt binders and can result in an improved performance of WMA equally or over-performing the asphalt concrete without fillers or containing conventionally used fillers in asphalt mixtures. Such beneficial interactions can help to tailor the asphalt mastics and asphalt concrete with enhanced performance.

## **1.3. OBJECTIVES**

- Perform scanning electron microscope (SEM) test on heavy cement incorporated (50% replacement by volume) mastic to investigate the moisture-induced self-healing property.
- Conduct characterization tests on the fillers (portland cement reactive powder and limestone filler) to investigate the physical, chemical, and morphological characteristics.

- Conduct rheological testing and analyze the performance of 4 types of asphalt binders and two production technologies (HMA and WMA) at 3 different dosages of reactive powder upto 50% bitumen replacement by weight (approximately, 25% by volume) and compare to a control limestone mineral filler as asphalt with no filler.
- Conduct the fatigue and multiple stress creep and recovery (MSCR) tests and evaluate the low-temperature performance using bending beam rheometer (BBR) and dynamic mechanical analysis (DMA) on aged specimens with portland cement.
- Develop a model to correlate the performance of investigated mastics under BBR and DMA tests at low temperatures.
- Conduct testing on WMA asphalt mixtures with optimal portland cement content (40% replacement of binder by volume) in terms of aggregate coating, workability, moisture damage resistance, and fatigue cracking resistance.

#### **1.4. RESEARCH METHODOLOGY**

The research objectives were met by completing the following tasks:

##### **Task 1: Literature Review**

- Conduct a comprehensive review on polymer-modification of asphalt binder, warm-mix addition in asphalt production, and filler incorporation into asphalt mastic and mixtures.
- Report on current research efforts on asphalt mastics with traditional fillers and investigate the limited research on asphalt mastics or mixtures that have been modified with portland cement.

## **Task 2: Experimental Design and Material Characterization**

- Determine the portland cement materials (reactive powders), asphalt binder types, polymer-modification type and dosage, and WMA additive to use in the mastic and mixture testing protocol.
- Evaluate the chemical, physical, and morphological properties of the reactive powder/filler.
- Access Superpave® testing specifications and evaluate mastics and mixtures to understand the influence of reactive powders on material performance.
- Assess the influence of reactive powders on non-traditional durability testing of asphalt specimens.

## **Task 3: Performance Characterization of Asphalt Mastics and Asphalt Mixtures**

- Access Superpave® testing specifications to evaluate the unaged, short-term aged, and long-term aged mastics at high, intermediate, and low temperatures.
- Conduct testing to evaluate the performance of WMA asphalt mixtures in terms of aggregate coating, moisture damage resistance, volumetric properties, workability, and fatigue resistance.

## **CHAPTER 2: LITERATURE REVIEW**

### **2.1 Asphalt Binder**

Asphalt is a highly viscous hydrocarbon that ranges in color from dark brown to black. It is derived from the residue of petroleum distillation. The distillation process can occur naturally, resulting in the formation of asphalt lakes. Alternatively, it can be achieved through refining crude oil at a petroleum refinery. According to the US EIA, the production of asphalt in the United States in 2020 amounted to approximately 21 million tons (U.S. Energy Information Administration 2021). Asphalt is predominantly utilized in the construction of roads and highways, which account for roughly 80% of its overall consumption. In hot mix asphalt (HMA), asphalt serves as a viscoelastic, thermoplastic, waterproof adhesive. By weight, asphalt typically represents 4% to 8% of HMA, and its cost comprises approximately 25% to 30% of the total cost of an HMA pavement structure, depending on its type and quantity. Additionally, the paving industry employs various forms of asphalt, including asphalt emulsions, asphalt cutbacks, and foamed asphalt.

The term "asphalt cement" typically denotes asphalt that has been ready for application in hot mix asphalt (HMA) and other pavement-related uses. However, in this particular section, the all-encompassing term "asphalt binder" is employed to refer to the primary binding agent in HMA. This is due to the fact that "asphalt binder" incorporates not only asphalt cement but also any added materials used to modify the initial asphalt cement characteristics.

The asphalt binder serves a critical function as a bonding agent in the asphalt mixture. The asphalt mixture is made up of asphalt binder, filler, and aggregates, and the asphalt binder is responsible for providing the overall strength and durability of the composite material. Essentially, it acts as a glue that binds the other components together and gives the asphalt mixture its resistance against distresses, including rutting, fatigue cracking, thermal cracking, or cracks caused by combined

effects of traffic load and environmental conditions (McGennis, Shuler et al. 1994). To ensure the optimal performance and longevity of asphalt pavements, it is crucial to fully characterize the rheological properties of the asphalt binder prior to its use in the field. This characterization process involves analyzing the flow and deformation properties of the binder, including its viscosity, stiffness, and elasticity. By comprehensively characterizing the asphalt binder's rheological properties, engineers can select and utilize binders that are best suited for the specific environmental and traffic conditions in which the pavement will be utilized.

To evaluate the performance and select the appropriate asphalt binder for a given pavement application, a grading system is typically employed. Three main grading systems are currently used worldwide: the penetration grading system, viscosity grading system, and Superpave performance grading (PG) system. These systems utilize various tests and criteria to assess the properties of the asphalt binder, including its consistency, stiffness, and ability to withstand traffic and environmental conditions. Once the grading has been established, engineers can then select an appropriate asphalt binder that meets the specific requirements of the pavement application (Zeiada, Liu et al. 2022).

The penetration grading system and the viscosity grading system both rely on key characterization tests to assess the properties of the asphalt binder. The penetration grading system, according to ASTM D946, utilizes the penetration test, which involves measuring the depth in tenths of a millimeter to which a standard needle will penetrate the asphalt binder sample under specific conditions. The viscosity grading system, on the other hand, relies on the viscosity test, which measures the kinematic viscosity of the asphalt binder at a specific temperature, as per ASTM D3381. These key characterization tests provide critical information about the consistency and flow properties of the asphalt binder and help to determine its appropriate grade. The penetration

grading system and the viscosity grading system, while widely used, have been identified as having three major limitations, as summarized below (Charoentham and Kanitpong 2012):

1. Empirical nature: both grading systems rely on empirical tests, and there is no direct correlation between the physical properties measured in the laboratory and the field performance of the asphalt binder. Field experience and observations are required to interpret the test results accurately.
2. Limited evaluation of long-term aging: neither the penetration grading system nor the viscosity grading system considers the long-term aging of asphalt binders, which can be critical in predicting the performance of asphalt pavements over a longer period. The simulation of long-term aging in the laboratory is essential to investigate fatigue cracking and thermal temperature cracking after a prolonged service period.
3. Insufficient consideration of pavement condition: the grading systems do not fully account for the pavement conditions, including temperature, traffic speed, volume, and structure, which can significantly affect the pavement performance. These factors must be considered to select an appropriate asphalt binder for a specific pavement application.

To address the limitations of the previous grading systems, the Superpave PG (performance grading) system was developed in the United States as part of the Strategic Highway Research Program (SHRP) in the early 1990s (McGennis, Shuler et al. 1994). The Superpave PG system utilizes two temperature limits, such as PG 70-22, where the upper temperature limit is determined by the average seven-day maximum pavement design temperature (in degrees Celsius), and the lower temperature limit is determined by the minimum pavement design temperature (in degrees Celsius). The Superpave PG system is the first grading system to directly relate the measured physical properties of asphalt binders to the field performance of asphalt pavements, with

consideration of aging and pavement conditions. The system includes novel tests and specifications to address performance requirements, such as rutting resistance, fatigue cracking resistance, and thermal cracking resistance. Many researchers have shown that using the Superpave PG system can more accurately and comprehensively characterize asphalt binders, resulting in improved pavement performance (Zeiada, Liu et al. 2022).

The Superpave Performance Grade (PG) system is a significant improvement over conventional grading systems; however, there is scope for further enhancement. Despite its adoption in the United States, several state highway agencies have identified crucial deficiencies in the test methods and evaluation criteria associated with the Superpave PG system. These gaps must be addressed to ensure that the system is effective in accurately characterizing the performance of asphalt materials under various conditions. Therefore, ongoing research and development efforts are necessary to refine the Superpave PG system and optimize its performance (Bahia, Perdomo et al. 1997, Bahia, Zhai et al. 1999, Chen and Tsai 1999, D'Angelo and Dongr 2002).

To address the gaps in the Superpave PG system, new test methods have been developed, particularly for polymer-modified asphalt binders. However, the Superpave rutting parameter  $|G^*|/\sin \delta$ , which measures the dynamic shear modulus and phase angle, has been identified to have several issues. Delgadillo et al. highlighted these problems, including the use of fully reversed load in testing, derivation from total dissipated energy based on linear viscoelastic theory, insufficient number of cycles for testing, and grade bumping for traffic speed and volume. The middle two problems with  $|G^*|/\sin \delta$  also apply to the Superpave fatigue parameter  $|G^*|\sin \delta$ . Additionally, Bahia et al. pointed out that fatigue in asphalt pavements begins and propagates in the asphalt binder, but  $|G^*|\sin \delta$  was derived based on the dissipated energy concept and measured in the linear viscoelastic range using small strains. As a result,  $|G^*|\sin \delta$  may not accurately reflect

the true damage induced in the asphalt binder. Their study demonstrated a poor correlation between  $|G^*|/\sin \delta$  and mixture fatigue indicators, indicating a need to control binder-associated damage in the binder specification. With respect to thermal cracking evaluation, the Bending Beam Rheometer (BBR) specification was found in many cases to underestimate the low temperature performance of some modified asphalt binders, despite improved performance indicated by field experience (Bahia, Hanson et al. 2001, D'Angelo 2009).

The value of the Superpave PG system lies not in its specific test methods but in its fundamental concept of using properties that directly relate to performance to classify and characterize asphalt binders. Therefore, it is reasonable to anticipate ongoing improvements as properties that more accurately reflect performance are identified. In recent years, considerable effort has been directed towards enhancing the Superpave PG system through the development of a more uniform and mechanistic asphalt binder testing scheme. Numerous performance-based/related test methods have been developed as potential modifications to the Superpave PG system. An example of a successful modification is the Multiple Stress Creep Recovery (MSCR) test, which has been integrated into the latest Superpave PG system to grade the high-temperature performance of asphalt binders. It is crucial to have a comprehensive understanding of these recently developed performance-based test methods, as they indicate the evolution of the Superpave PG system.

## **2.2 Polymer-modified Asphalt Binder**

The incorporation of polymers, which are chains of repeated units, into asphalt has been demonstrated to enhance its performance. Specifically, pavement with polymer modification displays increased resistance to rutting and thermal cracking, decreased fatigue damage, stripping, and temperature susceptibility. Polymer modified binders have proven successful in areas experiencing high stress, such as intersections of busy streets, airports, vehicle weigh stations, and

racetracks. Various polymers, such as styrene-butadiene-styrene (SBS), styrene-butadiene rubber (SBR), Elvaloy, rubber, ethylene vinyl acetate (EVA), polyethylene, and others, have been used to modify asphalt. Desirable characteristics of polymer modified binders include greater elastic recovery, a higher softening point, greater viscosity, greater cohesive strength, and greater ductility (Yildirim 2007).

Processes for modifying asphalt using natural and synthetic polymers have been patented since as early as 1843 (Hoiberg 1966). Test projects were initiated in Europe during the 1930s and neoprene latex was first used in North America during the 1950s (Yildirim 2007). In the late 1970s, Europe was ahead of the United States in the use of modified asphalts due to the European practice of using contractors who provided warranties and a greater focus on decreased life cycle costs, even at higher initial costs. The high initial costs associated with polymer modified asphalt limited its use in the U.S (Terrel and Walter 1986). In the mid-1980s, new polymers were developed, and European technologies began to be used in the U.S (Brûlé 1996). During this time, there was also an increased emphasis on the long-term economic outlook in the U.S (Roque, Birgisson et al. 2004). The current National Asphalt Specification in Australia includes guidelines and specifications for the polymer-modified binders (Association 2004).

The United States Federal Highway Administration (FHWA) has devised a life cycle cost analysis methodology for assessing the life cycle expenditures of pavements containing asphalt rubber binders and other treatments. According to the results, the utilization of asphalt rubber is economically beneficial, particularly in Arizona and California. However, the estimated lifespan of the pavement is based on a combination of interviews and engineering expertise and can be refined as the pavement matures and the long-term operational effectiveness is incorporated into the model (Kennedy, Cominsky et al. 1990).

In 1997, a survey of state transportation departments in the United States revealed that 47 out of 50 states reported intentions to adopt modified binders in the future, with 35 indicating plans to increase usage levels (Pauli 1996). Various research groups worldwide have investigated the effects of polymer modification on pavement performance, and testing and specifications for binders are continuously evolving. A study conducted in 2001 by Sargand and Kim for the Ohio Department of Transportation compared the fatigue and rutting resistance of three PG 70-22 binders, including an unmodified binder, an SBS-modified binder, and an SBR-modified binder (Sargand and Kim 2001). The findings revealed that the modified binders were more resistant to both fatigue and rutting than the unmodified binder, despite all three possessing the same performance grade. According to a Nevada-based study conducted in 2003, polymer-modified binders typically exhibit significantly higher viscosity than non-modified binders at 60°C, while penetration changes only slightly at all temperatures (Sebaaly, Bazi et al. 2003).

In 2003, Newcomb [12] presented the idea of "perpetual pavements" in Hot Mix Asphalt, disputing the notion that fatigue cracking is an inevitable occurrence (Newcomb 2003). Newcomb argued that several full-depth HMA pavements constructed 30-40 years ago have yet to demonstrate any signs of fatigue cracking and proposed that increasing the amount of polymer-modified binders at the bottom of the asphalt layer could increase the pavement's fatigue limit. A 2003 study by the US Army Corps of Engineers (Newman 2003) highlighted that for optimal cost-effectiveness, it is preferable to select an asphalt modifier that resists multiple types of stress, such as rutting, fatigue, thermal cracking, and water damage. The study found that the polymer choice can significantly impact fatigue properties, with the mixtures that exhibit the highest fatigue life containing reactive styrene-butadiene crosslinked polymer. Other polymers investigated included chemically modified crumb rubber, SBR, linear block SBS, and a proprietary modified SBS.

Four specific polymers have been introduced as common polymer-modifiers for asphalt binders: rubber, styrene-butadiene-styrene (SBS), styrene-butadiene-rubber (SBR), and Elvaloy. Rubber and SBS-modifier will be elaborated with details.

The terms "Crumb rubber modifier" (CRM) and "asphalt-rubber" refer to the addition of ground tire rubber to asphalt to improve its performance. The characteristics of asphalt-rubber depend on the type of rubber, asphalt composition, size of rubber crumbs, and reaction time and temperature. The rubber used is typically recycled from used automotive tires, which has the added benefits of saving landfill space and reducing costs. Natural rubber modification improves rutting resistance and ductility, but the modifier is sensitive to decomposition and oxygen absorption and has compatibility issues due to its high molecular weight. Recycled tire rubber reduces reflective cracking and increases durability. However, there are practical problems in using natural rubber, such as the need for elevated temperatures and long digestion times to disperse it in the bitumen (Behnood and Gharehveran 2019). In 1991, the Intermodal Surface Transportation Efficiency Act (ISTEA) mandated the use of pavement made with crumb rubber, processed recycled tires, or modified asphalt for 5% of roads built with federal funds starting in 1994, and 20% by 1997, to develop a national intermodal transportation system that is economically efficient, environmentally sound, and energy efficient (Camph, Siwek et al. 1997) .

Styrene-butadiene-styrene (SBS) is a block copolymer that enhances the elasticity of asphalt. A 2001 review published in *Vision Tecnologica* (Becker, Mendez et al. 2001) indicated that SBS is likely the most appropriate polymer for asphalt modification, although the use of SBS-type block copolymers has economic and technical limitations. While low-temperature flexibility is improved, some studies suggest that a reduction in strength and resistance to penetration may be

observed at higher temperatures. Despite these limitations, "SBS is the most commonly employed polymer for asphalt modification, followed by reclaimed tire rubber".

According to the Danish Road Directorate (Rieksts, Pettinari et al. 2019), an SBS-modified binder course did not exhibit superior rut resistance when compared to other asphalt courses used in Denmark. Examination of asphalt cores obtained from the job site revealed that separation had occurred, and the polymer phase was not homogeneously distributed, which may have contributed to the mediocre performance of the pavement. A study published in the *Journal of Materials in Civil Engineering* in 2002 (Chen, Liao et al. 2002) utilized transmission electron microscopy to investigate the behavior of SBS in asphalt binders. The morphology of the binder varied depending on the source of the asphalt and polymer, with possible configurations including a continuous asphalt phase with dispersed SBS particles, a continuous polymer phase with dispersed asphalt globules, or two interlocked continuous phases. The formation of a critical network between the binder and polymer was found to increase the complex modulus, indicating resistance to rutting. (Mohammad, Negulescu et al. 2003) conducted a study to investigate the feasibility of recycling SBS-modified asphalt for resurfacing pavement. They found that the extraction and recovery process had minimal impact on the binder. However, the recovered binder from an eight-year-old SBS-modified binder obtained from Route US61 in Louisiana had experienced intensive oxidative age hardening, resulting in brittle behavior at low temperatures. Blends of virgin and recovered polymer-modified binder were stiffer than expected at both low and elevated temperatures. The study also found that as the percentage of recovered binder increased, rutting resistance increased, while fatigue resistance decreased. In a 2004 report published by the Florida Department of Transportation and FHWA (Federal Highway Administration) (Roque, Birgisson et al. 2004), the effect of SBS modification on cracking resistance and healing characteristics of Superpave mixes

was investigated. It was found that SBS improved cracking resistance due to a reduced rate of micro-damage accumulation but had no effect on the healing or aging of the asphalt mixture. SBS has become the preferred replacement for SBR due to its broader compatibility and greater tensile strength under strain. It is currently the most commonly used polymer for modifying asphalt, as it enhances the elasticity of the asphalt and allows for its recycling. Additionally, SBS-modified binders have demonstrated superior performance at low temperatures compared to unmodified binders or binders modified with chemically reactive polymers (Tian, Li et al. 2021).

(Zhu 2015) examined the effects of thermal oxidative aging on polymer-modified asphalt binders. The study involves the preparation of various modified asphalt binders by adding different types of polymer additives, such as SBS and crumb rubber, to the base asphalt. The study prepared six different types of modified asphalt binders, including a control sample without any polymer additives. The other five samples were modified with varying dosages of either SBS or crumb rubber. After preparation, the samples were subjected to thermal oxidative aging at 163°C for 5, 10, 15, and 20 hours. The rheological properties of the modified asphalt binders were then evaluated using a dynamic shear rheometer (DSR). The prepared binders were then subjected to thermal oxidative aging in a laboratory setting. The study's results showed that thermal oxidative aging causes significant changes in the rheological properties of the modified asphalt binders, with an increase in stiffness and a decrease in ductility. The study also found that the type and dosage of polymer additives significantly affect the rheological properties of the modified asphalt binders after thermal oxidative aging. For instance, the addition of SBS can enhance the resistance to thermal oxidative aging, while the addition of crumb rubber can increase the ductility of the modified asphalt binder. (Lin, Huang et al. 2020) conducted a laboratory study to investigate the effects of long-term aging on high-content polymer-modified asphalt binder. The study involved

preparing six different asphalt binders, including a control binder and five binders modified with varying amounts of a styrene-butadiene-styrene (SBS) polymer. The prepared binders were then subjected to long-term aging at 85°C for up to 365 days. The researchers measured the binders' rheological properties using a dynamic shear rheometer (DSR) and evaluated their low-temperature cracking resistance using a bending beam rheometer (BBR). The study's findings revealed that long-term aging causes significant changes in the rheological properties of high-content polymer-modified asphalt binders, including an increase in stiffness and a decrease in ductility. The research also found that the effects of long-term aging on the binders' performance were dependent on the amount of polymer added. Additionally, the study showed that the high-content polymer-modified asphalt binders exhibited better low-temperature cracking resistance than the control binder, indicating their potential for use in cold climates.

(Yut and Zofka 2014) conducted a study to investigate the correlation between rheology and chemical composition of aged polymer-modified asphalt. The researchers prepared five different asphalt binders, including a control binder and four binders modified with varying amounts of a styrene-butadiene-styrene (SBS) polymer. The prepared binders were then subjected to aging in a laboratory setting at 163°C for 3, 7, and 14 days. The researchers analyzed the chemical composition of the aged binders using Fourier transform infrared (FTIR) spectroscopy and gas chromatography-mass spectrometry (GC-MS). The study's findings showed that aging causes significant changes in the chemical composition and rheological properties of the polymer-modified asphalt binders. The researchers found that the changes in the binder's chemical composition were related to the changes in its rheological properties. The study's results also suggested that the formation of polar functional groups, such as carboxylic acids and ketones, played a significant role in the aging process of the polymer-modified asphalt binders. These

functional groups were found to be related to the increase in the binder's stiffness and decrease in its ductility.

(Singh, Kumar et al. 2018) studied the thermal degradation of styrene-butadiene-styrene (SBS) polymer in bitumen during storage and its dependence on several factors such as temperature, SBS concentration, polymer type, and base bitumen. The researchers prepared different SBS-modified bitumen samples with varying SBS concentrations and base bitumen types. The samples were then subjected to thermal degradation by storing them at temperatures ranging from 50°C to 80°C for up to 180 days. The study's findings showed that the thermal degradation of SBS in bitumen during storage was dependent on several factors. The researchers found that the rate of degradation increased with increasing temperature and SBS concentration. They also observed that the rate of degradation was influenced by the type of base bitumen used, with some types of base bitumen being more susceptible to degradation than others. Furthermore, the study found that the degradation of SBS in bitumen resulted in a reduction in the binder's elasticity and increased stiffness, as measured by dynamic mechanical analysis (DMA) tests. The researchers also observed that the degree of degradation was dependent on the type of SBS polymer used.

Overall, the addition of polymers to asphalt binders is known to significantly improve their physical and rheological properties. However, this technique is not without its drawbacks, including the possibility of phase separation problems and reduced aging resistance. To address these issues, various techniques have been suggested, including functionalization, saturation, and sulfur vulcanization. Additionally, non-conventional modifiers such as reactive polymers, nanomaterials/clay minerals, and bio-oils can also improve asphalt binder properties. These modifiers can be used either alone or in combination with polymers. However, it is important to

note that while these techniques and non-conventional modifiers may improve the properties of asphalt binders, they can also introduce unexpected problems (Behnood and Gharehveran 2019).

### **2.3 Warm Mix Asphalt**

The utilization of Hot Mix Asphalt (HMA) in pavements has been associated with negative environmental effects, including high CO<sub>2</sub> emissions and energy consumption. In contrast, Warm Mix Asphalt (WMA) has been gaining attention due to its superior technical, environmental, and economic benefits, such as improved workability, reduced emissions, lower energy consumption, enhanced working conditions, reduced binder aging, and extended construction time (Bower, Wen et al. 2016, Tao, Xiao et al. 2019, Cloutier 2021, Cloutier, Farahi et al. 2021). The use of WMA began in European countries and Australia in 2000 and has since attracted researchers and engineers in North America (Vaitkus, Čygas et al. 2009). WMA technology incorporates various additives and techniques that enable the production of asphalt mixtures at lower temperatures compared to those required for HMA (about 20-60 degrees Celsius). Despite its numerous advantages, WMA has its limitations from a technical perspective.

The utilization of WMA technologies offers various environmental, technical, and economic advantages. However, these benefits are subject to the type of technology employed and may be influenced by other factors such as the properties of other materials, including binder, aggregate, and recycled materials, in the WMA mixtures and the quantity of WMA additives. Concerning environmental benefits, WMA technologies are capable of reducing energy consumption by approximately 18% to 30% as they require lower mixing and compaction temperatures when compared to conventional HMA (Almeida-Costa and Benta 2016). The production process of WMA results in decreased emissions of toxic and greenhouse gases, which can improve working conditions by reducing exposure to hazardous fumes. Additionally, lifecycle analysis of WMA has

shown that it is associated with a reduction of 18% in fossil fuel usage and 24% in air pollution (Hassan 2010). The implementation of WMA technologies can result in significant reductions in energy consumption and air pollution, depending on the specific technology used. These technologies can also improve the workability of paving operations and lead to earlier opening to traffic, longer hauling distances, and a longer construction season. Additionally, WMA can provide economic benefits, including reductions in fuel usage of up to 20-25% (Pérez-Martínez, Moreno-Navarro et al. 2014). WMA technologies offer potential cost savings of 10-30% in life cycle cost assessments, depending on the technology used. However, there are also some economic and technical drawbacks associated with WMA. These drawbacks include the initial cost of acquiring additional equipment and the additional cost of WMA additives, which may only partially offset the reduced energy consumption. Some WMAs may also exhibit reduced resistance to moisture damage and bonding/coating problems compared to HMA. One of the main reasons for these issues is the reduced optimal binder content in WMA compared to HMA. Additionally, the reduced oxidative aging and air void content in WMA may lead to distresses such as rutting, although they may also improve the WMA's durability (Behnood 2020).

Overall, WMA technologies can be classified into three main categories of foaming technologies, chemical additives, and organic or wax additives. Foaming technologies are diverse methods used to produce foamed binders by adding pulverized cold water or other liquids, such as ethanol, into a preheated binder (Hasan, Goh et al. 2013). Foaming technologies involve adding cold water or other liquids like ethanol into a preheated binder to create a foamed binder. However, the use of other liquids like ethanol may not be cost-effective due to their higher cost compared to water. The water added to the binder is vaporized as the temperature increases, and the steam produced is trapped in the binder, temporarily increasing its volume, and reducing its viscosity, which

improves the workability of the asphalt mixture. As the steam eventually dissipates, the binder returns to its original volume. Foaming technologies can be grouped into two categories: those that use additives containing water and those that are water-based (West, Rodezno et al. 2014). The addition of water-containing additives, like Aspha-min and Advera, to the binder is one method of foaming technology. These additives consist of finely crushed powders that contain water within their structure. When the temperature exceeds a certain level, depending on the type of additive, the water evaporates, causing the volume of the binder to expand by approximately 5-15 times and creating foamed asphalt binder. Aspha-min is a synthetic zeolite, while Advera can be natural or synthetic. Synthetic zeolite is more effective than natural zeolite as a water-containing agent. Aspha-min and Advera differ in their particle size, and lower dosages are recommended for use as a compaction aid, while higher dosages are recommended for mixtures with over 7% binder content. Apart from Aspha-min and Advera, other natural and synthetic zeolite structures have also been reported as foaming agents for asphalt (Woszuk, Zofka et al. 2017).

Chemical additives can be used in the production of WMA to improve adhesion and coating of the aggregates by the binder. These additives are typically formulated as a package of products and can include anti-stripping agents, aggregate coating promoters, emulsification agents, and surfactants. Examples of chemical additives used in WMA include Evotherm, Cecabase, Rediset, Iterlow T, and HyperTherm/QualiTherm. Evotherm is a chemical additive that enhances the adhesion, coating, and workability of WMA. It can be used in three main processes: Evotherm Emulsion Technology (ET), Evotherm Dispersed Asphalt Technology (DAT), and Evotherm Third Generation (3G). Evotherm ET was the original process developed in 2004 and uses hot aggregates mixed with an emulsion to decrease the mixing temperature. In 2007, Evotherm DAT was introduced, which diluted the same chemical additive in Evotherm ET with a small amount of

water. The third process, Evotherm 3G, does not contain water and can be added to the asphalt binder or mixture. Due to the benefits provided by Evotherm 3G and Evotherm DAT, the first process of Evotherm is no longer used in WMA. Evotherm DAT provides a higher reduction in production temperature than Evotherm 3G compared to Evotherm ET (Behnood 2020).

Organic wax can be added to the asphalt binder or blended into the asphalt mixture at high temperatures to reduce its viscosity. However, when the asphalt mixture cools down, the additive can crystallize and cause the binder to become stiffer. One commonly used method to produce organic additives is the Fisher-Tropsch (FT) process that uses natural gas. Sasobit is a widely used WMA additive produced using this process. Other organic additives, such as SonneWarmix, BituTech PER, Thiopave, LEADCAP, RPPW, Licomont BS 100, Rh-WMA, and Asphaltan-B, have also been used in WMA mixtures, but they are produced using other methods (Behnood 2020).

Chemical additives are known to have negligible impacts on the high, intermediate, and low-temperature properties of asphalt binders, while foaming-based technologies may have minor effects on high-temperature properties. Out of all the WMA additives, organic additives, specifically Sasobit, have the most significant positive effects on high-temperature properties. When the temperature is above Sasobit's melting point of around 115°C, it dissolves in the asphalt binder, making the mixture more workable. Below the melting point, Sasobit has a lattice-like structure that can improve the binder's resistance to permanent deformation. The apparent viscosity decreases linearly above 110°C with increasing additive content, while the dynamic viscosity increases exponentially at 60°C (Zhang, Yang et al. 2015). Studies have shown that the use of Sasobit as an additive in asphalt binders can significantly improve their resistance to rutting, while other additives such as Advera and Rediset may have a minor

negative impact on this property. Therefore, in order to achieve the desired Performance Grade, the use of Sasobit as a modifier in asphalt binders should be carefully considered and engineered (Jamshidi, Hamzah et al. 2013). The aging of the asphalt binders decreases the resistance to thermal cracking and fatigue cracking as it increases the stiffness of the binders (Behnood, Gharehveran et al. 2015). When using Recycled Asphalt Pavement (RAP) with aged and stiff binders, the construction temperatures can be increased. To reduce the construction temperatures of asphalt mixtures containing RAP or aged binders, WMA additives can be used. However, some of the common WMA additives used in the asphalt industry can increase the stiffness of binders at low temperatures. Therefore, careful consideration should be given when using WMA additives with recycled and aged binders, especially with regard to binder and mixture performance at low temperatures. To compensate for the rheological changes in aged asphalt binders containing WMA additives, it is recommended to use a binder with a lower performance grade, such as PG 58-28 instead of PG 64-22 (Kim, Lee et al. 2011). With regard to the moisture damage resistance, chemical additives such as Cecabase, Rediset, and Evotherm can be used to enhance the adhesion properties, however, careful consideration is needed to be taken since a reduction in asphalt's surface tension occurs without modifying the rheological properties). Surfactants, due to their polarized extremities, can attract the materials (aggregates) with opposite charges and increase the adhesion properties (Liu, Yan et al. 2018).

## **2.4 Fillers**

The aggregates are generally categorized as coarse if they are larger than 4.75 mm and fine if they are smaller than 4.75 mm. The aggregate particles that are finer than 75  $\mu\text{m}$  in size are referred to as fillers. Even though filler particles are small, they have a significant impact on the characteristics and performance of the asphalt-concrete mixture. Good packing of the coarse,

fine, and filler aggregates provides a strong backbone for the mixture. The presence of fillers leads to a reduced optimum asphalt content, stronger pavement, better asphalt cohesivity, and better internal stability due to the good packing contributed by the filler. The inclusion of mineral filler increases the resilient modulus of an asphalt-concrete mixture. However, excessive filler amounts may weaken the mixture by increasing the amount of asphalt needed to coat the aggregates or by making the asphalt stiff and thereby affecting the workability of the mixture. The presence of filler in the asphalt-concrete mixture is even more important because of its possible interaction with asphalt, leading to different mixture performance due to the interaction of filler with asphalt and the formation of asphalt-filler mastic during the mixing process (Zulkati, Diew et al. 2012).

## CHAPTER 3: MATERIALS AND METHODS

### 3.1 Materials Characterization

The reactive powders and fillers used in this study were investigated for chemical and physical properties. The experimental program included one reference limestone filler and one Type I portland cement reactive powder. Table 3.1 indicates the source of these components and their corresponding abbreviations used in the report.

**Table 3.1: Used Fillers in the Study**

Type	Supplier	Abbreviation
Limestone	Piqua Materials	LS
Portland Cement Type I	Lafarge	PC

#### 3.1.1 Chemical Properties

Chemical composition testing was performed on the utilized fillers. The assessed properties include chemical oxides, Loss on Ignition (LOI), and crystallographic analysis.

##### Chemical Oxide Composition

The chemical oxide composition of the investigated powders was tested using X-Ray Fluorescence (XRF) as per ASTM C114. It was necessary to determine the chemical composition to understand the potential effect of cement reactive powders on the performance of asphalt mastics and asphalt mixtures. Figure 3.1 indicates the SiO<sub>2</sub>, Al<sub>2</sub>O<sub>3</sub>, Fe<sub>2</sub>O<sub>3</sub>, CaO, and MgO content of LS and PC fillers that were used in the study. As reported in Figure 3.1, LS filler had a higher MgO content while PC powder had a higher SiO<sub>2</sub> content.

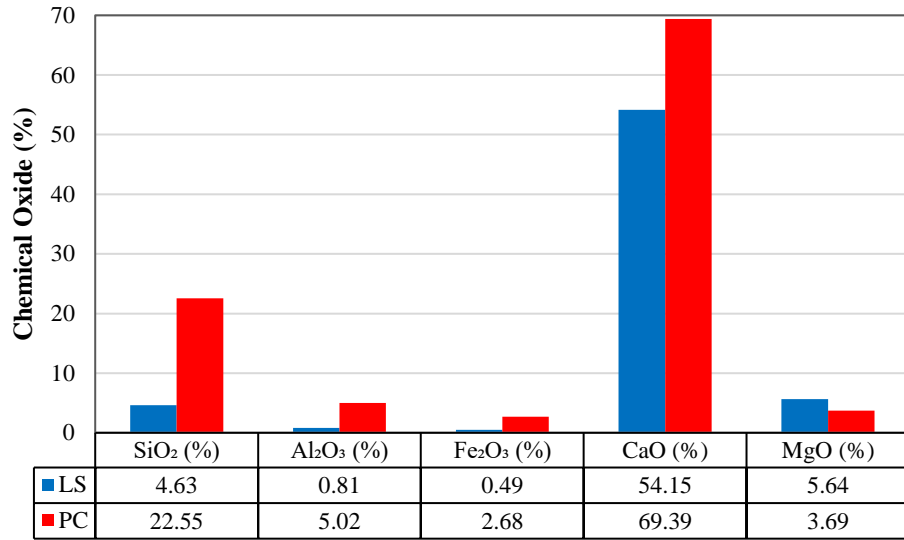


**Figure 3.1: Chemical Oxide Content for Investigated Fillers**

Based on the results of XRF testing, the investigated powders are positioned in a ternary diagram that indicates the distribution of calcium oxide (CaO), silicon dioxide (SiO<sub>2</sub>), and aluminum oxide (Al<sub>2</sub>O<sub>3</sub>), as reported in Figure 3.2. Some other reactive powders which have been used in some recent studies (Cloutier, 2021) are also demonstrated in the same figure. It can be observed that LS filler had a smaller amount of Al<sub>2</sub>O<sub>3</sub> and CaO, as compared with PC reactive powder.

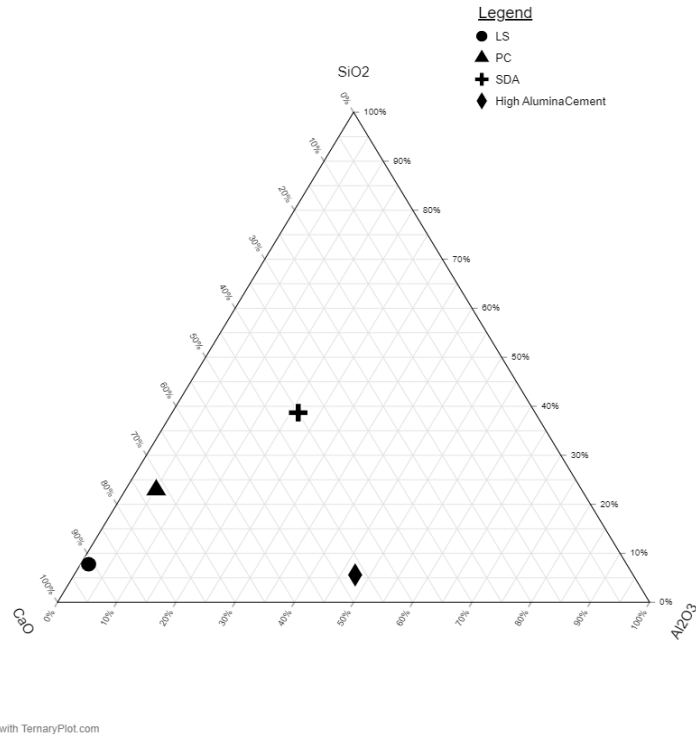


**Figure 3.2: Ternary Diagram of Filler/ Reactive Powders**

The chemical oxide composition is summarized in Table 3.2, and it can be observed that some chemical oxides such as Na<sub>2</sub>O, TiO<sub>2</sub>, and P<sub>2</sub>O<sub>5</sub> are present in minor quantities (< 1%).

**Table 3.2: Chemical Composition of Powder Components**

Sample ID	Na <sub>2</sub> O (%)	MgO (%)	Al <sub>2</sub> O <sub>3</sub> (%)	SiO <sub>2</sub> (%)	P <sub>2</sub> O <sub>5</sub> (%)	K <sub>2</sub> O (%)	CaO (%)	TiO <sub>2</sub> (%)	Fe <sub>2</sub> O <sub>3</sub> (%)
LS	0.04	5.64	0.81	4.63	0.03	0.14	54.15	0.02	0.49
PC	0.11	3.69	5.02	22.55	0.08	0.99	69.39	0.38	2.68

### Loss on Ignition (LOI)

Loss on ignition (LOI) can be described as the process of measuring the weight change of a sample after it has been heated to a high temperature causing some of its content to burn. This

test was conducted according to ASTM C311 to assess the organic content of the fillers. The investigated materials were required to be dried in an oven at  $750 \pm 50^\circ\text{C}$  in a controlled environment with an inert gas, then exposed to oxygen to allow the volatile matter to escape due to rapid oxidation. The procedure concluded when there was no more mass change. The results of this test were evaluated based on the percentage of total mass loss on the point of ignition. Figure 3.3 demonstrates the result of LOI content of LS and PC filler materials, and it can be observed that the LOI content for LS filler is significantly higher than that of PC. This can be attributed to the decomposition of  $\text{CaCO}_3$  in LS filler upon heating.

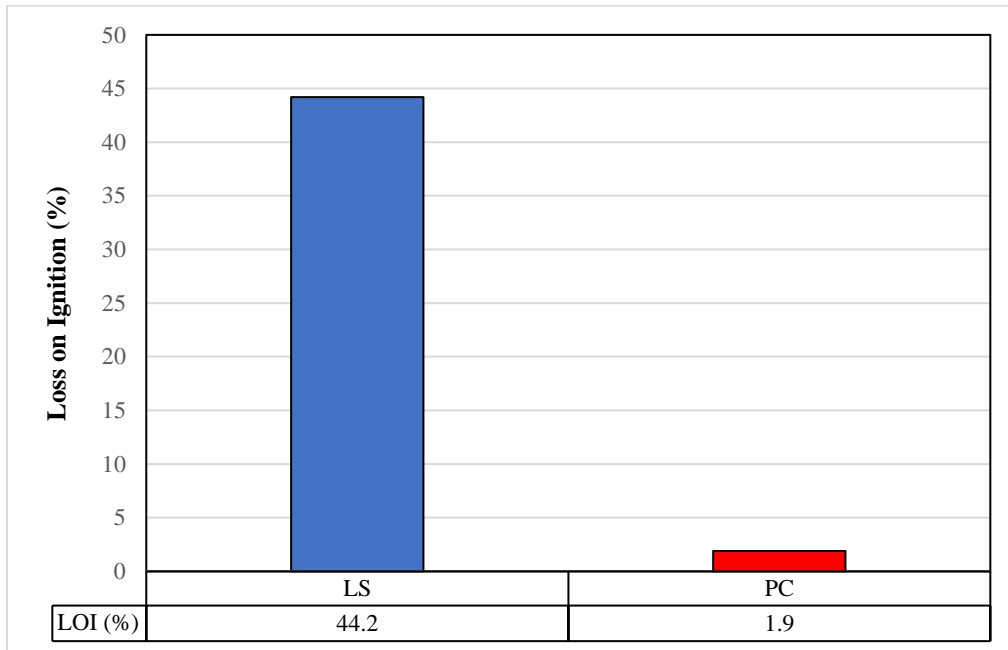


**Figure 3.3: LOI content of Investigated Fillers**

### **Crystallography Analysis**

The phase composition was evaluated using X-Ray Diffraction (XRD), which is a microstructural investigation technique developed to analyze the crystalline materials by evaluating the spacing for the atomic planes of a crystal and is commonly used to determine the phase

composition, unit cell lattice parameters, residual strains, crystal structure, and even crystal size. The samples used in this study were tested to determine if they were crystalline or amorphous. To prepare the powder samples for XRD, the samples were carefully placed onto a shallow well of the XRD sample holder, and once there was a small amount of material, the metal spatula was used to flatten the mound, which packed the sample into a dense configuration. The surface of the material needed to be flat and dense to ensure that the X-ray absorption did not reduce the intensity of low angle peaks. Once the sample was prepared on the holder, the sample was placed into the main compartment of the XRD machine and magnetically locked into place.

The model of the XRD machine that was used during the experiment was a Bruker D8 Discover, and data were collected from the DIFFRAC.COMMANDER software. The X-rays used were soft X-rays, produced from an anode consisting of a water-cooled block of copper. High-speed electrons were detected by colliding with the metal target. This experimental procedure evaluated the powder materials from 10 to 50 degrees of  $2\theta$ . Figure 3.4 reports the XRD results for the control LS filler material. The results demonstrate that the control limestone filler is a crystalline material based on the high-intensity peak of  $\text{CaCO}_3$  characterized by 143.02 CPS at  $2\theta$  of 29.38.

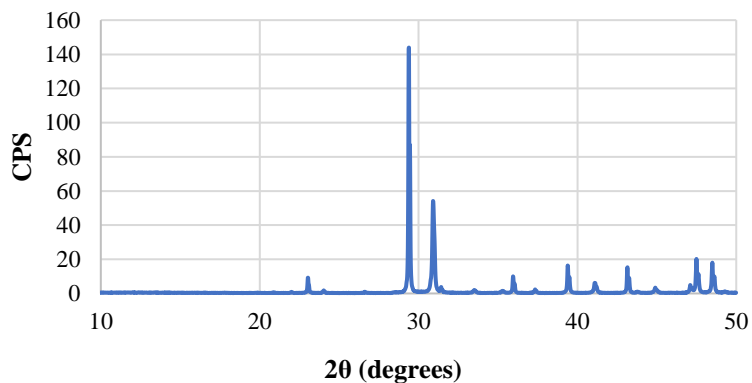


**Figure 3.4: XRD Spectrum for Control Limestone**

Figure 3.5 displays the XRD results for all the LF reactive powders. It can be observed that the reactive powder can be classified as crystalline material based on the low background and high-intensity peak. The cement had a max intensity peak of 32.22 CPS at 26.37  $2\theta$ .

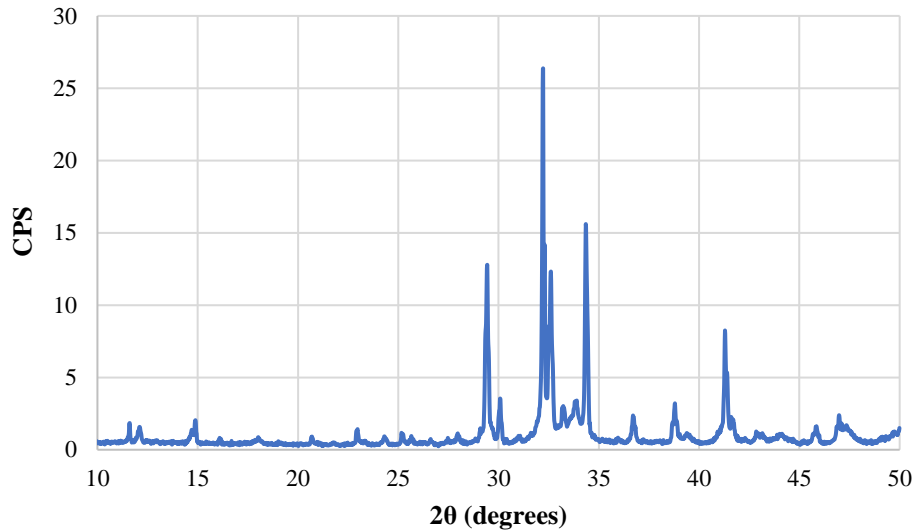


**Figure 3.5: XRD Spectrum for Portland Cement Reactive Powder**

### 3.1.2 Physical Properties

The physical properties tested for the LS filler and PC reactive powder were specific gravity (SG), particle size distribution (PSD), particle shape, and Rigden voids.

#### Specific Gravity

Specific gravity (SG) was evaluated based on ASTM D5550-06 using a Helium Pycnometer. The specific gravity is a significant parameter since it needed to calculate the Rigden voids and for converting mass to volume, which was also important as all compositions and comparisons in this research study were made for a specific volume of material. Figure 3.6 presents the results of the specific gravity testing. The results demonstrate that the specific gravity of LS filler is 2.76, whereas the specific gravity of PC reactive powder is 3.15. The SG values are important for this

research study since these were used for Rigden Void (RV) determination as well as for mixture proportioning of mastic and asphalt mixtures.

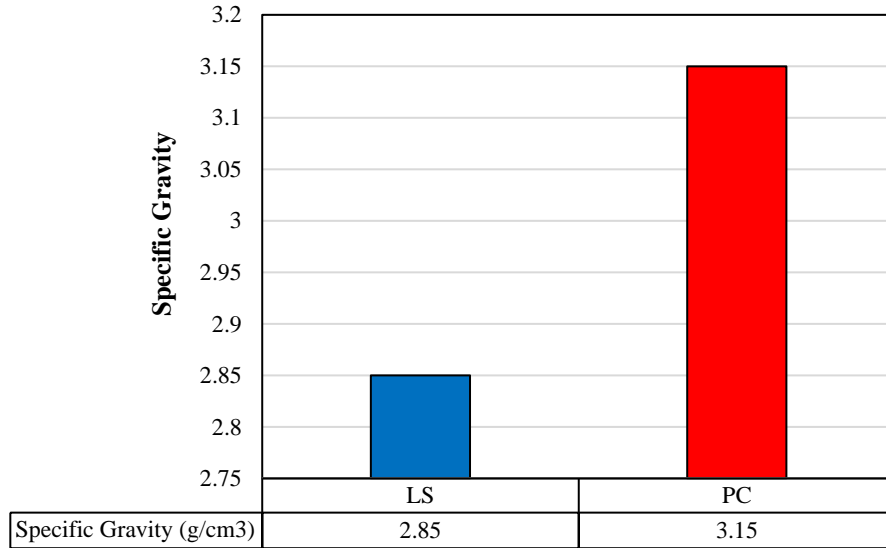
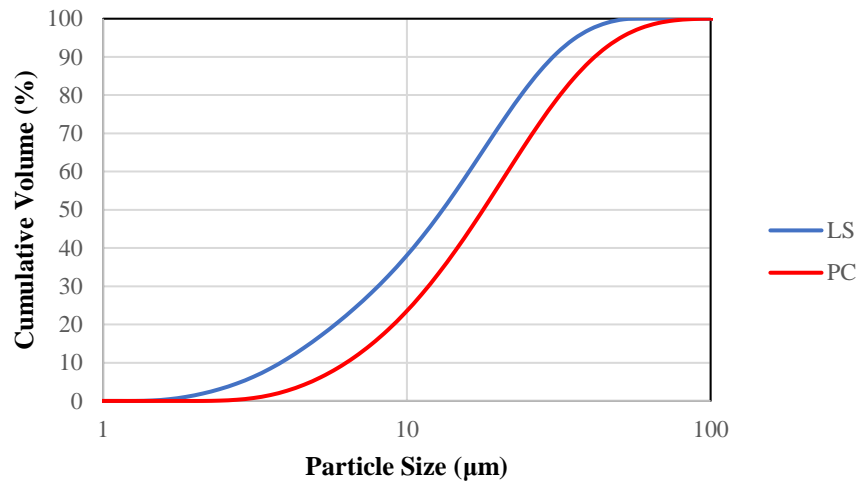


**Figure 3.6: Specific Gravity of Investigated Powders**

**Particle Size Distribution (PSD)**

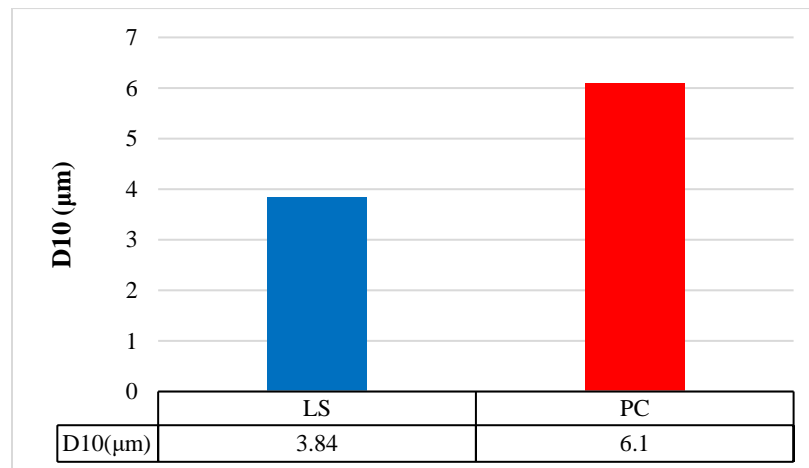
The filler materials' particle size distribution (PSD) was evaluated based on ASTM D4464-10 using laser light scattering. This test method can measure the equivalent spherical diameter for particle sizes in the range of 1 to 300 μm. To conduct the laser diffraction test, a sample of the material was dispersed in distilled water or a compatible organic liquid (IPA was used in this research) and circulated through the path of a laser light beam. When the light beam hits a particle, it is scattered. This scattered light is then collected by a photodetector and converted to an electrical signal, and analyzed with the assumption that all the particles are spherical. From this experiment the PSD curves, the D<sub>10</sub>, D<sub>50</sub>, and D<sub>90</sub> values are determined. The diameters D<sub>10</sub>, D<sub>50</sub>, and D<sub>90</sub> correspond to the portion of the material that is 10%, 50%, and 90% finer, respectively. Figure 3.7 presents the particle size distribution curves for the investigated powders. It can be noted that PC reactive powder had a larger average particle size compared with manufactured (not collected from baghouse) reference LS filler. The

reactive powder particle size of cement ranges between 2- 98  $\mu\text{m}$ , whereas the LS filler particle size ranges between 1-59  $\mu\text{m}$ . Still, LS filler, used as reference material in this study, can be considered to be similar to portland particle shape and size distribution, and other characteristics are imposed by the industrial grinding process.



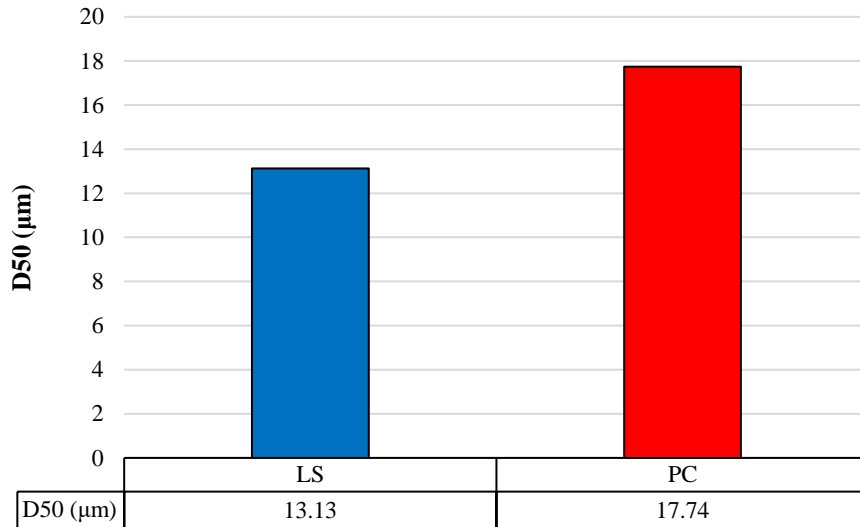
**Figure 3.7: Particle Size Distribution of Investigated Powders**

Figure 3.8 reports the  $D_{10}$  values for investigated materials. It can be observed that the LS filler material is characterized by smaller particles since the  $D_{10}$  value is only 3.84  $\mu\text{m}$  when compared with PC reactive powder having a  $D_{10}$  value of 6.3  $\mu\text{m}$ .



**Figure 3.8:  $D_{10}$  Values of Investigated Powders**

The values for  $D_{50}$  of LS and PC materials are demonstrated in Figure 3.9. It can be seen that LS filler has a  $D_{50}$  value of 13.13  $\mu\text{m}$ , while the value for PC reactive powder is 17.74  $\mu\text{m}$ .



**Figure 3.9:  $D_{50}$  Values of Investigated Powders**

Figure 3.10 presents the  $D_{90}$  values for the investigated powders, and it can be noted that these results represent the same trend, with the PC reactive powder being a coarser material and the LS filler; LS and PC materials have  $D_{90}$  values of 30.38 and 41.71  $\mu\text{m}$ , respectively.

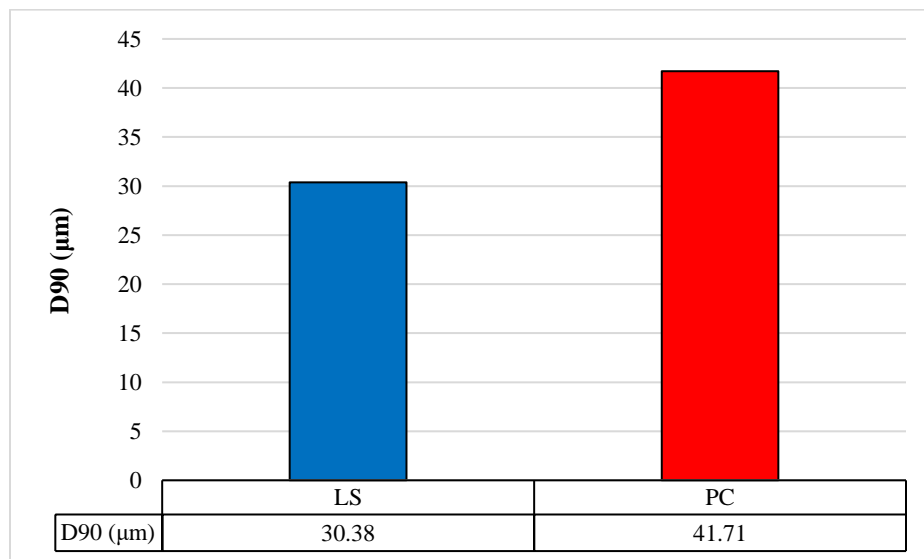


**Figure 3.10:  $D_{90}$  Values of Investigated Powders**

### Particle Shape

Particle shape was evaluated using a TOPCON® SM-300 Scanning Electron Microscope (SEM) in accordance with ASTM E986. An SEM is an electron imaging microscope that has the spatial resolution to examine microscopic structures by scanning material surfaces. The SEM is used for inspecting the topography of specimens at very high magnifications. Materials can be analyzed for physical defects, bond failures, fracture surfaces, and cracks. The SEM image is formed by a focused electron beam that scans over the surface area of a specimen. In this research study, the control LS filler and PC reactive powder were evaluated to examine the surface texture and shape. Figure 3.11 reports on the SEM images for the investigated powders. The control LS powder is composed of individual flake-shaped angular particles, whereas the PC reactive powder is represented by small flake particles with larger rigid forms. Here, similarities in particle shape and a variety of sizes (with larger grains  $> 20\mu\text{m}$  for LS specimen) were observed.

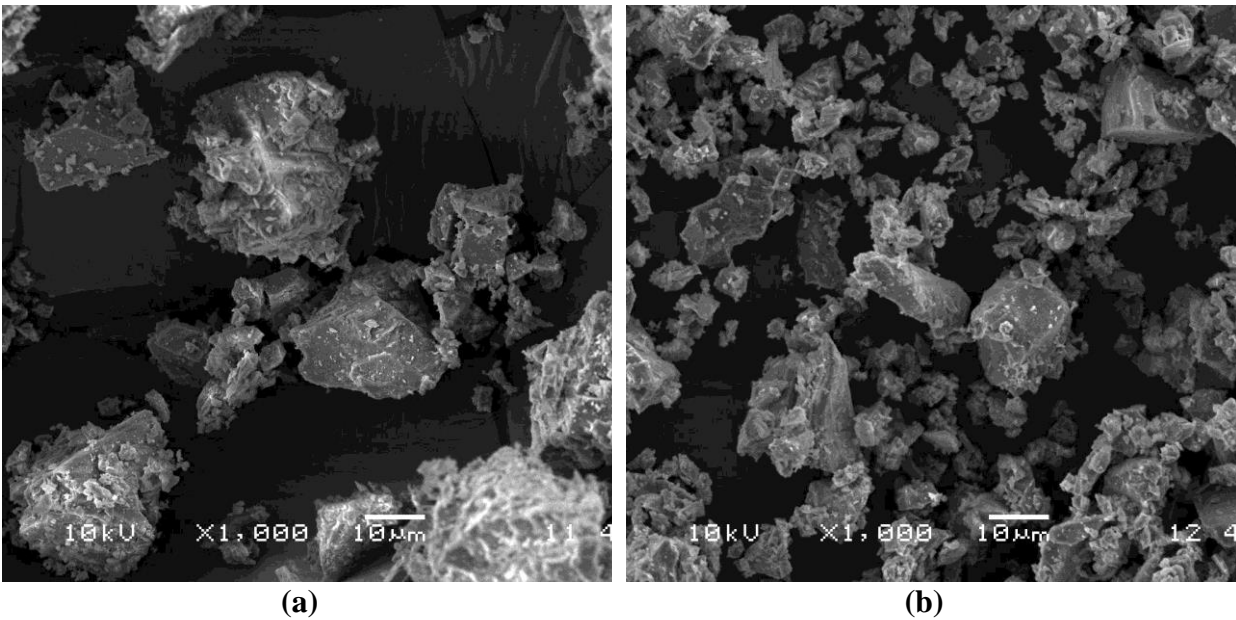


**Figure 3.11: SEM Images of (a) LS Filler and (b) PC Reactive Powder**

## **Rigden Voids**

The fractional void test, also known as the Rigden Voids Test (RV), was developed by Rigden (1947) in order to obtain a unique simple filler characteristic that could be related to the performance of asphalt binders. The significance of the Rigden void test which reports the percentage of void in compacted powder sample has been emphasized by different researchers (Rigden 1947), (Zulkati, Diew et al. 2012), (Faheem, Hintz et al. 2012). Several studies have demonstrated that a higher stiffening effect is related to higher RV values, suggesting that more asphalt binder is required to fill the voids, reducing the separation between the filler particles (Harris and Stuart 1995, Bautista, Flickinger et al. 2015, Sangiorgi, Tataranni et al. 2017, Farahi, Cloutier et al. 2021).

In this research, Rigden voids testing was conducted according to the European Standard EN 1097-4. This test was developed to evaluate the particle packing of powder materials directly associated with a filler in asphalt mastics. Here, the Rigden voids are important when understanding the interactions between filler void characteristics and asphalt binders and the associated stiffness properties that result from these interactions.

Figure 3.12 reports on the Rigden void values for the investigated materials. The Rigden voids value for the LS filler material is 37.66%, whereas the Rigden voids parameter for the PC reactive powder is 34.47%, which can be explained by the presence of larger particle ranges. Despite only a 3% difference, it can be expected that PC powders can be a more effective filler in asphalt systems.

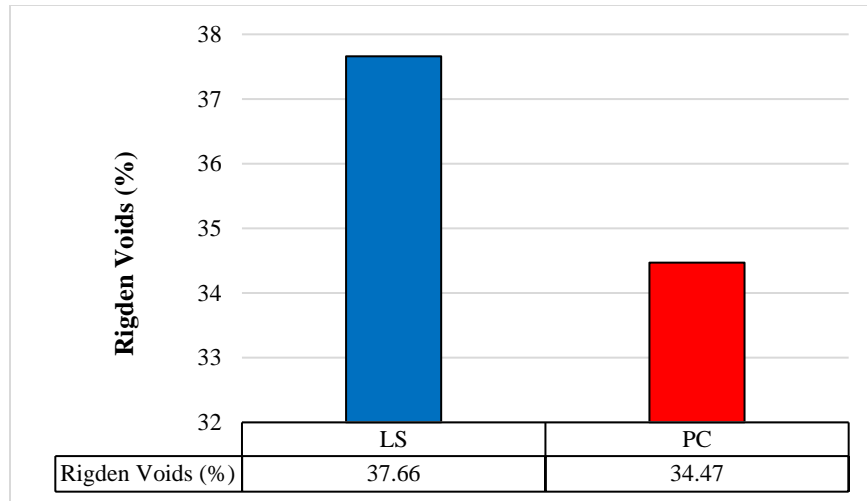


**Figure 3.12: Rigden Void Values for Investigated Powders**

### 3.2 Test Methods for Superpave® Asphalt Mastic Testing Protocol

This section details the experimental testing matrix employed for evaluating hot mix asphalt (HMA) and warm mix asphalt (WMA) mastics that are composed of both LS-based and PC-based binders, with plain and polymer-modified binders used in their production. In total, 40 different mastics were created and tested. Table 3.3 provides an overview of the characteristics of each mastic, including the type of filler, binder, production technology (HMA or WMA), and filler dosage. The primary objective of this phase was to assess the properties of the mastics according to Superpave® performance specifications and to determine the extent of interaction and feedback related to WMA mixture design.

During this phase, the viscosity of unaged asphalt mastics was assessed as an estimate of their workability using a Brookfield rotational viscometer (RV). Additionally, the rutting and fatigue resistance of the mastics were evaluated using the dynamic shear rheometer (DSR) after undergoing rolling thin film oven (RTFO) and pressure aging vessel (PAV) aging. The DSR measured Superpave®  $G^*/\sin(\delta)$ , non-recoverable compliance ( $J_{nr}$ ), % Recovery at high temperature, and Superpave®  $G^*\sin(\delta)$  at intermediate temperature. To assess thermal cracking

resistance, the bending beam rheometer (BBR) and dynamic mechanical analysis (DMA) machine were utilized to measure the creep stiffness  $S(t)$  and  $m$ -value at low service pavement temperature, and DMA was used for additional analysis. Table 3.4 describes the testing matrix for the mastic section of the study.

**Table 3.3: Characteristics of Investigated Mastics**

Filler	Without filler		LS				PC			
			Concentration by volume				Concentration by volume			
			10%		25%		10%		25%	
Tech Binder	HMA	WMA	HMA	WMA	HMA	WMA	HMA	WMA	HMA	WMA
PG58-28	x	x	x	x	x	x	x	x	x	x
Polymer Modified PG58-28	x	x	x	x	x	x	x	x	x	x
PG64-10	x	x	x	x	x	x	x	x	x	x
Polymer Modified PG64-10	x	x	x	x	x	x	x	x	x	x

**Table 3.4: Experimental Matrix for Asphalt Mastic Tests**

Mastic Property	Measured Parameter	Test Method	Aging	Asphalt Binders	Fillers	Replicate	Temperature
Complex Modulus and Phase Angle	$G^*$ and $\delta$	DSR (25mm)	Unaged	8	2	2	PG
Constructability	Viscosity	Rotational Viscometer	Unaged				135°C
Rutting Resistance	$G^*/\sin(\delta)$	DSR (25mm)	RTFO				PG
	$J_{nr}$ and %Recovery	MSCR (25mm)	RTFO				PG
Fatigue Resistance	$G^* \sin(\delta)$	DSR (8mm)	PAV				Intermediate PG + 4°C
Thermal Cracking	$S(t)$ & $m$	BBR	PAV				-PG + 10°C
	Creep compliance & Relaxation Modulus	DMA	PAV	-PG+ 10°C			

### **3.2.1 Mastic Preparation**

The optimization of the mixing process for the LS reference filler and PC reactive powder with asphalt binder was carried out to prevent the introduction of excessive air into the mastic blend. This was achieved through the utilization of an appropriate mixing apparatus, mixing speed, properly aligned propeller, and precise control of the mixing temperature by the hot plate. Specifically, a mechanical stirrer in the form of a Cowles Dissolver was employed, with a mixing speed of 1,300 rpm. The amount of powder required was calculated based on the mass of the asphalt binder using the volume concentration and specific gravity of the materials. The asphalt binder was then mixed with the powders for 30 minutes at  $135 \pm 5^\circ\text{C}$  for HMA and  $120 \pm 5^\circ\text{C}$  for WMA. Additionally, during this mixing time, the powders were added in increments of 5 minutes to ensure proper distribution and integration into the blend.

#### **Mixing Procedure**

The proposed procedure for blending the powders with asphalt binder was as following:

1. Preheat the powder in an oven at  $\pm 5^\circ\text{C}$  for HMA,  $120 \pm 5^\circ\text{C}$  for WMA.
2. Heat asphalt at  $135 \pm 5^\circ\text{C}$  for HMA,  $120 \pm 5^\circ\text{C}$  for WMA.
3. Place an empty quarter of a gallon paint can on top of a piece of wood or plywood on the scale to prevent heat from reaching the platen.
4. Zero the scale.
5. Pour target mass of asphalt into the can (recommended 500 – 600 grams in a quarter of a gallon can).
6. Measure Evotherm using a dropper (skip this step for HMA).
7. Determine the mass of filler required based on the mass of asphalt according to the target filler concentration by mass.

8. Put the can of asphalt in the heat mantel and adjust temperature to  $135 \pm 5^{\circ}\text{C}$  for HMA,  $120 \pm 5^{\circ}\text{C}$  for WMA.
9. Heat asphalt in the mantel for 10 minutes.
10. Insert the mechanical stirrer such that it is located at the bottom third of the can depth. (Use dispersing stirrer to prevent filler agglomeration).
11. Start the mechanical stirrer at 1,300 revolutions per minute.
12. Put an aluminum foil over the can and make a hole to allow space for adding filler into it and make sure to prevent dust going into air.
13. Add Evotherm to asphalt binder (skip this step for HMA).
14. Add filler in small increments while stirring, targeting mixing time of 30 minutes.
15. After all the filler is added continue stirring for five minutes. This makes the total stirring time to be 30 minutes.
16. After blending, the mix is poured into smaller ointment tins. (50 – 60 grams each in 8 oz ointment tins).
17. Cover the ointment tins and store at room temperature for future testing.

### **3.2.2 Aging Procedures**

#### **Rolling Thin Film Oven (RTFO)**

The Superpave® PG binder specification necessitates the testing of the short-term aged asphalt binder at high service temperatures to evaluate its resistance to rutting damage. To simulate the aging of the asphalt binder during the mixing and construction stages, the rolling thin film oven (RTFO) is utilized, which is outlined in the AASHTO standard designation T240. The RTFO method involves subjecting the asphalt binder to elevated temperatures and replicating the aging process during manufacturing and

placement. Furthermore, the RTFO provides a quantitative measure of the volatiles that are lost during the aging process.

The fundamental procedure for RTFO, which is shown in Figure 3.13, involves placing unaged asphalt binder samples into cylindrical glass bottles and mounting these bottles in a rotating carriage within an oven. The carriage then rotates within the oven for a period of 85 minutes while the temperature is maintained at 163°C (325°F) to facilitate the aging of the samples. Following the aging process, the samples are either subjected to physical properties testing or further processed with the pressure aging vessel (PAV).

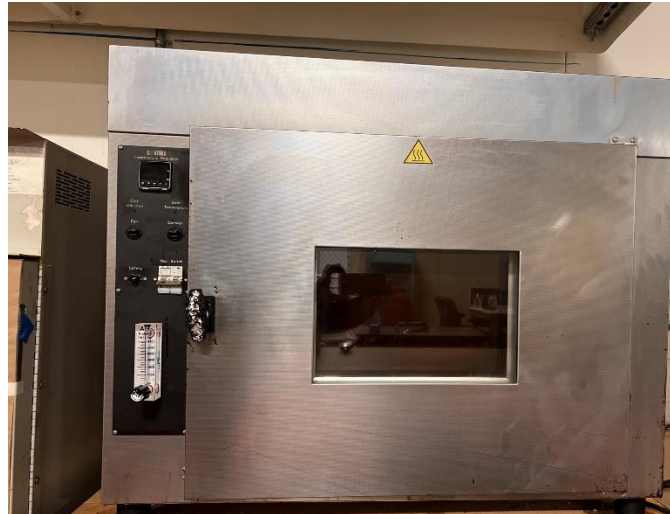


**Figure 3.13: Rolling Thin Film Oven (RTFO)**

### **Pressure Aging Vessel (PAV)**

In addition to short-term aging, the Superpave® PG binder specifications also consider long-term aging of the asphalt binder for testing at intermediate and low temperatures to determine the fatigue and thermal damage resistance, respectively. AASHTO standard R28 describes a method in which RTFO-aged asphalt binder is subjected to heat and pressure to simulate in-service aging over a period of 7 to 10 years in the pressure aging vessel (PAV) unit. The basic PAV procedure, as

illustrated in Figure 3.14, involves further aging of the RTFO-processed asphalt binder samples by placing them into stainless steel pans and subjecting them to a heated vessel that is pressurized to 305 psi (2.10 MPa or 20.7 atmospheres) for 20 hours. The heating temperature depends on the climate for which the asphalt binder will be used and typically ranges from 90°C to 110°C. After the process is complete, the final material is degassed for 30 minutes in a vacuum oven at 170°C. The samples are then stored for performance testing.



**Figure 3.14: Pressure Aging Vessel (PAV)**

### **3.2.3 Brookfield Rotational Viscometer (RV)**

Under the Superpave® testing protocol, the Rotational Viscometer (Figure 3.15) was utilized to determine the asphalt viscosity at high construction temperatures (above 100°C). As the behavior of most asphalt binders is predominantly viscous at such high temperatures, a measurement of viscosity suffices to represent the workability of the asphalt.

The determination of the viscosity of the asphalt binder at high construction temperatures (above 100°C) is an important parameter for evaluating its workability during the production of HMA. The ASTM D4402 standard describes the measurement of the resistance to rotation of a rotating spindle in a thermostatically controlled sample holder containing the asphalt binder. The torque and speed of rotation are then used to estimate the viscosity of the asphalt in units of Pascal seconds (Pa.s), miliPascal seconds (mPa.s) or centipoises (cP). The viscoelastic behavior of asphalt is influenced by both temperature and load, with higher temperatures resulting in more flowable (less viscous) material. Proper heating of asphalt binder to the appropriate temperature during HMA production is crucial for achieving the desired followability for proper mixing with aggregates, as well as ensuring that the resulting product can be easily handled, pumped, and compacted.

The Superpave® binder specifications set the viscosity limit for unfilled asphalt at a maximum of 3 Pa.s at 135°C. For the Rotational Viscometer (RV) test, the viscosity at 135°C is reported as the average of three readings. The viscosity of mastics was measured at 135°C using a #27 spindle, a type of spindle with specific dimensions and geometry used in the RV test. The schematic of the spindle is shown in Figure 3.16.

The test started with 30 minutes of conditioning of the specimen at the testing temperature. During the last 10 minutes of equilibrium, the spindle started to rotate at 20 rpm for 900 seconds. The viscosity measurements were taken every 300 seconds of testing, recording the average of the apparent viscosity to evaluate the effect of reactive powders and reference filler on mastics workability. Although mastics are known to be shear-dependent materials, the shear rate speed was kept at 20 rpm because it is the most commonly used shear rate in binder testing in accordance with Superpave® binder protocol. Work conducted under the NCHRP 9-45 found that the relative ranking of mastics did not change as a function of shear rate. (Bautista 2015).

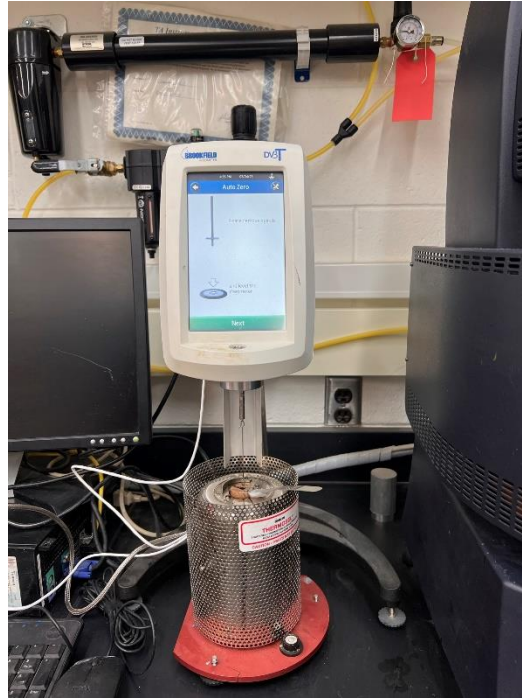


**Figure 3.15: Rotational Viscometer (RV)**

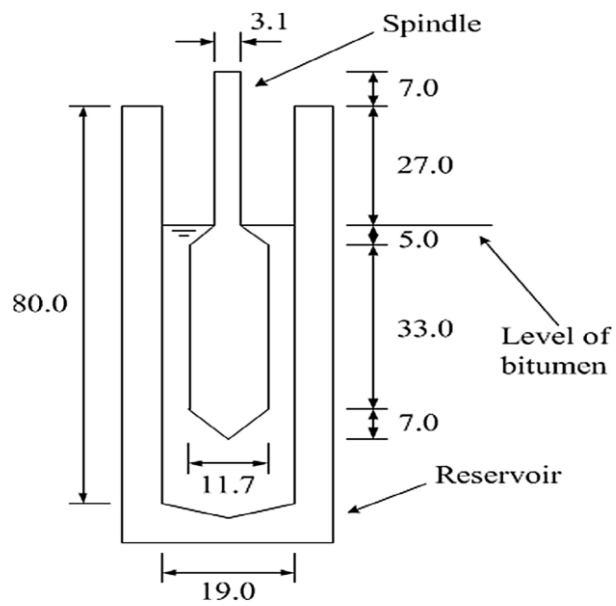


**Figure 3.16: Schematic of Spindle #27 in Viscosity Test (Dimensions are in mm) (Presti, Giancontieri et al. 2017)**

### 3.2.4 Dynamic Shear Rheometer (DSR)

#### Time Sweep

Viscoelastic materials can be characterized by subjecting them to dynamic testing using sinusoidal stress or strain loads. The resulting response strain or stress is typically sinusoidal, and a time lag between the stress and strain sinusoids is observed, referred to as the phase angle ( $\delta$ ). The dynamic shear rheometer (DSR) can measure a material's complex shear modulus ( $G^*$ ) and phase angle ( $\delta$ ). The  $G^*$  represents the total resistance of the sample to deformation under repeated shearing, while  $\delta$  represents the time lag between the applied shear stress and the resulting shear strain. This phenomenon is illustrated in Figure 3.17, where the time lag ( $\Delta t$ ) is equivalent to the observed phase angle.

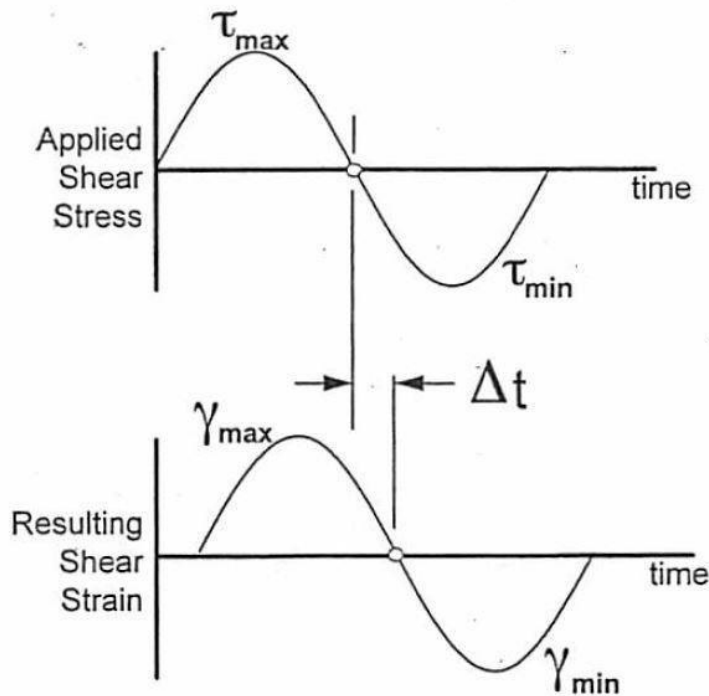


Figure 3.17: Stress-Strain Response of Viscoelastic Materials

For elastic materials, the stress/strain reaction to load is immediate resulting in the  $\delta = 0^\circ$ . For viscous materials, since the stress is proportional to the strain rate, the  $\delta = 90^\circ (\pi/2)$ . For viscoelastic materials, the  $\delta$  is in between  $0^\circ$  and  $90^\circ (\pi/2)$ .

The stress and strain function on Figure 3.17 can be expressed mathematically by:

$$\sigma(t) = \sigma_0 \sin(\omega t + \delta) \quad \text{Eq. 3.1}$$

$$\epsilon(t) = \epsilon_0 \sin(\omega t) \quad \text{Eq. 3.2}$$

where:

$\sigma_0$  = peak stress;

$\epsilon_0$  = peak strain ;

$\omega$  = frequency of loading, rad/s ;

T = period.

For analysis, the stress function can be broken into two functions of the same frequency, one in phase with the strain ( $\sin \omega t$ ) and another out of phase with the strain ( $\cos \omega t$ ) (Eq. 3.3).

$$\sigma(t) = \sigma_0 \sin \delta \cos \omega t + \sigma_0 \cos \delta \sin \omega t \quad \text{Eq. 3.3}$$

The function that is in phase ( $\sin \omega t$ ) represents the elastic component ( $\delta = 0^\circ$ ) and the function that is out of phase represents the viscous component ( $\delta = 90^\circ$ ). Since Hooke's Law is also applicable to shear stress ( $\tau$ ) and shear strain ( $\gamma$ ), Eq. 3.3 can be written as:

$$\tau(t) = \tau_0 \sin \delta \cos \omega t + \tau_0 \cos \delta \sin \omega t \quad \text{Eq. 3.4}$$

By dividing Eq. 3.4 by the shear strain ( $\gamma_0$ ), two dynamic moduli can be identified. One with the in-phase function called Shear Storage Modulus ( $G'$ ) (Eq. 3.5) and another with the out-phase function called Shear Loss Modulus ( $G''$ ) (Eq. 3.6).

$$G' = \frac{\tau_0 \cos \delta}{\gamma_0} \quad \text{Eq. 3.5}$$

$$G'' = \frac{\tau_0 \sin \delta}{\gamma_0} \quad \text{Eq. 3.6}$$

In viscoelastic materials, the Shear Storage Modulus ( $G'$ ) represents the elastic portion and it is a measure of the stored energy. On the other hand, the Shear Loss Modulus ( $G''$ ) represents the viscous portion and it is a measure of the energy dissipated as heat (Tao, Xiao et al. 2019).

Using trigonometry, it can be seen that:

$$\tan \delta = \frac{G''}{G'} \quad \text{Eq. 3.7}$$

The prime and double prime notation has its origin in complex numbers (Pahlavan, Hosseinnzhad et al. 2019).

In this way a Complex Shear Modulus ( $G^*$ ) can be defined as:

$$G^* = G' + iG'' \quad \text{Eq. 3.8}$$

Where  $G'$  is the real component and  $G''$  the imaginary component of the Complex Shear Modulus ( $G^*$ ).

The Complex Shear Modulus ( $G^*$ ) represents the stiffness of material for a specific frequency of loading and its graphical representation is reported in Figure 3.18. It is observed that the higher the time lag between the stress and strain ( $\delta$ ), the higher the  $G''$  is and the more viscous the material is. Then again, the smaller the time lag between the stress and strain ( $\delta$ ), the higher the  $G'$  is and the more elastic the material is.

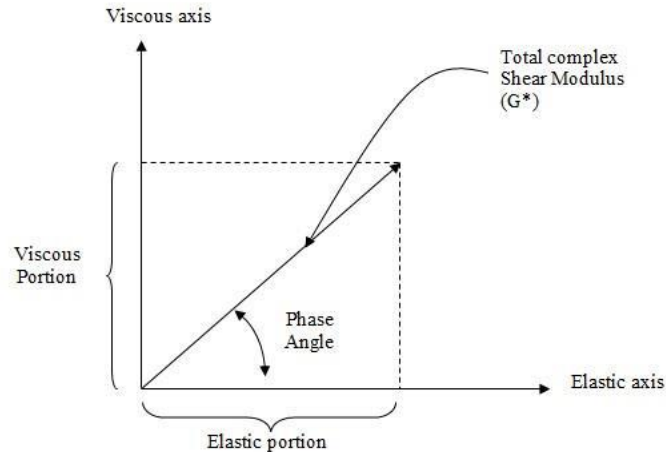


**Figure 3.18: : Complex Shear Modulus Representation**

To simulate the shearing action equivalent to a traffic speed of approximately 55 mph (90 km/h), an oscillation rate of 10 radians/second (1.59 Hz) was selected for the DSR testing. The resulting Complex Shear Modulus ( $G^*$ ) and phase angle ( $\delta$ ) are used as predictors of Hot Mix Asphalt (HMA) rutting and fatigue cracking. During the initial stages of pavement life, rutting is the primary concern, whereas fatigue cracking becomes the primary concern as the pavement ages.

The Superpave® system utilizes a rutting factor  $G^*/\sin(\delta)$  to evaluate the rutting resistance of asphalt cement under high pavement service temperatures. According to AASHTO M320, unaged asphalt cement tested under dynamic loading at maximum pavement service temperature must have a rutting factor of 1.00 kPa or greater. Conversely, when testing RTFO-aged asphalt binder under dynamic loading at the maximum pavement service temperature, the rutting factor must be 2.20 kPa or greater.

In a controlled strain test, the Superpave® defines the target strain level for unaged materials as 12%, which corresponds to the point at which the asphalt binder remains within the linear viscoelastic region. AASHTO T315 recommends a target strain level of 12% for unaged materials. However, as this study exclusively focuses on asphalt mastics, the target strain level for unaged asphalt binder was reduced to 5%.

The Superpave® system uses a fatigue factor  $G^*\sin(\delta)$  to evaluate the fatigue cracking resistance of the asphalt binder under intermediate pavement service temperatures. When RTFO and PAV-aged asphalt binders are tested under dynamic loading at the intermediate pavement service temperature, the maximum allowable fatigue factor is 5,000 kPa, according to Superpave®. The intermediate testing temperature depends on the specific asphalt binder used and is determined by calculating the average of the high and low Performance Grade (PG) temperatures, adding 4°C to the result, and then dividing it by two.

Similar to unaged materials, the target strain level for PAV-aged materials was reduced to 0.6% to ensure testing in the linear viscoelastic region for this research. According to AASHTO T325, the target strain value for PAV-aged asphalt binder is 1%. These strain levels were chosen based on limited experiments to ensure the linear viscoelastic response of the material.

### **Multiple Stress Creep and Recovery (MSCR)**

The multiple stress creep and recovery (MSCR) test, which utilizes the dynamic shear rheometer, is a relatively new addition to the Superpave® Performance Graded (PG) asphalt binder specification. This test, as per the AASHTO standard T350, is performed at high pavement service temperatures and is indicative of the asphalt binder's resistance to pavement damage caused by rutting. The MSCR test method evaluates asphalt binders based on their elastic recovery, toughness, and force ductility, making it a useful tool for characterizing binder performance.

The DSR test that measures the  $G^*/\sin(\delta)$  value is not sufficient to fully characterize the rutting resistance of polymer-modified binders. Therefore, it is often used in conjunction with another test to assess the deformation resistance and recovery influenced by the polymer modification (D'Angelo, 2009). This additional test involves the application of an initial conditioning load of 0.1 kPa for 1 second, followed by a 9-second recovery period, repeated for a total of 10 cycles.

Subsequently, a load of 3.2 kPa is applied for 1 second, followed by a 9-second recovery period, also repeated for 10 cycles (as shown in Figure 3.6). In this research, an additional load of 10 kPa was applied to supplement the standard 0.1 kPa and 3.2 kPa sequence. This test is performed on samples aged using the rolling thin film oven (RTFO) method at a high Performance Grade (PG) temperature.

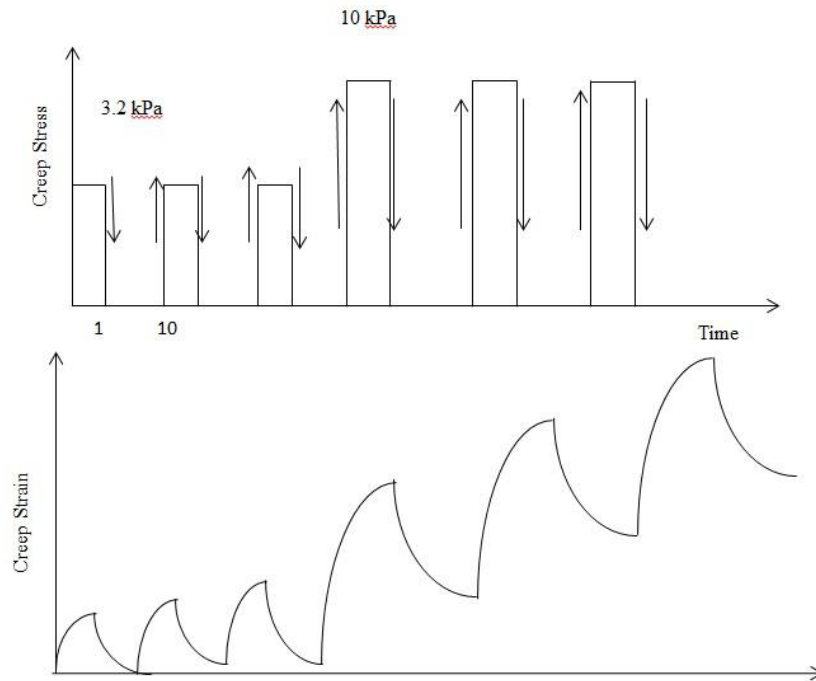


**Figure 3.19: Multiple Stress Creep and Recovery Test Principle**

The method for calculating the non-recoverable creep compliance ( $J_{nr}$ ), which is the inverse of complex modulus, is illustrated in Figure 3.20. The percent recovery is then determined by computing the strain values obtained from Figure 3.21. Recent studies have indicated a strong correlation between  $J_{nr}$  and pavement rutting. Specifically, as the stiffness of the asphalt binder increases, the value of  $J_{nr}$  decreases while the percent recovery increases (Fini, Hajikarimi et al. 2016).

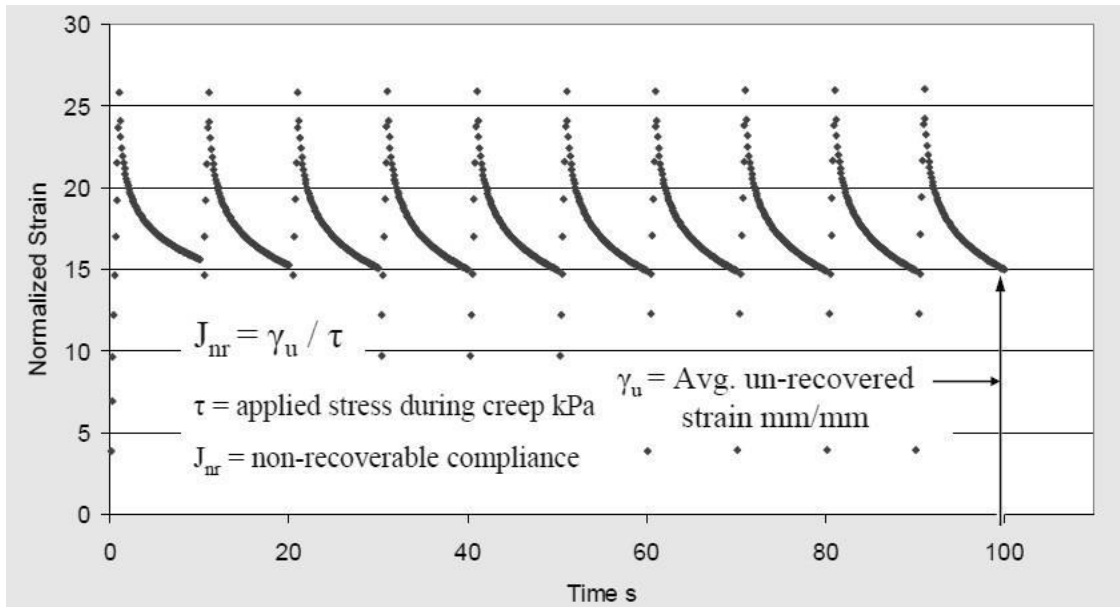


Figure 3.20: Plot Showing Determination of  $J_{nr}$  from MSCR Test (D'Angelo 2009)

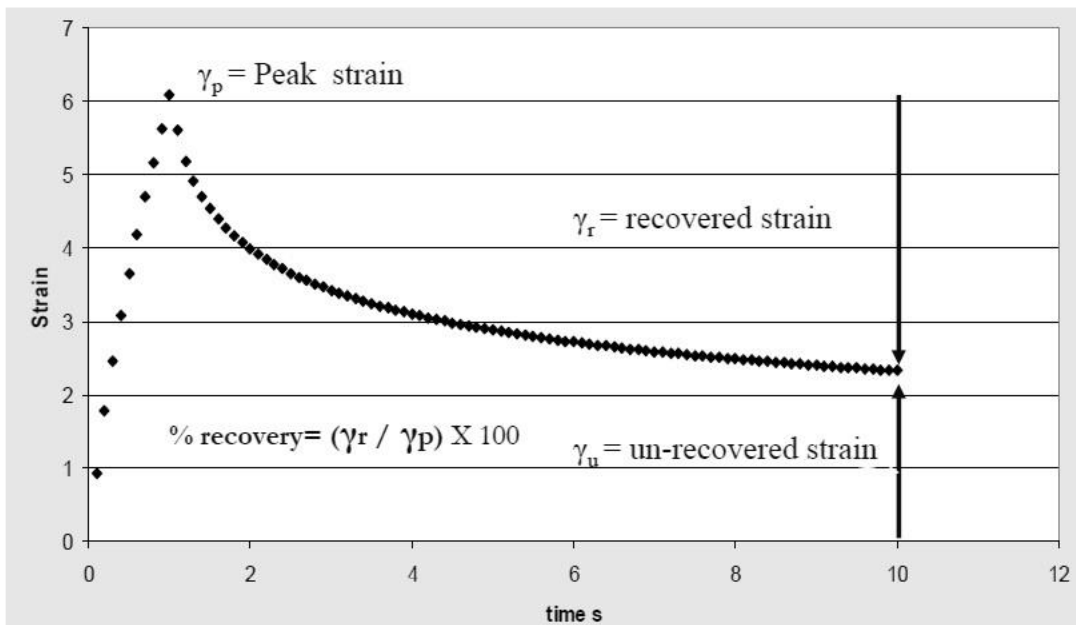
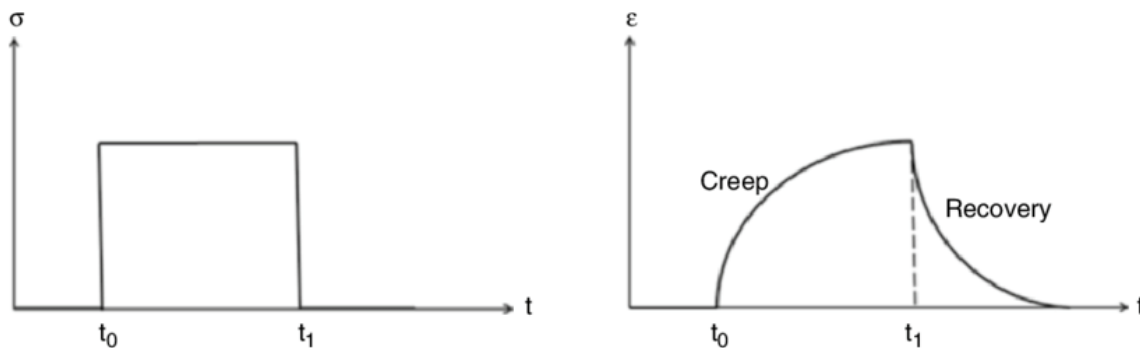


Figure 3.21: Plot Showing Determination of % Recovery from MSCR Test (D'Angelo 2009)

### 3.2.5 Bending Beam Rheometer (BBR)

The Superpave® system employs two parameters, namely the creep stiffness  $S(t)$  and the slope of the creep stiffness (m-value), to evaluate the thermal cracking resistance of asphalt cement under low pavement service temperatures. Creep is a phenomenon where a material undergoes a gradual deformation under constant stress. In a creep test, the stress is suddenly increased from 0 to  $\sigma_0$ , and the resulting strain  $\epsilon(t)$  is measured over time.

As reported in Figure 3.22, a typical creep response of a viscoelastic material can be demonstrated by the instantaneous deformation at  $t_0$  as soon as the stress is applied, then an increase in strain from  $t_0$  to  $t_1$  when the applied stress is continued and observed; once the stress has been removed the material responds with partial or total recovery (Lakes and Lakes 2009).



**Figure 3.22: Creep and Recovery Stress ( $\sigma$ ) and Strain ( $\epsilon$ ) Versus Time ( $t$ )**

The bending beam rheometer (Figure 3.23) test was conducted according to the standard AASHTO T313. Low temperature cracking is generally found in older, brittle pavements; therefore, the test is performed on the long-term aged material, after pressure aging vessel (PAV). When asphalt binder aged in the RTFO and PAV is tested under the creep loading at low pavement service temperature, the creep stiffness  $S(t)$  is calculated using the Bernoulli beam classic theory as a function of time, sample geometry and deflection (Eq. 3.9).

$$S(t) = \frac{PL^3}{4bh^3\delta(t)} \quad \text{Eq. 3.9}$$

where:

$S(t)$  = creep stiffness (MPa) at time  $t$ ;

$P$  = applied constant load, (N);

$L$  = distance between beam supports, 102 mm;  $b$  = beam width, 12.5 mm;

$h$  = beam thickness, 6.25 mm;

$\delta(t)$  = deflection (mm) at time,  $t$ .

In accordance with Superpave® methodology, the maximum allowable value for creep stiffness  $S(t)$  in asphalt binders is 300 MPa. Additionally, the slope of the creep stiffness, or  $m$ -value, is calculated to evaluate the relaxation behavior of asphalt binders at low temperatures, and it must be no less than 0.300. The Superpave® standard requires reporting the stiffness value at 60 seconds, as this value is correlated with two hours of actual traffic loading, a significant factor leading to pavement cracking. To determine the response of the asphalt binder at the low PG temperature, the test is conducted at a temperature 10°C higher than the specified low PG temperature, and the time temperature superposition principle is applied. This approach results in shorter testing times (Xiao, Yao et al. 2018). Therefore, for PG58-28 the test was conducted at -18°C and for PG64-10 the test was conducted at 0°C.



**Figure 3.23: Bending Beam Rheometer**

### **3.2.6 Dynamic Mechanical Analysis (DMA)**

DMA has been widely used to evaluate the rheological performance of asphalt materials. In this study, DMA was used to evaluate the thermal cracking resistance of asphalt mastics. Despite rutting and fatigue cracking, thermal cracking is not associated with the applied load, particularly in cold climates. Thermal cracking occurs when asphalt shrinks, or contracts due to low temperatures, and the resulting tensile stresses within the layer exceed the tensile strength of the material, causing it to crack. Thermal cracking can occur from a single cycle of low temperatures or repeated freezing and thawing cycles.

To resist thermal cracking, proper asphalt binder selection is essential. Asphalt binders that are harder tend to perform poorly at low-temperature conditions, while excessively aged binders have inferior performance due to age-hardening originating from excessive oxidation. Therefore, mixtures should be designed with soft asphalt binders that are still sufficiently ductile upon aging to minimize the effects of low-temperature thermal cracking.

Researchers have recommended limiting asphalt binder stiffness values in Hot Mix Asphalt (HMA) mixtures to reduce the risk of thermal cracking. By carefully selecting and testing the binder, engineers can design asphalt pavements that are more resistant to thermal cracking, ensuring longer pavement life and lower maintenance costs.

The DMA test was conducted using a TA instrument DMA Q-800 apparatus (New Castle, DE, USA) and a dual cantilever loading clamp, as shown in Figure 3.24. First, the asphalt binders PG58-28 and PG64-10-based mastics were heated up for one hour. The PG58-28, PG64-10, and polymer-modified PG58-28-based mastics were heated to 135°C, and the polymer-modified PG64-10 binder was heated to 165°C. This was because polymer-modified PG64-10-based mastics had higher viscosity and required to be heated to higher temperatures to be poured into the mold. The molds for the specimens (size of 12.7 mm by 5.6 mm by 60 mm) were prepared by covering each side of the mold with a thin layer of petroleum jelly and then covering the mold with plastic strips. The plastic strips were then covered with another thin layer of petroleum jelly. After the conditioning time, the specimens were then tested using the Dynamic Mechanical Analysis machine. The testing included cooling the DMA to -18°C for PG58-28-based mastics and 0°C for PG64-10 using liquid nitrogen. The next step involved removing the specimen from the -18°C alcohol bath and putting the specimen into the apparatus using forceps. The apparatus was then closed and allowed to isotherm at -18°C for PG58-28-based mastics and 0°C for PG64-10-based mastics for 10 minutes. A force of 6 Newtons was then applied and ramped at 0.001 N/min. for a total of 5 minutes. This ensured conformance with the parameters set forth by BBR testing standard AASHTO T313. Duplicate specimens were tested for each mastic.



**Figure 3.24: DMA Machine and Cantilever Clamp (Wang, Wang et al. 2022)**

The creep compliance of a polymer, as defined in Equation 3.10, is the ratio of shear strain to shear stress, expressed in units of  $\text{Pa}^{-1}$ . This quantity provides a measure of the instantaneous and continuous flexural deformation of a material under static loading over time. The use of creep compliance as a metric allows for the characterization of the time-dependent deformation behavior of the polymer under study, which is critical for applications in which long-term mechanical stability is essential. It should be noted that the units of  $\text{Pa}^{-1}$  are commonly used in the field of materials science and engineering to express the ratio of stress to strain, and as such, are well-suited for the quantification of creep compliance.

$$J(t) = \frac{\gamma(t)}{\sigma} \quad \text{Eq. 3.10}$$

Creep compliance is mathematically the inverse of the material's shear complex modulus and can be considered a normalized strain (displacement) based on the applied stress. The creep behavior of elastic, viscous, and viscoelastic behavior is demonstrated in Figure 3.25.

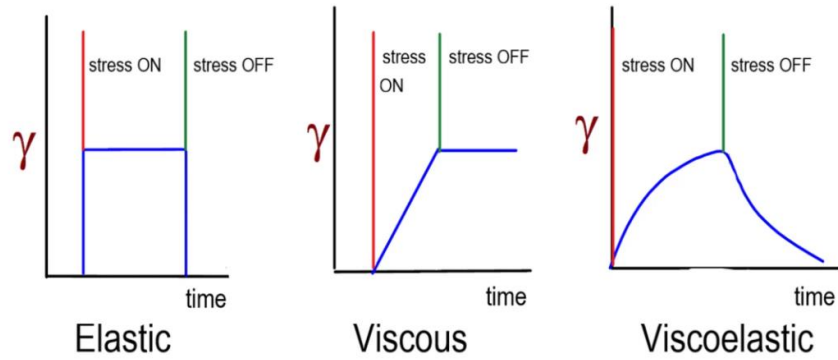


**Figure 3.25: Behavior of Different Materials Under Creep Testing**

As reported in Figure 3.25, the ideal elastic material recovers all the applied deformation after unloading. As elastic behavior is a desirable performance of asphalt mastics at low temperatures, a smaller creep compliance for a given mastic is satisfactory.

The relaxation modulus is a characteristic property of a viscoelastic material that describes how it responds to a sudden deformation, such as a step strain. It is defined as the ratio of the stress response to the strain input, over time, after the input has been removed. In other words, it is a measure of how much the material continues to deform over time after an initial deformation. The relaxation modulus is an important property of viscoelastic materials and is often used to characterize the material's behavior under various loading conditions. It is commonly denoted by  $G(t)$  and is reported in units of stress over strain, such as Pa or  $N/m^2$ . The higher amount of relaxation modulus for a given mastic under DMA testing is a desirable outcome at low temperatures.

### 3.3 SUPERPAVE® ASPHALT MIXTURE TESTING PROTOCOL

This section outlines the experimental testing plan for both the control asphalt mixtures and the mixtures containing reactive powders. The testing plan encompassed various performance indicators, including aggregate coating, workability, moisture damage resistance, and fatigue-cracking resistance. Table 3.5 provides an overview of the experimental testing plan for all asphalt mixtures. At least two samples were tested for each test, and the average results were reported. For the aggregate coating, workability, and aging comparison, nine replicates were produced and compared. On the other hand, for the moisture damage resistance and fatigue cracking resistance, two replicates were produced and tested. The experimental testing methods are discussed in detail in the subsequent sections.

**Table 3.5: Experimental Matrix for Asphalt Concrete Tests**

Test	Measured Indicator		Aging	Filler	Filler Dosage	Replicates per Test
Aggregate Coating	Asphalt Binder Film Thickness		Short-Term	PC + control with LS	Two replacement levels as defined by Phase I	3
Workability	Number of Gyration to Compact to 92% Gmm		Short-Term			3
			Long-Term			3
Moisture Damage	Tensile Strength Ratio	Dry Condition	Long-Term			2
		Saturated Condition <sup>+</sup>				2
Fatigue	Number of Cycles Drop in E* using IDT		Long-Term	2		

### 3.3.1 Mixture Preparation

This study employed two distinct types of mix designs: control mixtures without any fillers, and mixtures containing LS filler or PC reactive powder as 40% replacement of binder by volume. The control mixtures utilized a total added binder content of 6.1%. In contrast, the mixtures containing LS filler and PC reactive powder had a 40% (by volume) bitumen replacement, resulting in a reduction of the total added binder content to 3.5%. The aggregate quantities remained constant across all the mixtures to ensure a more equitable comparison among the three different mixture types. To produce Warm Mix Asphalt (WMA), all mixtures were modified with Evotherm, an asphalt additive by Ingevity®. The total mass of the mixtures and the added binder mass can be calculated using the following equations:

$$\text{Total Asphalt Mixture Mass} = \frac{\text{Aggregate Mass}}{1 - P_b} \quad \text{Eq. 3.11}$$

$$\text{Added Binder Mass } (P_b) = \left[ \frac{\text{Aggregate Mass}}{1 - P_b} \right] - \text{Aggregate Mass} \quad \text{Eq. 3.12}$$

Where:

Aggregate Mass = Total mass of aggregates ( in this experiment, 4700 g or 1500 g);

$P_b$  = added binder content.

The quantity of total mixture mass and binder content per batch was dependent on the specific test for which the mixtures were utilized. To calculate the bulk specific gravity ( $G_{mb}$ ) using ASTM D6857/D6857M-11 procedure, a total mass of 4700 g of aggregates was required for compaction. In contrast, to determine the maximum specific gravity ( $G_{mm}$ ) according to ASTM D6752/D6752M-11, only 1500 g of aggregates were necessary. These quantities are outlined in the respective procedures for each test.

## **Mixing Procedure**

Conforming to AASHTO T312-12, the asphalt mixing process adhered to a prescribed protocol. The initial step involved the precise weighing of all the constituents, followed by the thorough blending of the aggregates, which were subsequently heated to a specified temperature within an oven. For mixtures incorporating fillers, the LS and PC were introduced to the blended aggregates before heating. Mixing took place at 120°C, and compaction occurred at 115°C, except for polymer-modified PG64-10-based mixtures. Due to high viscosity, such mixtures were mixed at 150°C and compacted at 145°C. The compaction temperature was lower than the mixing temperature to replicate the temperature loss that occurs during delivery in real-world applications. The required amount of asphalt binder was also warmed to the mixing temperature. Once all the components reached the mixing temperature, the aggregates were deposited into a heated mixing container, and a concave depression was made at the center of the mixture. The required batch mass was attained by adding the precise amount of asphalt binder to the blend. The mixing container was then positioned in the Humboldt asphalt mixer and mixed for 3 minutes at a velocity of 60 revolutions per minute (RPMs). Upon completion of the mixing process, it was observed that all aggregates were evenly coated. It is pertinent to note that despite the fillers being considered as substitutes for asphalt binder, they were treated as aggregates during the mixing procedure (no premixing of fillers and bitumen).

### **3.3.2 Aging Procedures**

#### **Short-Term Aging**

The short-term aging conditioning process was conducted according to the guidelines outlined in AASHTO R30-02. The primary objective of this process is to replicate the effects of producing, placing, and compacting asphalt mixtures in the short term. The process involved spreading the

loose mixture of aggregates and asphalt binder evenly in a pan to achieve a thickness ranging from 25 to 50 mm. Subsequently, the mixture was placed in a forced-draft oven for 2 hours  $\pm$  5 minutes at a temperature equivalent to the compaction temperature of the mixture  $\pm$  3°C to simulate short-term aging. Stirring was performed after 60  $\pm$  5 minutes to ensure uniform conditioning. Following the completion of the 2-hour  $\pm$  5-minute period, the mixture was removed from the forced-draft oven and ready for compaction.

### **Long-Term Aging**

To evaluate the long-term aging effects on the asphalt mixtures, the AASHTO R30-02 standard and methods established by Elwardany et al (Elwardany, Yousefi Rad et al. 2017). can evaluate the effects of aging on the asphalt mixtures using either compacted specimens or loose mixtures, and are designed to simulate a 5 to 10-year aging process. After undergoing the short-term aging process, the mixtures were subjected to a force-draft oven for 24 hours at a temperature of 115°C, which corresponded to the compaction temperature. Subsequent to the 24-hour duration, the specimens were available for compaction and subsequent testing.

### **3.3.3 Asphalt Mixture Volumetric**

#### **Aggregate Volumetrics**

The evaluation of asphalt mixtures requires a thorough knowledge of numerous volumetric parameters associated with aggregates and binders. These parameters play a vital role in the assessment of asphalt mixtures. The basic calculation of aggregate volumetrics is reported in Figure 3.26.

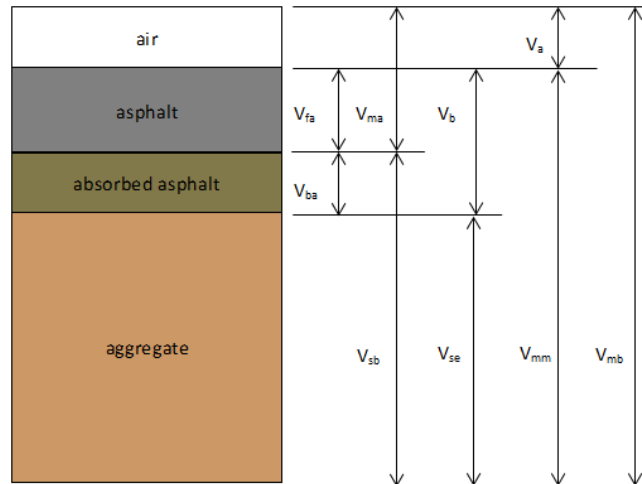


**Figure 3.26: Component Diagram of Compacted HMA Specimen (Asphalt Institute 2001)**

% VMA = Volume of voids in mineral aggregate;

%  $V_{mb}$  = Bulk volume of compacted mix;

%  $V_{mm}$  = Voidless volume of paving mix;

% VFA = Volume of voids filled with asphalt;

%  $V_a$  = Volume of air voids;

%  $V_b$  = Volume of asphalt;

%  $V_{ba}$  = Volume of absorbed asphalt;

%  $V_{sb}$  = Volume of mineral aggregate (by bulk specific gravity);

%  $V_{se}$  = Volume of mineral aggregate (by effective specific gravity).

Asphalt mixtures comprise aggregates that are capable of absorbing both water and asphalt binder. The assessment of the interaction between the aggregates and binder is dependent on several critical factors, including the quantity of voids present in the mineral aggregates, the amount of air voids in the mixture, and the volume of voids that are filled with asphalt. These

variables significantly influence the bonding strength, the thickness of the coating film, and the overall strength and durability of the mixture against moisture damage.

### **Determination of $G_{mm}$ and $G_{mb}$**

The determination of the maximum specific gravity ( $G_{mm}$ ) of the asphalt mixtures was carried out by employing the ASTM D6857/D6857M-11 procedure, which utilized a vacuum-sealed material method. Similarly, the bulk specific gravity ( $G_{mb}$ ) of the mixtures was determined in accordance with the ASTM D6752/D6752M-11 specification, also using a vacuum-sealed material method. To comply with the AASHTO R30-02 standard, the asphalt mixtures were heated and subsequently allowed to cool for  $16 \pm 1$  hour at room temperature prior to the commencement of the tests. The InistroTek CoreLok vacuum machine was utilized to conduct the tests.

To determine the maximum specific gravity, the loose samples were uniformly spread on a pan and the aggregates were carefully separated to ensure they were not fractured. The fine aggregate portion was broken down to ensure that the size of the aggregates did not exceed 6.3 mm. The bags containing the asphalt mixture were weighed, and the sample was then placed in the CoreLok machine. The machine was then operated to vacuum out the air, after which the sealed sample was submerged in water. The top of the bag was cut open to allow water to enter, and then the bags were manually opened to ensure complete water entry. The sample was weighed again, and the  $G_{mm}$  was calculated directly using the CoreLok computer program.

The bulk specific gravity ( $G_{mb}$ ) of asphalt mixtures was determined using the ASTM D6752/D6752M-11 specification and a vacuum sealed material method. After heating the mixtures, the samples were allowed to cool at room temperature for  $16 \pm 1$  hour, following the AASHTO R30-02 standard. Subsequently, the compacted sample was weighed and placed in a bag, which was then inserted into the CoreLok machine to remove air from the chamber and bag.

Once the test was completed, the sealed sample was taken out of the CoreLok machine and weighed underwater, with the weight being recorded once the scale had stabilized. To ensure that no water had entered the bag while it was submerged, the sample was weighed again, without the bag, out of the water. Finally, the CoreLok computer program was used to calculate  $G_{mb}$  directly using the collected data.

Using the  $G_{mm}$  and  $G_{mb}$  values, the  $\%G_{mm}$  could be calculated using the following equation. It is essential to note that 100% minus the  $\%G_{mm}$  is the percentage of air in the mixture.

$$\%G_{mm} = \frac{G_{mb}}{G_{mm}} \frac{h_m}{h_x} * 100 \quad \text{Eq. 3.13}$$

$$\%V_a = 100 - \%G_{mm} \quad \text{Eq. 3.14}$$

where:

$\%G_{mm}$  = corrected relative density expressed as a percent of the maximum theoretical specific gravity;

$G_{mb}$  = bulk specific gravity of the extruded specimen;

$G_{mm}$  = max specific gravity of the of the mix;

$h_m$  = height of the extruded specimen (mm);

$h_x$  = height of the specimen after x gyrations (mm).

$\%V_a$  = Air content percent within the asphalt mixture

### 3.3.4 Workability

The compaction effort required to densify the mixtures was measured using the Superpave® Gyratory Compactor, and the densification curve was used to determine the  $\%G_{mm}$  and  $\%V_a$  values. The  $\%G_{mm}$  value represents the maximum theoretical specific gravity that can be achieved through compaction, while the  $\%V_a$  value represents the voids in the compacted mixture. Higher  $\%G_{mm}$  values and lower  $\%V_a$  values indicate better workability performance. The study aimed to

assess the compatibility of the hybrid reactive powder mixtures by comparing their workability performance to that of the LS-based mixtures and short-term aged control mixtures. The reduction in workability was considered desirable if the hybrid reactive powder mixtures demonstrated higher % $G_{mm}$  values, indicating a more challenging compaction process.

The Superpave® Gyratory Compactor (SGC) is a laboratory compaction device used to prepare asphalt samples for testing. It was developed by the Strategic Highway Research Program (SHRP) to meet several objectives, including producing samples with realistic densities, accommodating larger aggregate sizes, and evaluating compaction problems.

The SGC uses a vertically applied pressure and an angle of gyration to compact the asphalt sample over time. The machine, which is shown in Figure 3.27, applies pressure to the sample through a series of compaction cycles, during which the mold containing the sample is rotated around its axis at a specific angle of gyration. The height of the sample is measured during each compaction cycle, allowing for the determination of the specimen height over time.

The resulting densification curve provides information on the compaction characteristics of the asphalt mixture, including the maximum specific gravity ( $G_{mm}$ ) and the percent air voids (% $V_a$ ). The SGC is commonly used in the development and testing of asphalt mixtures to ensure that they meet specific performance requirements for use in pavement construction.



**Figure 3.27: Superpave® Gyratory Compactor**

The Superpave® Gyratory Compactor (SGC) is a specialized equipment used in asphalt compaction testing. The SGC comprises a rotating base that is inclined at an angle of 1.25 degrees and rotates at a rate of 30 gyrations per minute. The compaction mold, as demonstrated in Figure 3.28, has a diameter of 150 mm, and the loading system applies 600 kPa of compaction pressure on the specimen while the base and compaction mold rotate. The device is connected to a computer program that records various parameters, including the gyration number, angle, pressure (kPa), and specimen height (mm). The specimen height is essential to measure since it enables the calculation of material density. Additionally, the percentage of air in the material after compaction can be calculated from these values, which is a critical characteristic in the context of asphalt pavement.

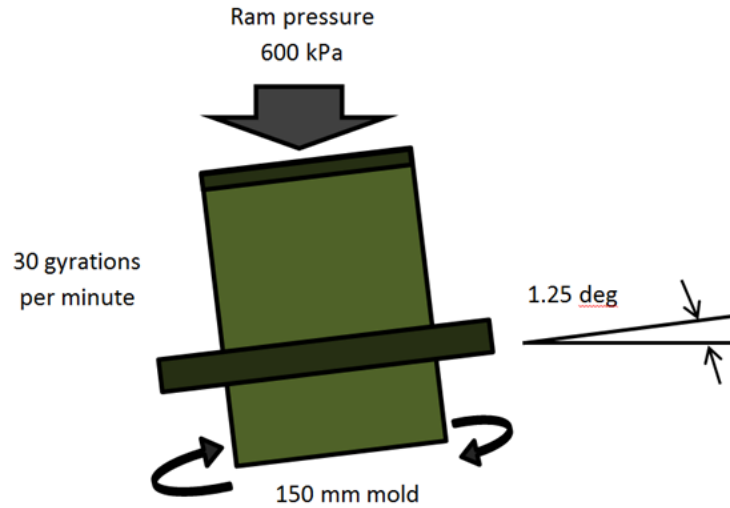


**Figure 3.28: Superpave® Gyratory Compactor Mold**

Asphalt mixtures are formulated to meet specific compaction requirements, and the number of gyrations required to achieve the appropriate amount of air voids can be directly linked to the compaction effort when utilizing a Superpave® Gyratory Compactor (SGC). In the Superpave® system, these variables are commonly expressed as the design number of gyrations ( $N_{des}$ ), which signifies the number of gyrations necessary to attain the designated compaction level and asphalt density expected in the field after being exposed to the projected amount of traffic. Typically, after  $N_{des}$  gyrations, the compacted asphalt specimen will possess approximately 4% air voids.

Aside from  $N_{des}$ , other gyrations levels of importance in asphalt mixture design are  $N_{ini}$  and  $N_{max}$ .  $N_{ini}$  represents the initial number of gyrations and provides a measure of mixture compatibility. Tender mixtures, which compact too quickly, are generally undesirable. At  $N_{ini}$ , the compacted specimen typically contains around 11% air voids.  $N_{max}$ , on the other hand, represents the maximum number of gyrations that should produce a density that should never be exceeded in the field. At  $N_{max}$ , the number of air voids in the compacted specimen should generally be less than 2%. Mixtures with air voids of less than 2% are typically more susceptible to rutting and fracture.

All values of  $N_{ini}$ ,  $N_{des}$ , and  $N_{max}$  are utilized in the design process as a function of traffic levels. The traffic levels are represented by the design equivalent single axel loads (ESALs).

Estimating the number of wheel/axle loads a pavement will endure during its lifetime can be a difficult undertaking. These cyclic loading and unloading forces can have adverse effects on the pavement structure, making it imperative to have an accurate assessment of the traffic loads when evaluating pavement design. To this end, Equivalent Single Axle Loads (ESALs) are frequently used to convert daily traffic loads into magnitudes and repetitions representing a standard number of equivalent loads. An 80.0 kN standard axle load is commonly utilized to predict the pavement's performance over its service life.

The air void content in asphalt mixtures is typically assessed through  $\%G_{mm}$ , which represents the corrected relative density as a percentage of the maximum theoretical specific gravity. Densification curves usually depict  $\%G_{mm}$  on the y-axis and the number of gyrations on the x-axis, as exemplified in Figure 3.29. It is noteworthy that the air void percentage ( $\%V_a$ ) can be computed as 100% minus  $\%G_{mm}$  at any given point on the curve. To achieve a 4% air void content, for example,  $\%G_{mm}$  would need to be 96%. The densification curve facilitates the identification of certain points, such as  $N_{ini}$ ,  $N_{des}$ , and  $N_{max}$ , by locating them on the plot.

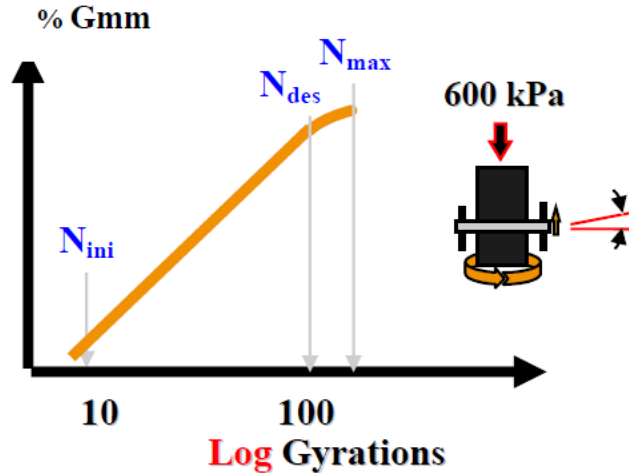


**Figure 3.29: Maximum Theoretical Specific Gravity vs. Number of Gyration (Faheem, Hanz et al. 2008)**

Table 3.6 further summarizes the Superpave® compaction efforts and  $N_{des}$  characteristic values for different roadway applications.

**Table 3.6: Superpave® Gyratory Compaction Parameters for Different Roadway Applications**

Deign ESALs (millions)	Compaction Parameters			Typical Roadway Applications
	$N_{ini}$	$N_{des}$	$N_{max}$	
< 0.3	6	50	75	Very light traffic (local/county roads, city streets where truck traffic is prohibited)
0.3 to <3	7	75	115	Medium Traffic (collector roads; mostly county roadways)
3 to <30	8	100	160	Medium to high traffic (city streets; state routes; US highways; some rural interstates)
$\geq 30$	9	125	205	High traffic (most of the interstate system; climbing lanes; truck weighing stations)

The compaction was performed using a Pine Co. Superpave Gyratory Compactor (SGC) in accordance with the AASHTO T312-12 procedure. The compaction mold and base plate were preheated for at least 30 minutes at the required compaction temperature, which was 115°C for the

mixtures based on PG58-28 and polymer-modified PG58-28 binders and 145°C for the mixtures based on polymer-modified PG64-10 binder.

To determine the bulk specific gravity, approximately 4,700 g of asphalt material was used for compaction. Additionally, 1,500 g of the same material was used in a loose mixture to determine the maximum specific gravity. The material was placed into the mold in a single lift and leveled with paper disks on top and bottom.

The compactor applied a pressure of  $600 \pm 18$  kPa to the specimen at an angle of 1.25° while the rotating base spun at a constant 30 gyrations per minute. During each gyration, the Superpave Gyratory Compactor recorded the height, pressure, and angle of the compacted sample, which were used to develop the compaction densification curve. The compaction parameters used in this study are consistent with typical roadway applications, with varying parameters depending on the anticipated traffic levels.

The study employed 115 gyrations to comprehensively analyze the workability of the mixtures. After the compaction was completed, the mold angle and ram pressure were removed, and the ram was retracted from the mold. The specimens were then extruded from the mold, and the paper disks were removed using the same procedure for the duplicate sample. The compacted specimen was crucial for evaluating the bulk specific gravity, while the loose mixture was significant in determining the maximum specific gravity.

### **3.3.5 Aggregate Coating**

The evaluation of aggregate coating in the study involved physical observations and calculated parameters. Comparative photographs were taken to assess the coating quality between the control and hybrid samples. As the total binder content for the control mixtures was higher (6.1%) than

that for the hybrid powder mixtures (3.5%), it was important to examine the aggregate coating to ensure optimal long-term performance.

The thickness of the asphalt film on the aggregate particles is influenced by various factors such as the percentage of asphalt binder, diameter, particle size distribution, and surface area of the aggregate particles. When the average diameter of the aggregate particle decreases, the surface area increases, resulting in a decrease in asphalt film thickness. The surface area factors provided in Table 3.7 can be used to estimate the total aggregate surface area in a given asphalt mixture. This method assumes that all particles are rounded, which provides a suitable approximation. To calculate the surface area, the surface area factor is multiplied by the percent passing that specific sieve size. The resulting units are square feet per pound of aggregate, as stated by (Roberts, Kandhal et al. 1991).

**Table 3.7: Surface Area Factors for Different Aggregate Sizes**

Sieve Size	Surface Area Factors
Percent Passing Maximum Sieve Size	2
Percent Passing No. 4	2
Percent Passing No. 8	4
Percent Passing No. 16	8
Percent Passing No. 30	14
Percent Passing No. 50	30
Percent Passing No. 100	60
Percent Passing No. 200	160

After the surface area of the aggregates has been determined and converted to m<sup>2</sup>/kg, a volumetric analysis must be performed to determine the film thickness. The following equations outline the required calculations for determining the variables necessary to determine film thickness:

$$Total\ volume\ Pbv = \frac{(total\ weight\ of\ mixture) * (Pb)}{Gb} \quad Eq. 3.15$$

$$P_{ba} = \frac{G_{se}-G_{sb}}{G_{sb}*G_{se}} * G_b \quad \text{Eq. 3.16}$$

$$P_{baw} = (P_{ba})*(total\ weight\ of\ mixture*(1-P_b)) \quad \text{Eq. 3.17}$$

$$P_{bav} = \frac{\text{Weight of absorbed asphalt}}{G_b} \quad \text{Eq. 3.18}$$

$$P_{bev} = 100% * \frac{G_{se}-G_{sb}}{G_{sb}*G_{se}} * G_b \quad \text{Eq. 3.19}$$

where:

$P_{bv}$  = total volume of asphalt cement, by total mass of mixture (mL);

$P_b$  = asphalt content, by total mass of mixture;

$P_{ba}$  = absorbed asphalt content, by total mass of mixture;

$G_{se}$  = effective specific gravity of aggregate;

$G_{sb}$  = bulk specific gravity of aggregate;

$G_b$  = specific gravity of asphalt;

$P_{baw}$  = weight of absorbed mixture (g);

$P_{bav}$  = volume of absorbed asphalt (mL);

$P_{bev}$  = effective volume of asphalt (mL);

After these variables are determined, the film thickness can then be calculated using the

equation below:

$$T_F = 1000 * \frac{V_{asp}}{SA*W} \quad \text{Eq. 3.20}$$

where:

$T_F$  = Average film thickness (microns);

$V_{asp}$  = Effective volume of asphalt cement (liters);

SA = Surface area of the aggregate ( $m^2$  per kg of aggregate);

W = weight of aggregate (kg).

It is imperative to comprehend that, in the estimation of surface area, units must be converted from square feet per pound to  $m^2$  per kg of aggregate when utilizing this equation. Upon converting the units, the equation can be applied to the given data.

### **3.3.6 Moisture Damage**

#### **Specimen Conditioning**

The testing protocol utilized in this study adheres to the guidelines outlined in the AASHTO T283-07 standard. Moisture damage, which arises from the detrimental effects of water or air on the adhesive bond between aggregate particles and the layer of asphalt binder, is a significant concern. It is essential that the compacted asphalt mixtures demonstrate sufficient resistance to this form of damage when saturated with water. To assess the ability of the asphalt mixtures to resist moisture damage, specimens were prepared and conditioned according to the prescribed methodology. In order to increase the reliability of the findings, two identical samples were examined for each experimental scenario.

Following long-term aging and compaction to 93%  $G_{mm}$ , the asphalt mixtures underwent core drilling and saw cutting to create specimens with a diameter of  $101.6 \pm 2.0$  mm and thickness of  $50.8 \pm 2.0$  mm. Core drilling and saw cutting were performed using standard protocols. Two

specimens were obtained from each compacted sample subsequent to core drilling and saw cutting. The specimens selected for each testing procedure were chosen at random from those obtained from the compacted cores.

During the testing procedure, the saturated and conditioned specimens were submerged in a water container such that there was at least 25 mm of water above the top surface and an additional 25 mm of water below the bottom surface. To lift the specimen off the base of the water container, a perforated spacer was employed. Subsequently, using the Instron Corelok machine, the samples underwent vacuuming in order to extract any remaining air from the specimen. Following the completion of the vacuum cycle, the specimens were left submerged in the water bath for a period of approximately 5 to 10 minutes. After this time interval had elapsed, the specimens were removed from the water bath, and the degree of saturation ( $S'$ ) was determined through the application of the following equations:

$$S' = \frac{100*J'}{V_a} \quad \text{Eq. 3.21}$$

$$V_a = \frac{P_a * E}{100} \quad \text{Eq. 3.22}$$

$$J' = B' - A \quad \text{Eq. 3.23}$$

where:

$V_a$  = volume of air voids ( $\text{cm}^3$ );

$P_a$  = air voids, (percent);

$E$  = volume of the specimen, ( $\text{cm}^3$ ).

$J'$  = volume of absorbed water, (mL);

$B'$  = mass of the saturated, surface-dry specimen after partial vacuum saturation, (g);

$A$  = mass of the dry specimen in air, (g).

According to the guidelines specified in AASHTO T283-07, all of the saturated and conditioned specimens must exhibit a degree of saturation that falls within the range of 70 to 80%. In cases where the degree of saturation is found to be lower than 70%, the specimen must undergo further vacuuming in order to increase the degree of saturation. Conversely, if the degree of saturation exceeds 80%, the specimen must be discarded due to excessive damage. The degree of saturation is of utmost importance since it provides an acceptable range within which the asphalt pavement is not excessively damaged yet still permits realistic water penetration.

Subsequent to the saturation of all specimens to ensure that their degree of saturation was within the prescribed range of 70 to 80%, specimens were immersed in a water bath at a temperature of  $25 \pm 0.5$  °C for a duration of  $2 \text{ h} \pm 10 \text{ min}$  with a minimum of 25 mm of water above the surface of the specimens. The specimens were then prepared for testing using the Indirect Tension Machine.

Post-saturation, the conditioned specimens were placed in a water bath at a temperature of  $60 \pm 1$  °C for a duration of  $24 \pm 1 \text{ h}$ , with the specimens submerged such that at least 25 mm of water was above the top surface of the asphalt specimens. After the completion of the  $24 \pm 1 \text{ h}$  period, the specimens were withdrawn from the water bath and transferred to a different water container maintained at a temperature of  $25 \pm 0.5$ °C for a period of  $2 \text{ h} \pm 10 \text{ min}$ , with at least 25 mm of water above the top surface of the specimens.

The precise control of temperature in the water bath was crucial in ensuring that the temperature of the specimens did not exceed  $25 \pm 0.5$ °C. After the completion of the prescribed procedure, the specimens were extracted from the water bath and subjected to testing using the indirect tensile (IDT) test.

### 3.3.7 Indirect Tensile (IDT) Test

In this study, the MTS 858 Mini Bionix II Machine was employed to assess the moisture damage resistance, as per the guidelines stipulated by ASTM D4123. The IDT test is designed to subject the specimen to a single compressive load, which acts parallel to the vertical plane of the specimen. As the vertical compressive load is applied to the specimen, horizontal tensile forces begin to develop, at a rate of 50 mm/min. (Figure 3.30). The loading strip required for a 101.6 mm diameter asphalt specimen was 12.7 mm thick, which ensured uniform loading conditions and a nearly uniform stress distribution.

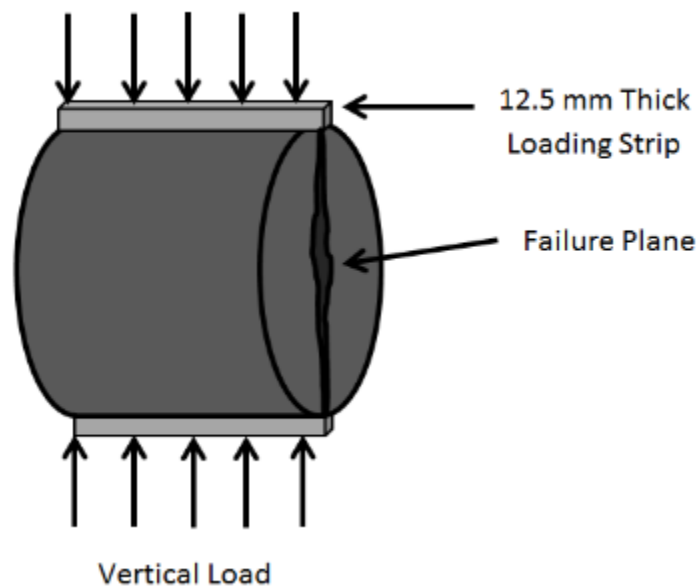


**Figure 3.30: Indirect Tension Test at Failure**

The IDT test provides a quick and reliable method to evaluate the moisture damage resistance and tensile strength properties of asphalt mixtures. The tensile strength ratio (TSR) is calculated by dividing the tensile strength of the conditioned specimen by the tensile strength of the vacuum-saturated specimen. The TSR value provides an indication of the asphalt mixture's ability to resist moisture damage, with a higher value indicating better performance.

In addition to TSR, the IDT can also measure the tensile strain at failure. This property is important because it helps predict the cracking potential of the asphalt mixture. Mixtures with higher tensile strain at failure are generally more resistant to cracking and are, therefore, more desirable for asphalt pavement applications. Overall, the IDT test is an important tool for evaluating the performance of asphalt mixtures and ensuring the long-term durability of asphalt pavements.

Equations for tensile stress and tensile strain have been developed (Hadley, Hudson et al. 1969) and are reported below:

$$\sigma_x = \frac{2P}{\pi dt} \quad \text{Eq. 3.24}$$

$$\sigma_y = \frac{6P}{\pi dt} \quad \text{Eq. 3.25}$$

where:

$\sigma_x$  = horizontal tensile stress at center of specimen, (MPa);

$\sigma_y$  = vertical tensile stress at center of specimen, (MPa);

P = applied load, (N);

d = diameter of specimen, (mm);

t = thickness of specimen, (mm).

$$\epsilon_f = 0.52x_t \quad \text{Eq. 3.26}$$

where:

$\epsilon_f$  = tensile strain at failure (mm/mm);

$x_t$  = horizontal deformation across the specimen (in.).

$$TSR = \frac{S_c}{S_s} \quad \text{Eq. 3.27}$$

where:

$S_c$  = average tensile strength of conditioned specimen (MPa);

$S_s$  = average tensile strength of saturated specimen (MPa).

The methods explained in this section were used to convert the loads and deflections to stresses and strains. Moisture damage resistance was also calculated, and evaluations of test data were performed.

### **3.3.8 Fatigue-Cracking Resistance**

To assess the resistance of the mixtures to fatigue cracking, fatigue testing was conducted. Fatigue cracking is caused by repeated loading occurring at intermediate temperatures, resulting in the gradual deterioration of asphalt pavement material over its life cycle. Fatigue cracking is primarily influenced by factors such as asphalt content, air void content, aggregate characteristics, temperature, and traffic. In addition, aging of the asphalt binder can result in stiffening and reduced fatigue resistance. Ideally, asphalt materials should exhibit a soft and elastic behavior when subjected to loading and unloading. Given that fatigue cracking is an unfavorable feature of asphalt pavements, evaluating this parameter and the potential impact of reactive powders was crucial.

Figure 3.31 illustrates a typical fatigue testing curve, with the horizontal axis representing the number of cycles and the vertical axis representing the displacement of the material. As demonstrated in Figure 3.31, various zones can be identified within this type of fatigue curve. Of particular importance for the present research are the secondary fatigue section and the point at which the tertiary fatigue section commences. During the secondary fatigue stage, the material

experiences constant cyclic loading, resulting in a constant rate of deformation. The slope of this line reflects the consistent deformation per cycle, which is crucial in demonstrating perfect elastic deformation over time. The tertiary section marks the point at which the material ultimately fails, and it was important to understand where this occurs ( $N_f$ ). Although the curve continues beyond the tertiary fatigue section, the material was considered to have failed once the tertiary fatigue section began.

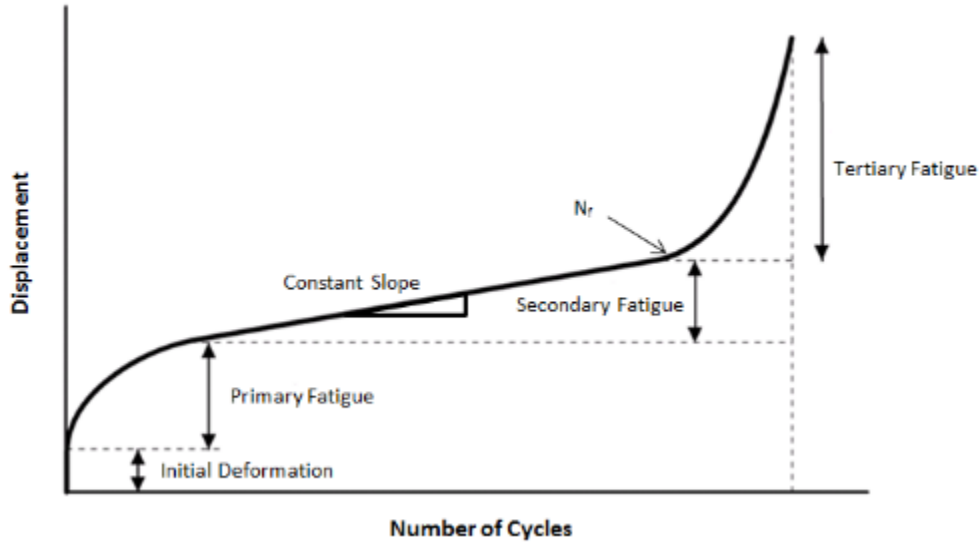


**Figure 3.31: Typical Fatigue Curve**

The complex modulus,  $E^*$ , is a measure of the storage and loss moduli of a viscoelastic material and is defined as a complex number that quantifies the relationship between the stress and strain.

This relationship can be mathematically described using the following equation:

$$E^* = E' + iE'' \tag{Eq. 3.28}$$

where:

$E$  = storage modulus or elastic component of the complex modulus (MPa);

$E''$  = loss modulus or the viscous component (MPa).

The complex modulus can also be determined by assessing the stress and strain rates at various locations. Specifically, the dynamic modulus can be determined by calculating the ratio of the stress amplitude to the strain rate observed during cyclic testing, expressed as:

$$E^* = \frac{\sigma_0}{\epsilon_0} \quad \text{Eq. 3.29}$$

where:

$\sigma_0$  = stress amplitude (MPa);

$\epsilon_0$  = strain-rate (mm/cycle).

During the cyclic testing, the amplitude of the load cycle (i.e., stress) remains constant, while the deformation (i.e., strain) varies. As a result,  $E^*$  remains constant over the secondary fatigue section, where the strain rate increases at a consistent rate. The number of cycles until  $E^*$  decreases in magnitude, represented by  $N_f$ , is, therefore, a critical parameter to evaluate, as it marks the onset of tertiary fatigue. Since  $E^*$  is a function of both stress and strain, the strain rate directly affects  $E^*$ , given that stress is held constant. As such, the final reduction in  $E^*$  can be attributed to the increasing strain rate (as it is the denominator of the function). When the tertiary fatigue section begins, the strain rate increases, resulting in a decrease in  $E^*$ . In this research,  $N_f$  is employed to determine the precise point at which  $E^*$  decreases.

The fatigue testing performed in this study was adapted from the methods outlined in AASHTO T322-03, AASHTO T342-11. The procedure involves the evaluation of fatigue using various parameters, including loading curve, temperature, load amplitude, and frequency of applied load. In this study, fatigue was assessed using a sine wave loading condition, a test temperature of  $20 \pm$

1°C, a 2% pre-loading condition, a 10% ultimate loading condition, and a frequency of 10 Hz (as depicted in Figure 3.32). Consistent loading conditions were employed for all specimens to enable direct comparison between the data. The loading conditions were calculated based on the ultimate loads obtained from the dry specimens tested in IDT test.

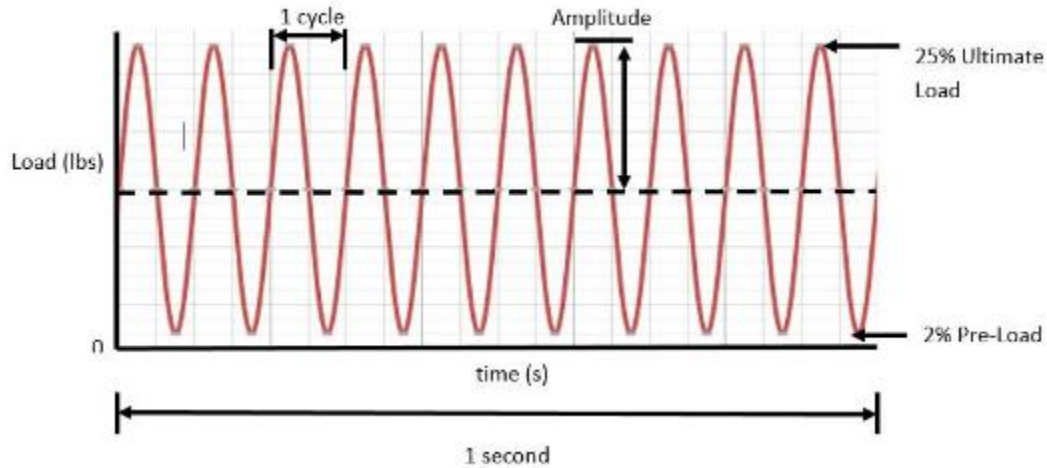


**Figure 3.32: 10 Hz Sine Wave Representation of Fatigue Test**

The cyclic loading condition to the specimen during the fatigue testing was represented by a sine wave. The equation used to represent the loading cycle is presented below:

$$y(t) = A \cdot \sin(2\pi f t + \varphi) \quad \text{Eq. 3.30}$$

where:

$A$  = Amplitude (peak from the reference line) (N);

$f$  = frequency (number of oscillations, or cycles, per second) (Hz);

$t$  = time (s);

$\varphi$  = phase (where the oscillation is at  $t = 0$ ) (radians).

The MTS 858 Mini Bionix II loading frame is a type of testing equipment commonly used to perform mechanical testing on materials. It is designed to apply different types of loads to a sample, such as compression, tension, and fatigue loading. The MTS 651 Environmental Chamber is an

accessory that is used to control the temperature and humidity of the testing environment. The chamber is connected to a temperature controller that ensures the temperature inside the chamber is accurate and stable throughout the testing process. The MTS data acquisition software is a computer program that is used to collect and analyze data from testing equipment. It allows the user to monitor the performance of the material being tested in real-time and to generate graphs and reports based on the collected data.



**Figure 3.33: MTS Environmental Chamber with IDT Testing Frame**

The specimens subjected to fatigue testing had a semicircular shape with dimensions of  $101.6 \pm 2.0$  mm in diameter and  $50.8 \pm 2.0$  mm in thickness, and duplicate specimens were tested. The testing procedure involved measuring both horizontal and vertical displacements, which constituted a crucial aspect of the testing process. The load applied and vertical displacement were

recorded directly from the testing frame of the MTS system. Upon loading, the specimen was subjected to testing according to a predefined protocol utilizing the MTS software.

## **CHAPTER 4: PERFORMANCE OF MASTICS**

Based on the characterization of the filler and the reactive powder, this chapter describes the performance of mastics (asphalt binder + filler) at high, medium, and low temperatures.

The fillers were added to a range of asphalt binders (HMA PG58-28, WMA PG58-28, HMA polymer-modified PG58-28, WMA polymer-modified PG 58-28, HMA PG64-10, WMA PG64-10, HMA polymer-modified PG64-10, and WMA polymer-modified PG64-10) at a concentration of 10 and 25% by volume of the binder replacement and compared with the response of the plain binders without fillers. The warm mix modification was performed by adding Evotherm by Ingevity®, used at 0.5% of binder mass. Evotherm is a warm mix modifier comprising approximately 60-70% alkyl acid phosphates and 30-40% modified tall oil fatty acids. The polymer modification of both PG58-28 and PG64-10 binders was performed by incorporating SBS D1101 cross-linked with PPA (polyphosphoric acid). It should be noted that polymer-modified PG58-28 was provided by an asphalt binder supplier, and, to match the performance of reference PG64-10, the polymer-modified PG64-10 binder was manufactured by the manufacturer's asphalt laboratory facility in the state of Wisconsin.

### **4.1 Self-Healing Characteristic**

Prior to the research based on an experimental matrix for mastics, the self-healing characteristics of cement-based mastics were investigated. To realize this objective, two mastics were fabricated, one based on 50% replacement of PG58-28 bitumen with reactive cement powder and the second based on 50% replacement of PG58-28 bitumen with a limestone filler. The mastics were then applied on a 5 mm x 5 mm limestone tile as a thin liquid layer at 115°C. When the thin layer was cooled and adhered to the surface of the tile at room temperature, the tile was quenched by liquid

nitrogen at  $-196^{\circ}\text{C}$  to induce a thermal cracking. The tiles were then placed in a curing room for three days. The curing room had a temperature of  $20 \pm 3^{\circ}\text{C}$  and a relative humidity of 90%. The tiles were then investigated under a scanning electron microscope (SEM). The SEM images revealed that the cement-based mastics are able to present moisture-induced self-healing properties and can “self-weld” these cracks with the hydration products of cement. On the other hand, the SEM images of the limestone-based mastic demonstrated that the cracks remained unfilled as the limestone powders are not reactive fillers. Figures 4.1 and 4.2 report the SEM images taken from cement-based and limestone-based mastics, respectively. The results from this test are promising, since proving that using cement as a reactive powder in asphalt mixtures can lead not only to cost reduction but also can produce a product that has a moisture-induced self-healing property, especially in colder and wet climates.

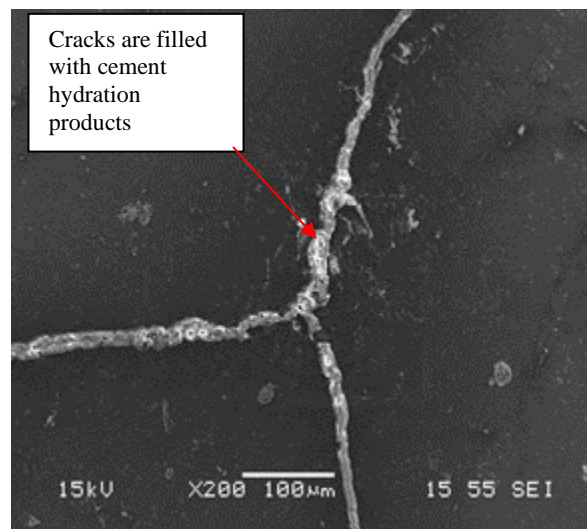


**Figure 4.1: SEM image of cement-based mastic after self-healing**



**Figure 4.2: Thermally-induced cracks in limestone-based mastics**

## **4.2 Constructability**

Workability was evaluated by comparing the viscosity of unaged mastics at high construction temperatures using the guidelines of ASTM D4402-12. The constructability of the asphalt mastic at a high temperature is an important parameter to evaluate as it corresponds to the workability efforts associated with aggregate coating, mixing, and compacting of asphalt mixtures (since the asphalt binder is completely viscous at these temperatures).

In this study, the viscosity was measured using a Brookfield Rotational Viscometer (RV) with a #27 spindle size at 135°C. The Superpave® testing protocol limits the viscosity for unfilled unaged binders to be less than 3.0 Pa-s. If the viscosity is above 3.0 Pa-s, the binder has a viscosity that is high and, therefore, there is a need for additional compaction effort and supplementary compaction energy. For this reason, lower values of viscosity at a specific temperature are desirable for compaction and workability as this helps to reduce the efforts for compaction.

Table 4.1 reports on the viscosity comparisons between the unaged HMA PG58-28 and WMA PG58-28 binders. As can be observed, a warm mix modification with only a 9% increase did not substantially affect the viscosity response of the binder.

**Table 4.1: Viscosity for Unaged HMA and WMA PG58-28 Binders at 135°C**

	PG58-28 (HMA)	PG58-28 (WMA)
Viscosity (Pa-s) $\leq$ 3.0 Pa-s	0.33	0.36

Table 4.2 indicates the measured viscosity for unaged HMA and WMA polymer-modified PG58-28 binders. Comparing the results with those reported for plain PG58-28 binders, it can be concluded that polymer modification results in an increase in the viscosity of the binder, yielding a more viscous material. However, the use of a WMA additive in polymer-modified systems helps to reduce the viscosity of these binders by 6%.

**Table 4.2: Viscosity for Unaged HMA and WMA Polymer-modified PG58-28 Binders at 135°C**

	Polymer-modified PG58-28 (HMA)	Polymer-modified PG58-28 (WMA)
Viscosity (Pa-s) $\leq$ 3.0 Pa-s	0.89	0.84

Table 4.3 reports the viscosity of unaged HMA and WMA PG64-10 binders. As reported in the table, warm mix modification did not change the viscosity of the binder.

**Table 4.3: Viscosity for Unaged HMA and WMA PG64-10 Binders at 135oC**

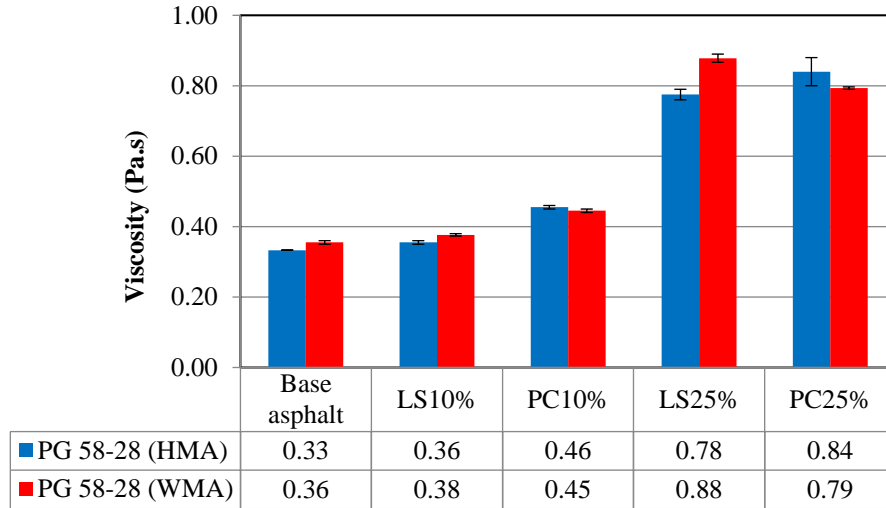
	PG64-10 (HMA)	PG64-10 (WMA)
Viscosity (Pa-s) $\leq$ 3.0 Pa-s	0.36	0.36

Table 4.4 indicates the measured quantities for the viscosity of HMA and WMA polymer-modified PG64-10 binders, which was increased by 4.5 times due to the polymer addition compared with the base binder. Here, the warm mix modification did not change the rheological response; however, the polymer modification itself increased the viscosity of PG64-10 significantly. This can be seen by comparing the results of Table 4.3 and Table 4.4.

**Table 4.4: Viscosity for Unaged HMA and WMA Polymer-modified PG64-10 Binders at 135oC**

	Polymer-modified PG64-10 (HMA)	Polymer-modified PG64-10 (WMA)
Viscosity (Pa-s) $\leq$ 3.0 Pa-s	1.96	1.95

Figures 4.3 and 4.4 report on the viscosity of the PG58-28 and polymer-modified PG58-28-based mastics. The results demonstrate that an increase in the filler content yields more viscous asphalt mastics. The increase in the viscosity of the mastics became more pronounced when 25% of the volume of the binder was replaced with fillers. Both PG58-28 and polymer-modified PG58-28-based mastics had viscosity below 3 Pa-s, the threshold in Superpave® specification (for plain bitumen). Further, it is observed that the viscosity of LS-based and PC-based mastics are similar for the same filler volume concentrations. Among plain mastics, WMA LS 25% PG58-28 was the most viscous mastic with 2.47 times higher viscosity compared with the unfilled HMA PG58-28 binder. In the case of polymer-modified mastics, HMA PC25% PG58-28 mastic had the highest viscosity, which was 2.62 times greater than that of the HMA polymer-modified PG58-28 binder. Furthermore, it can be noted that warm-mix modification resulted in a reduction in the viscosity of polymer-modified PG58-28-based mastics. For example, WMA polymer-modified PG58-28 mastic with 25% by volume replacement with LS and PC had 12% and 10% smaller viscosity than the corresponding HMA mastics, respectively.



**Figure 4.3: Viscosity for Unaged PG58-28 Mastics at 135°C**

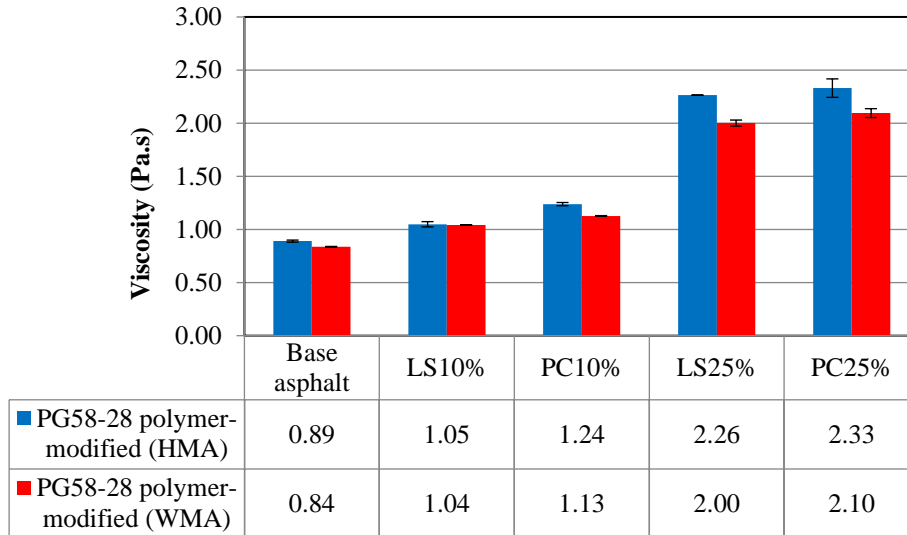


**Figure 4.4: Viscosity for Unaged Polymer-modified PG58-28 Mastics at 135°C**

Figures 4.5 and 4.6 demonstrate the measured viscosity of HMA and WMA PG64-10 and polymer-modified PG64-10-based mastics. As expected, the filler content had a significant effect on the viscosity of investigated mastics. All of the HMA and WMA PG64-10-based mastics had a viscosity smaller than 3 Pa-s, but HMA and WMA polymer-modified PG64-10 mastics passed the limit of Superpave® specification; when 25% of binder was replaced with fillers, which is

undesirable because the use of such mastics would need a higher effort for compaction. It is worth mentioning that Superpave® specifications are developed for unfilled binders, not for mastics, so having a mastic with a viscosity higher than specified as a criterion for viscosity, which cannot serve as a benchmark for acceptance of the mastic viscosity, is acceptable. Among the plain binders, HMA PC25% PG64-10 mastic was the most viscous mastic, experiencing a 297% increase in viscosity compared with the corresponding binder. Among the polymer-modified mastics, HMA LS25% polymer-modified PG64-10 mastic had the highest viscosity, which was 141% higher than HMA polymer-modified PG64-10 binder.

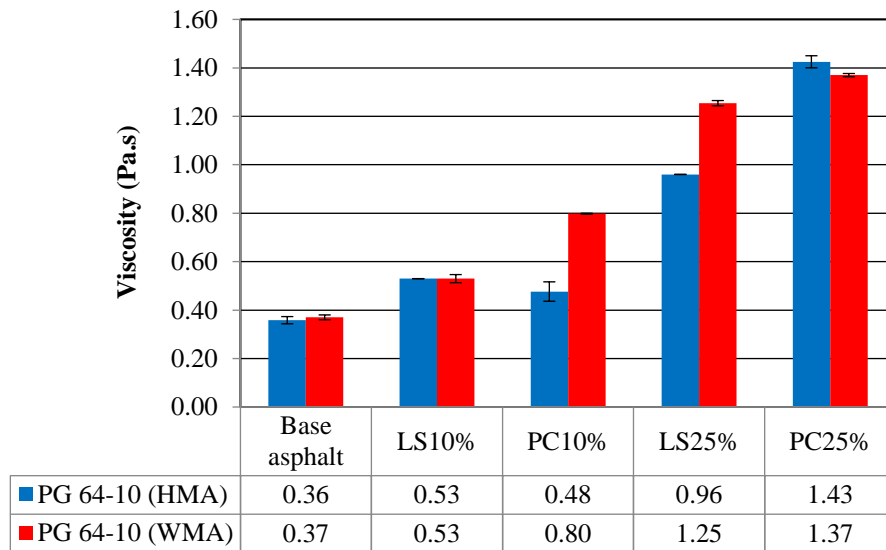


**Figure 4.5: Viscosity for Unaged PG64-10 Mastics at 135°C**

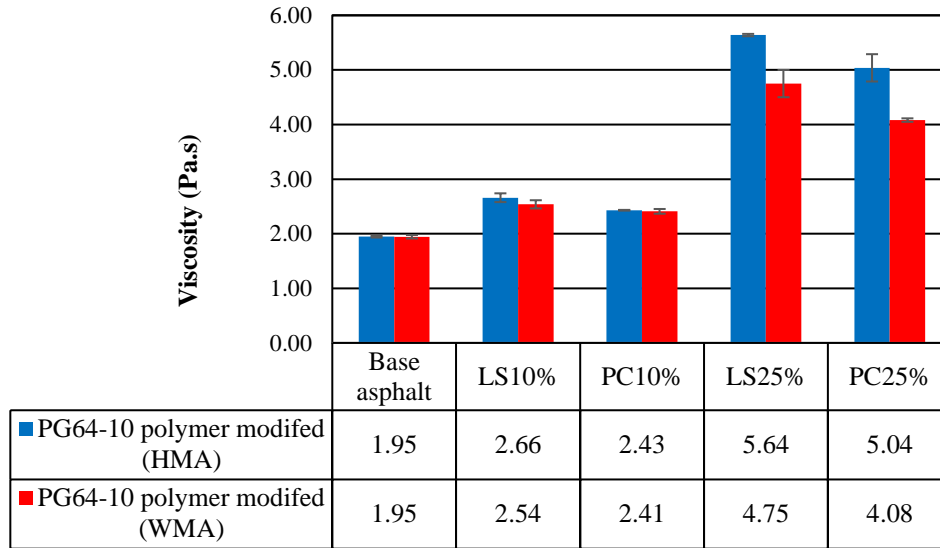


**Figure 4.6: Viscosity for Unaged Polymer-modified PG64-10 Mastics at 135°C**

### 4.3 Complex Shear Modulus ( $G^*$ )

The Dynamic Shear Rheometer (DSR) was used in accordance with AASHTO T315 to determine the specimen's response to shear and reporting on the complex shear modulus ( $G^*$ ) and the phase angle ( $\delta$ ) of mastics at high PG temperatures (58°C for PG58-28 and 64°C for PG64-10). The  $G^*$  is the measure of the total resistance of a material to shear deformation while the sample is repeatedly sheared and  $\delta$  is the phase angle between the recoverable and non-recoverable deformation. This section summarizes the results for unaged mastic testing, using DSR for all the mastics produced from the aforementioned asphalt binders.

Table 4.5 compares the results for  $G^*$  and  $\delta$  for unaged HMA PG58-28 and WMA PG58-28 asphalt binders. The results demonstrate that the WMA binder is stiffer than the HMA since the  $G^*$  is larger. However, the phase angle stays relatively the same regardless of the binder/modification type.

**Table 4.5: Complex Modulus and Phase Angle Results for Unaged PG58-28-based samples of HMA and WMA at 58°C**

	PG 58-28 (HMA)	PG58-28 (WMA)
Test Temp (°C)	58	58
$G^*$ (Pa)	1331	1438
Phase Angle	86.8	86.5

Table 4.6 reports the results for  $G^*$  and  $\delta$  for unaged HMA polymer-modified PG58-28 and WMA polymer-modified PG58-28 asphalt binders. The same trend as observed for PG58-28 binders can be reported, proving that the WMA binder is stiffer than the HMA binder and incorporation of a warm mix modifier does not change the phase angle.

**Table 4.6: Complex Modulus and Phase Angle Results for Unaged Polymer-modified PG58-28-based samples of HMA and WMA at 58°C**

	Polymer-modified PG 58-28 (HMA)	Polymer-modified PG58-28 (WMA)
Test Temp (°C)	58	58
$G^*$ (Pa)	2749	3033
Phase Angle	69.9	71

The results for  $G^*$  and  $\delta$  for unaged HMA PG64-10 and WMA PG64-10 asphalt binders are reported in Table 4.7. It can be noted that PG64-10 binders have lesser stiffness compared with PG58-28 binders due to lower  $G^*$  values. Also, the WMA and HMA binders have a very similar phase angle.

**Table 4.7: Complex Modulus and Phase Angle Results for Unaged PG64-10-based samples of HMA and WMA at 64°C**

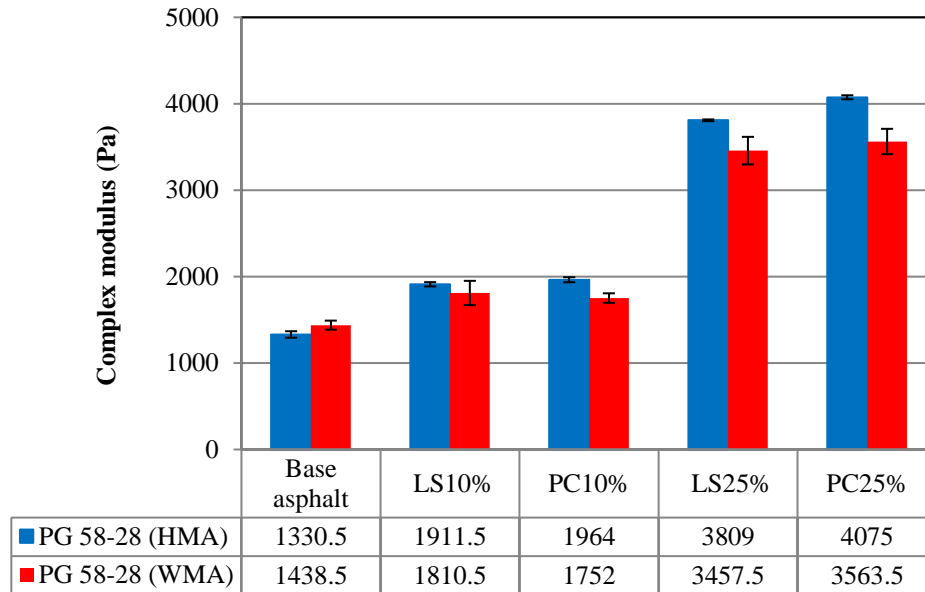
	PG 64-10 (HMA)	PG64-10 (WMA)
Test Temp (°C)	64	64
$G^*$ (Pa)	1055	969
Phase Angle	84.5	84.09

Table 4.8 reports the results for  $G^*$  and  $\delta$  for unaged HMA polymer-modified PG64-10 and WMA polymer-modified PG64-10 asphalt binders. Here, it can be observed that the polymer modification largely increased the stiffness of PG64-10 binders. As an example, HMA polymer-modified PG64-10 experienced a 229% increase in  $G^*$  value compared with HMA PG64-10. This can indicate the synergetic interaction between the type of polymer used and the WMA additive. However, the incorporation of the warm mix modifier did not change the phase angle drastically.

**Table 4.8: Complex Modulus and Phase Angle Results for Unaged Polymer-modified PG64-10-based samples of HMA and WMA at 64°C**

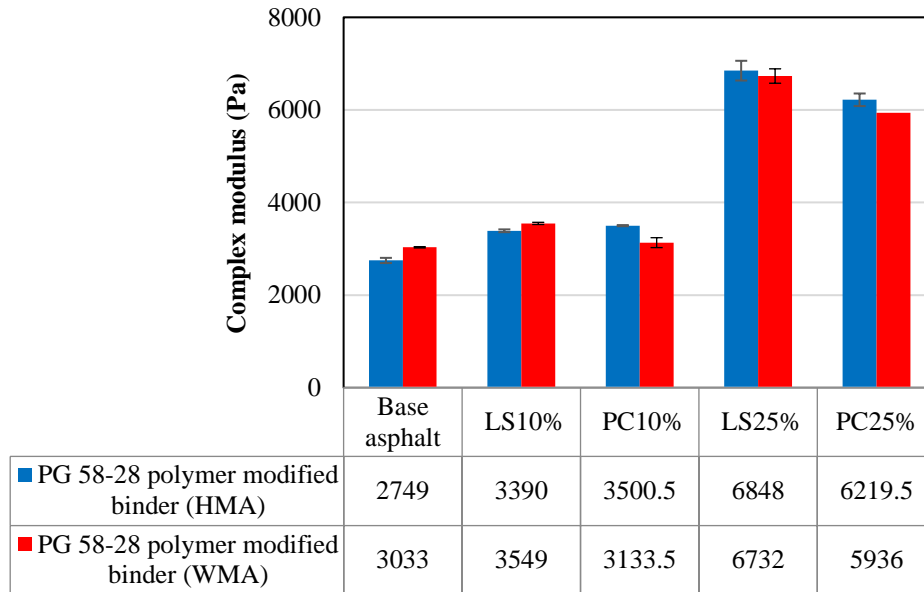
	Polymer-modified PG64-10 (HMA)	Polymer-modified PG64-10 (WMA)
Test Temp (°C)	64	64
$G^*$ (Pa)	3474	7324
Phase Angle	65.66	68.10

Figure 4.7 demonstrates the results for all  $G^*$  values for the unaged HMA PG58-28, and WMA PG58-28 mastics that tested at a higher PG temperature (58°C). The stiffness of these mastics varies significantly depending on both the quantity and the type of filler material. Typically, larger values of  $G^*$  are desirable as they reduce the overall shear deformation when repeatedly sheared. Using a warm-mix modifier reduces the complex modulus of mastics when the filler is added to the binder. This can be attributed to the softening or plasticizing effect of Evotherm that helps to reduce the mixing temperature. Adding a warm-mix modifier reduced the complex modulus of LS25% PG58-28 and PC25% PG58-28 mastics by 9.2% and 12.6%, respectively. Based on the graphs in Figure 4.6, it can be concluded that PC-based mastics had a larger  $G^*$  compared with LS-based mastics in the same filler volume concentration. The largest  $G^*$  value belongs to HMA PC25% PG58-28 mastic, which had a 206% increase in complex modulus when compared with the base asphalt binder. Moreover, the HMA PG58-28 mastic, with 25% of PC, had 7% higher  $G^*$  in comparison with the corresponding LS-based mastic.



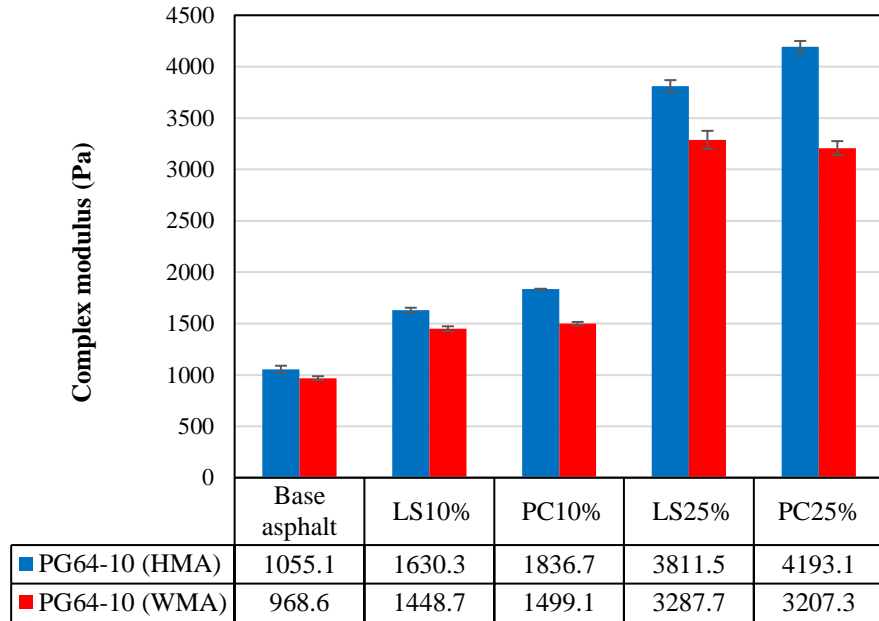
**Figure 4.7: Complex Modulus ( $G^*$ ) for Unaged HMA and WMA PG58-28 Mastics at 58°C**

Figure 4.8 reports the results for all  $G^*$  values for unaged HMA and WMA polymer-modified PG58-28 mastics. It can be observed that the incorporation of fillers drastically increases the  $G^*$  value of the polymer-modified HMA/WMA PG58-28 mastics. Here, at a low concentration (10%), LS and PC fillers work in a very similar way. However, replacing 25% by volume of the binder with LS and PC materials leads to a 122% and 96% increase in  $G^*$  value, compared with a polymer-modified WMA PG58-28 binder, respectively. Also, it can be observed that in most cases, adding the warm mix modifier reduced the  $G^*$  value due to the plasticizing effect. The highest complex modulus for polymer-modified PG58-28-based mastics belongs to HMA LS25% polymer-modified PG58-28 with a  $G^*$  value of 6,848 Pa.



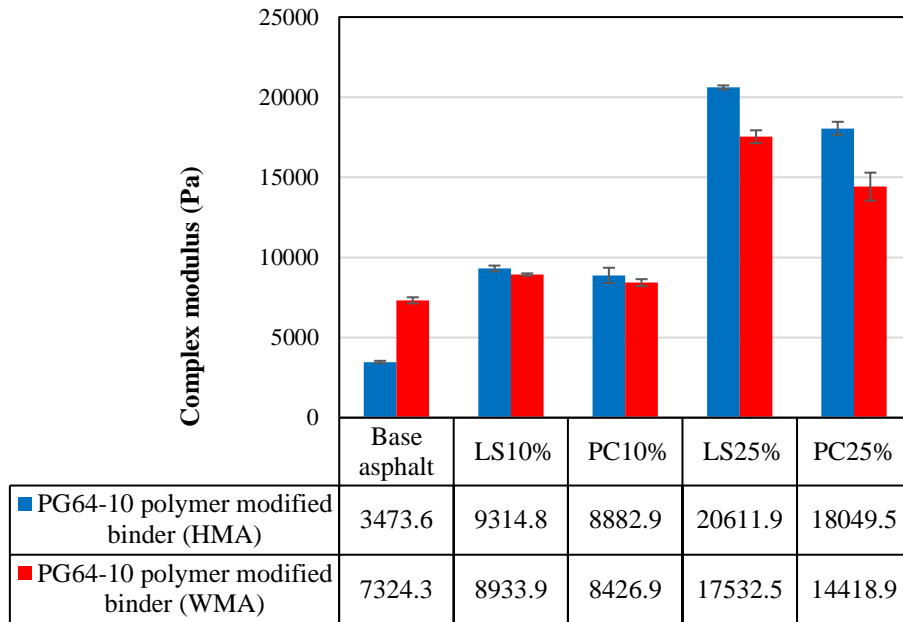
**Figure 4.8: Complex Modulus ( $G^*$ ) for Unaged HMA and WMA Polymer-modified PG58-28 Mastics at 58°C**

Figure 4.9 reports on the results for  $G^*$  values for unaged HMA PG64-10 and WMA PG64-10 mastics. It can be observed that in all of the cases, a warm mix modification resulted in a reduction of the complex modulus of the mastics. Here, the incorporation of fillers increased the  $G^*$  values; for example, replacing only 10% by volume of the asphalt binder with LS and PC filler material would increase the complex modulus in a similar way by 50% and 54%, respectively, when compared with WMA PG64-10 binder. Further, all HMA PC-based mastics had a higher complex modulus compared with the corresponding LS-based mastics. For example, PC25% PG64-10 HMA mastic had the largest complex modulus (4,193 Pa). However, minor difference was observed between the high-temperature performance of LS and PC-modified binders with WMA, with some reduction of  $G^*$  observed for WMA with 25% of PC.



**Figure 4.9: Complex Modulus ( $G^*$ ) for Unaged HMA and WMA PG64-10 Mastics at 64°C**

Figure 4.10 reports the results for all  $G^*$  values for the unaged HMA polymer-modified PG64-10 with considerable polymer addition (4% SBS incorporation) and corresponding WMA polymer-modified PG64-10 mastics. As noted in the figure, polymer modification of PG64-10- based mastics drastically increases the complex modulus. In addition, the  $G^*$  value for WMA polymer-modified PC25% PG64-10 mastic is 4.5 greater than the corresponding to non-polymer-modified material (See Figure 4.9). However, the addition of a warm mix modifier results in a reduction in the complex modulus of mastics with fillers. The highest complex modulus for polymer-modified PG58-28- based mastics corresponds to HMA LS25% polymer-modified PG64-10 mastic reaching  $G^*$  value of 20,612 Pa. However, using 25% by volume of PC instead of LS helps to reduce the  $G^*$  by 12% in the case of HMA and by 18% in the case of WMA compositions. Generally, a very high  $G^*$  value for a given mastic can be a sign of compositions which are very difficult to compact at a selected temperature.



**Figure 4.10: Complex Modulus ( $G^*$ ) for Unaged HMA and WMA Polymer-modified PG64-10 Mastics at 64°C**

### Relative Complex Shear Modulus ( $G^*_r$ )

To directly compare the complex modulus ( $G^*$ ) of the mastics, it was important to determine the relative complex shear modulus ( $G^*_r$ ). The relative complex shear modulus is the ratio of the complex modulus of the asphalt mastics over the complex modulus of the unfilled asphalt binder. By evaluating  $G^*_r$  it is easier to understand the relationships between the asphalt binders and the powders.

Figures 4.11 and 4.12 display the relative complex modulus ( $G^*_r$ ) for PG58-28 asphalt mastics and for PG64-10 asphalt mastics, respectively. In these figures, R represents the plain (reference) binder, P denotes the polymer-modified binder, LS and PC represent the type of incorporated filler, and HMA and WMA stand for hot mix asphalt and warm mix asphalt, respectively. As it can be concluded from these figures, the relative  $G^*_r$  is significantly dependent on the filler volume concentration. Also, it can be observed that the sensitivity of the results decreases in the case of

WMA- based mastics compared with HMA-based mastics; that is; the warm mix modifier reduces the relative  $G^*$  when the filler volume concentration increases. As reported in Figure 4.10, polymer-modified-PG58-28-based mastics had less sensitivity to relative  $G^*$  compared with plain PG58-28-based mastics; on the other hand, based on the results reported in Figure 4.12, the sensitivity of polymer-modified PG64-10 base mastics to relative  $G^*$  was higher than that of PG64-10-based mastics.

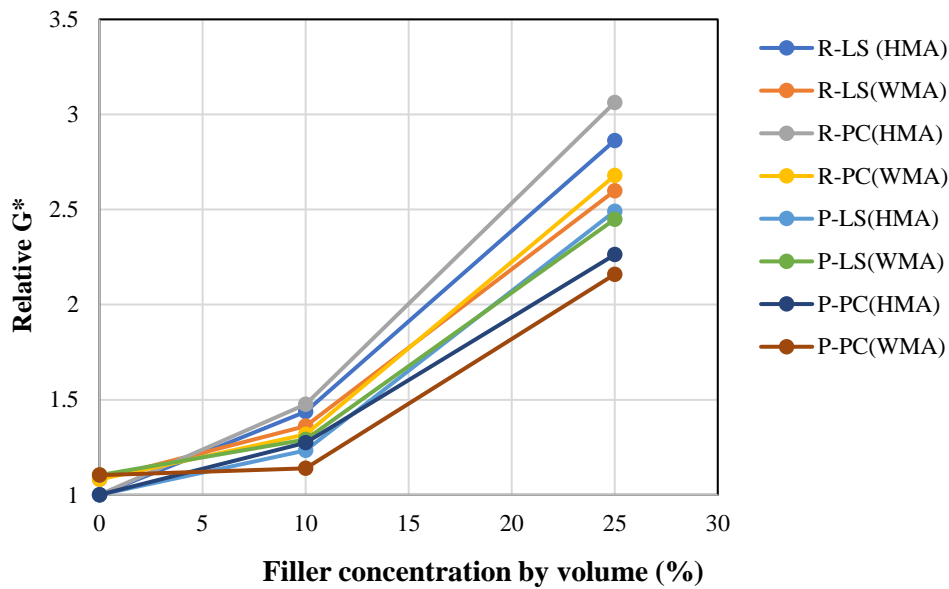


**Figure 4.11: Relative Complex Modulus ( $G^*$ ) for Unaged PG58-28 Mastics**

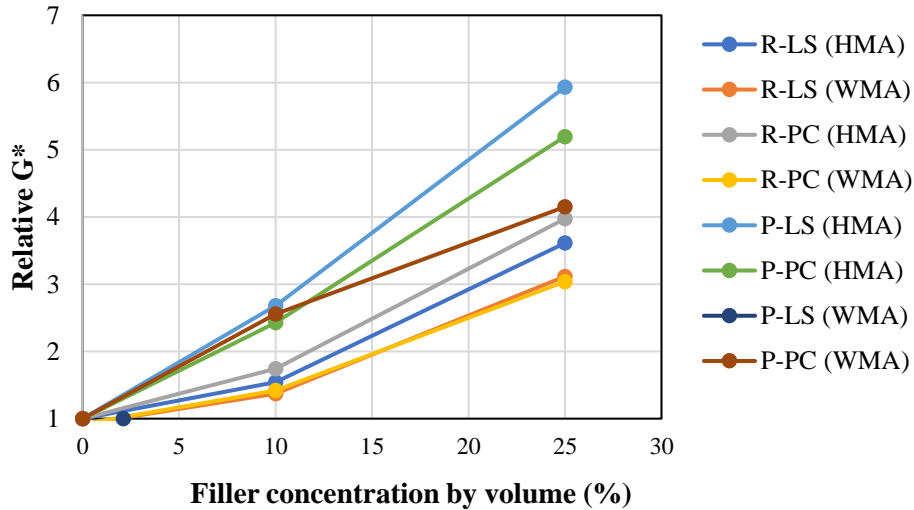


**Figure 4.12: Relative Complex Modulus ( $G^*$ ) for Unaged PG64-10 Mastics**

### Relative Phase Angle ( $\delta_r$ )

Relative phase angle ( $\delta_r$ ) was calculated to investigate the effect of polymer modification, the addition of a warm mix modifier, and incorporation of filler into PG58-28 and PG64-10 based mastics. The phase angle is the lag between the elastic and inelastic (viscous) response of the asphalt binder. When the phase angle is low, the binder experiences a more elastic response. The relative phase angle is the ratio of the phase angle of the asphalt mastic over the phase angle of the plain unfilled asphalt binder. By evaluating  $\delta_r$  it is easier to understand the relationships between the asphalt binders and the powders.

Tables 4.9 and 4.10 report on the relative phase angle ( $\delta_r$ ) for PG58-28 and PG64-10-based asphalt mastics. From these tables, it is evident that the phase angle is unaffected by the filler type, filler dosage, and warm mix modification, and the relative phase angle does not change dramatically; however, it can be seen that polymer modification reduces the relative phase angle substantially; hence making the polymer-modified-based mastics more elastic.

**Table 4.9: Relative Phase Angle ( $\delta r$ ) for Unaged PG58-28 based Mastics at 58°C**

Sample ID	Relative Phase Angle ( $\delta r$ )		
	0%	10%	25%
R-LS (HMA)	1.000	1.000	0.994
R-PC (HMA)	1.000	0.999	0.993
R-LS (WMA)	0.994	0.998	0.995
R-PC (WMA)	0.994	1.002	0.997
P-LS (HMA)	0.805	0.820	0.810
P-PC (HMA)	0.805	0.812	0.819
P-LS (WMA)	0.818	0.832	0.820
P-PC (WMA)	0.818	0.833	0.843

**Table 4.10: Relative Phase Angle ( $\delta r$ ) for Unaged PG64-10-based Mastics at 64°C**

Sample ID	Relative Phase Angle ( $\delta r$ )		
	0%	10%	25%
R-LS (HMA)	1.000	1.037	1.025
R-PC (HMA)	1.000	1.031	1.025
R-LS (WMA)	0.995	1.008	1.008
R-PC (WMA)	0.995	0.974	1.015
P-LS (HMA)	0.777	0.810	0.795
P-PC (HMA)	0.777	0.815	0.770
P-LS (WMA)	0.806	0.819	0.811
P-PC (WMA)	0.806	0.813	0.816

The testing requirements for the Superpave® binder testing protocol were developed to evaluate the performance of asphalt binders, not asphalt mastics. The purpose of this study was to adopt the Superpave® binder testing protocol for asphalt mastics and make comparisons between the binder and mastic performance. It was important to use this established protocol to make conclusions on the fundamental properties of the mastics based on the experimental results. Therefore, for this study, Superpave® limitations were not considered for characterizing the mastics (as these were developed for asphalt binders only) but rather used as a guideline to assess the relative effects of the fillers, warm mix conversion, and polymer modification on the overall performance of asphalt mastics. Duplicates were used for all tests to reduce the uncertainty and possibility of testing errors.

#### **4.4 Rutting Resistance**

Rutting in asphalt mixtures refers to a progressive, permanent deformation of a material under repeated traffic load, which can occur from consolidation or through plastic flow. Rutting results from permanent distortion of the material at higher temperatures due to wheel track loading affecting short-term aged materials, which is the most generic form of permanent deformation. A Superpave® rutting factor  $G^*/\sin(\delta)$  is used to assess the asphalt binders at the high PG temperature (58°C for PG58-28 and 64°C for PG64-10) under the testing protocol to evaluate rutting resistance. In this study, the rutting factor was used to compare all investigated asphalt mastics to understand the effects of warm mix addition, polymer modification, and filler incorporation on the enhancement of rutting resistance. In this regard, higher values of  $G^*/\sin(\delta)$  are desirable as this indicates better rutting resistance.

Still, the rutting factor  $G^*/\sin(\delta)$  may not be an effective parameter to characterize asphalt binders, especially polymer-modified binders, for rutting resistance. Therefore, Superpave® specifications require that the rutting factor  $G^*/\sin(\delta)$  to be accompanied by a Multiple Stress Creep and Recovery (MSCR) test conducted at the high PG temperature to evaluate the rutting resistance. For the MSCR test, Non-Recoverable Compliance ( $J_{nr}$ ) and % Recovery are evaluated to understand the response of the mastics. The  $J_{nr}$  values represent the residual strain of the material after the creep and recovery cycle, whereas the % Recovery is used to evaluate the elastic response of the asphalt binder. Here, lower values of  $J_{nr}$  are desirable, and higher values of % Recovery are desirable for the best performance.

#### **Superpave® Rutting Factor ( $G^*/\sin(\delta)$ )**

Rutting resistance testing was performed in accordance with AASHTO T315 specifications with the DSR to evaluate the rutting factor  $G^*/\sin(\delta)$ . According to the standard, to reduce rutting,

$G^*/\sin(\delta)$  must be larger than 1.00 kPa for unaged asphalt binders and larger than 2.20 kPa for RTFO-aged asphalt binders. Higher values of  $G^*/\sin(\delta)$  are desirable as they present a more elastic response which is desirable for rutting resistance.

Tables 4.11 through 4.14 report on the performance of unaged PG58-28- based and PG64-10- based asphalt binders. Regardless of warm mix additive or polymer modification, it can be reported that all the binders met the Superpave® testing specifications since all values of  $G^*/\sin(\delta)$  are greater than 1.00 kPa.

**Table 4.11:  $G^*/\sin(\delta)$  for Unaged HMA and WMA PG58-28**

	PG58-28 (HMA)	PG58-28 (WMA)
Test Temp (°C)	58	58
$G^*/\sin(\delta) \geq 1.00$ kPa	1.33	1.44

**Table 4.12:  $G^*/\sin(\delta)$  for Unaged HMA and WMA Polymer-modified PG58-28**

	Polymer-modified PG 58-28 (HMA)	Polymer-modified PG58-28 (WMA)
Test Temp (°C)	58	58
$G^*/\sin(\delta) \geq 1.00$ kPa	2.9	3.2

**Table 4.13:  $G^*/\sin(\delta)$  for Unaged HMA and WMA PG64-10**

	PG64-10 (HMA)	PG64-10 (WMA)
Test Temp (°C)	64	64
$G^*/\sin(\delta) \geq 1.00$ kPa	1.09	1.02

**Table 4.14:  $G^*/\sin(\delta)$  for Unaged HMA and WMA Polymer-modified PG64-10**

	Polymer-modified PG64-10 (HMA)	Polymer-modified PG64-10 (WMA)
Test Temp (°C)	64	64
$G^*/\sin(\delta) \geq 1.00$ kPa	3.92	7.89

Tables 4.15 through 4.18 report on the  $G^*/\sin(\delta)$  results for the RTFO-aged asphalt binders. These results demonstrate similar trends observed from the unaged asphalt binders when tested for rutting resistance. Here, all of the binders meet the Superpave® testing protocol requirements since the  $G^*/\sin(\delta)$  values are greater than 2.20 kPa. Further, it can be observed that polymer modification had a significant impact on the rutting resistance of the binders since the  $G^*/\sin(\delta)$  values of the polymer-modified binders are significantly higher than those of corresponding plain binders. As an example, the  $G^*/\sin(\delta)$  values of RTFO-aged HMA polymer-modified PG58-28 and HMA polymer-modified PG64-10 are 2 and 7 times greater than those of RTFO-aged HMA PG58-28 and HMA PG64-10, respectively.

**Table 4.15:  $G^*/\sin(\delta)$  for RTFO Aged HMA and WMA PG58-28**

	PG58-28 (HMA)	PG58-28 (WMA)
Test Temp (°C)	58	58
$G^*/\sin(\delta) \geq 2.20$ kPa	3.56	3.96

**Table 4.16:  $G^*/\sin(\delta)$  for RTFO Aged HMA and WMA Polymer-modified PG58-28**

	Polymer-modified PG 58-28 (HMA)	Polymer-modified PG58-28 (WMA)
Test Temp (°C)	58	58
$G^*/\sin(\delta) \geq 2.20$ kPa	7.13	6.79

**Table 4.17:  $G^*/\sin(\delta)$  for RTFO Aged HMA and WMA PG64-10**

	PG64-10 (HMA)	PG64-10 (WMA)
Test Temp (°C)	64	64
$G^*/\sin(\delta) \geq 2.20$ kPa	2.63	2.85

**Table 4.18:  $G^*/\sin(\delta)$  for RTFO Aged HMA and WMA Polymer-modified PG64-10**

	Polymer-modified PG64-10 (HMA)	Polymer-modified PG64-10 (WMA)
Test Temp (°C)	64	64
$G^*/\sin(\delta) \geq 2.220$ kPa	17.88	14.35

The results for RTFO aged rutting resistance testing are reported in Figures 4.13 through 4.16. The results demonstrate that the addition of the powders increases the rutting factor  $G^*/\sin(\delta)$  and, therefore, increases the rutting resistance. Also, it can be reported that polymer modification greatly enhances the rutting resistance of the mastics. For example, the rutting resistance for WMA polymer-modified PC10% PG58-28 is 2.25 times greater than that for WMA PC10% PG58-28.

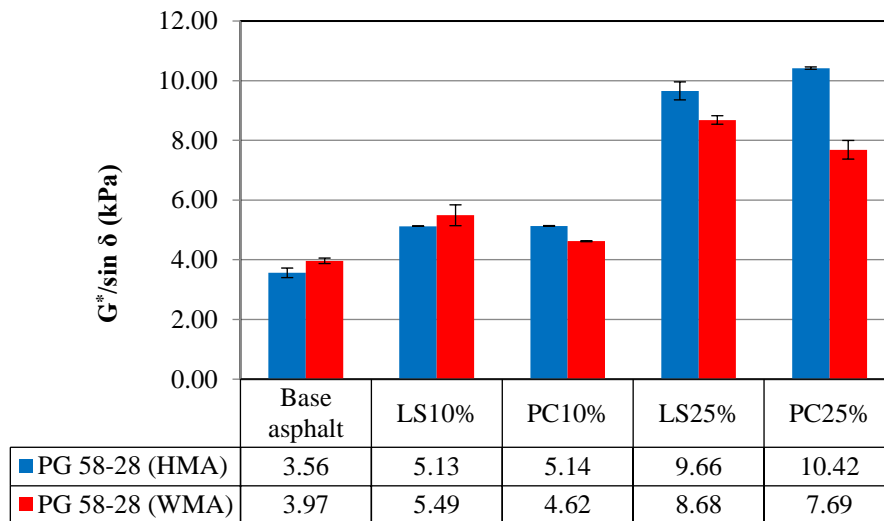


**Figure 4.13:  $G^*/\sin(\delta)$  for RTFO Aged PG58-28 Mastics at 58°C**

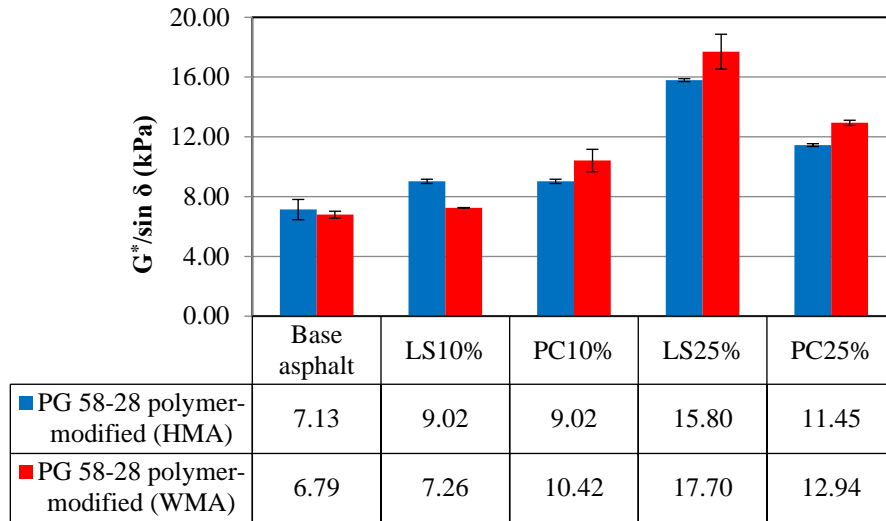


Figure 4.14:  $G^*/\sin(\delta)$  for RTFO Aged Polymer-modified PG58-28 Mastics at 58°C

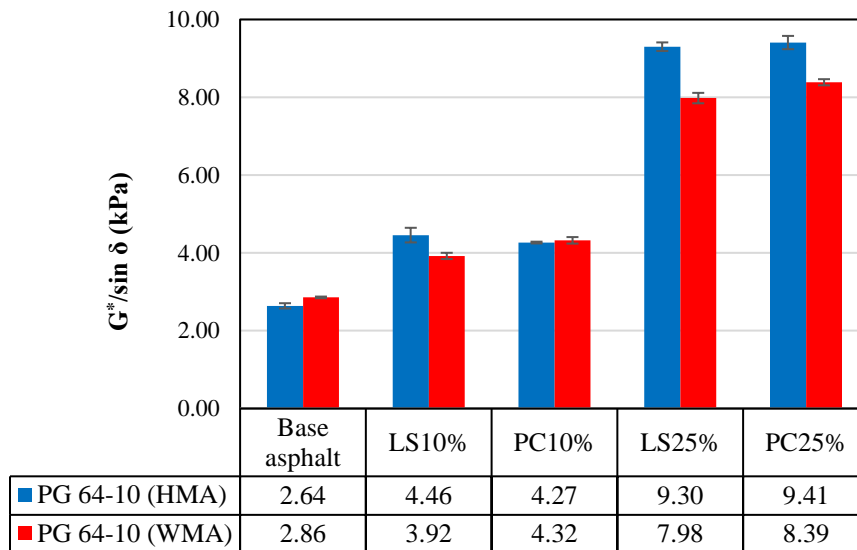
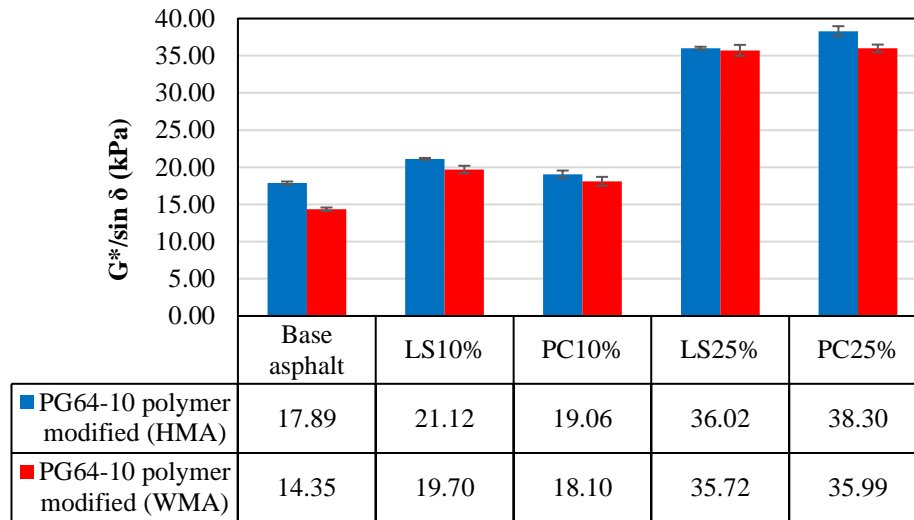


Figure 4.15:  $G^*/\sin(\delta)$  for RTFO Aged PG64-10 Mastics at 64°C



**Figure 4.16:  $G^*/\sin(\delta)$  for RTFO Aged Polymer-modified PG64-10 Mastics at 64°C**

### Non-Recoverable Compliance ( $J_{nr}$ )

The Multiple Stress Creep & Recovery (MSCR) testing was performed according to ASTM T315 and AASHTO T350-14 with the DSR at the high PG temperature on RTFO-aged materials to evaluate both Non-Recoverable Compliance ( $J_{nr}$ ) and % Recovery. The testing stress of 0.1 kPa was used for conditioning, and testing stresses of 3.2 and 10.0 kPa are commonly used to evaluate the rutting resistance of the asphalt mastics. Previous studies proved the stress sensitivity correlations between  $J_{nr}$  values at 3.2 kPa and 10.0 kPa levels for mastics at 5, 10, 15, 25, and 40% concentrations by volume (Bautista, 2014). The trends between the different stress levels had a strong linear correlation, so it was determined that the stress dependencies of the results could be ignored since the characteristics were affected by the Newtonian behavior of the asphalt binders. For this reason, this research reports on testing at 3.2 kPa stress levels. Here, lower values of  $J_{nr}$  and higher values of % Recovery are desirable.

Tables 4.19 and 4.20 report the  $J_{nr}$  results for the RTFO aged HMA/WMA PG58-28 and polymer-modified PG58-28 binders. From the tables below, it can be concluded that adding the warm-mix

modifier increased the  $J_{nr}$  values of the mastics. This can be attributed to the softening effect of the Evotherm. Also, it can be observed that polymer modification resulted in a significant decrease in the  $J_{nr}$  values, which is desirable. For example, The  $J_{nr}$  value for the RTFO-aged WMA polymer-modified PG58-28 is 8 times smaller than that of the non-polymer-modified binder.

**Table 4.19:  $J_{nr}$  for RTFO Aged HMA and WMA PG58-28 at 58°C at 3.2 kPa loading level**

	PG58-28 (HMA)	PG58-28 (WMA)
Test Temp (°C)	58	58
$J_{nr}$ (1/kPa)	2.81	2.88

**Table 4.20:  $J_{nr}$  for RTFO Aged HMA and WMA Polymer-modified PG58-28 at 58°C at 3.2 kPa loading level**

	Polymer-modified PG58-28 (HMA)	Polymer-modified PG58-28 (WMA)
Test Temp (°C)	58	58
$J_{nr}$ (1/kPa)	0.38	0.44

Tables 4.21 and 4.22 report on the  $J_{nr}$  results for the RTFO aged HMA/WMA mastics based on PG64-10 and polymer-modified PG64-10 binders. Again, it can be observed that polymer modification had a significant effect on the improvement of rutting resistance of the RTFO-aged plain and polymer-modified binders.

**Table 4.21:  $J_{nr}$  for RTFO Aged HMA and WMA PG64-10 at 64°C at 3.2 kPa loading level**

	Polymer-modified PG64-10 (HMA)	Polymer-modified PG64-10 (WMA)
Test Temp (°C)	64	64
$J_{nr}$ (1/kPa)	0.21	0.16

**Table 4.22:  $J_{nr}$  for RTFO Aged HMA and WMA PG64-10 at 64°C at 3.2 kPa loading level**

	Polymer-modified PG64-10 (HMA)	Polymer-modified PG64-10 (WMA)
Test Temp (°C)	64	64
$J_{nr}$ (1/kPa)	0.21	0.16

The MSRC testing results for PG58-28-based and polymer-modified PG58-28-based mastics are reported in Figures 4.17 and 4.18. The results demonstrate that the  $J_{nr}$  values improved as the filler volume concentration increased, which leads to a better performance in terms of rutting resistance. The mastics experience an improved elastic response under the 3.2 kPa loading level and continue to perform better with higher filler volume concentrations. Further, it can be noted that polymer modification resulted in a significant enhancement in the elastic response of the investigated mastics.

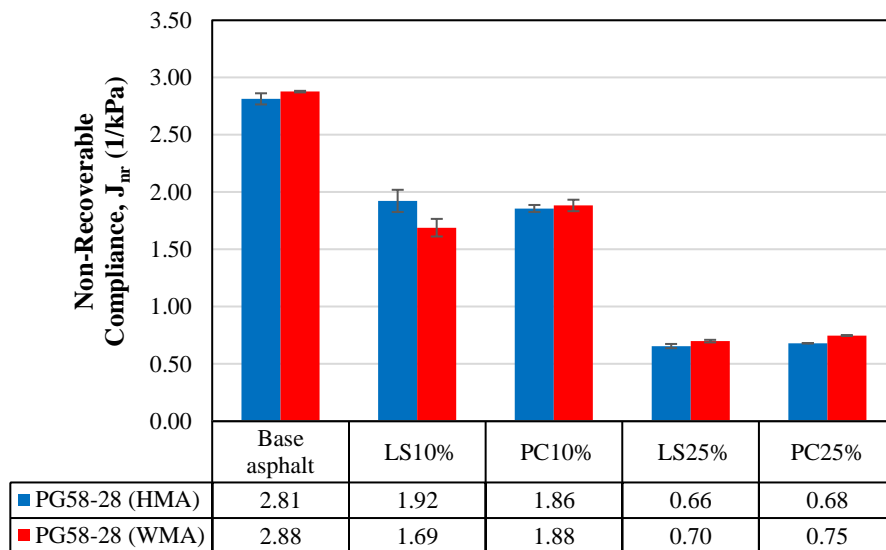


**Figure 4.17:  $J_{nr}$  for RTFO Aged HMA and WMA PG58-28 Mastics at 58°C**

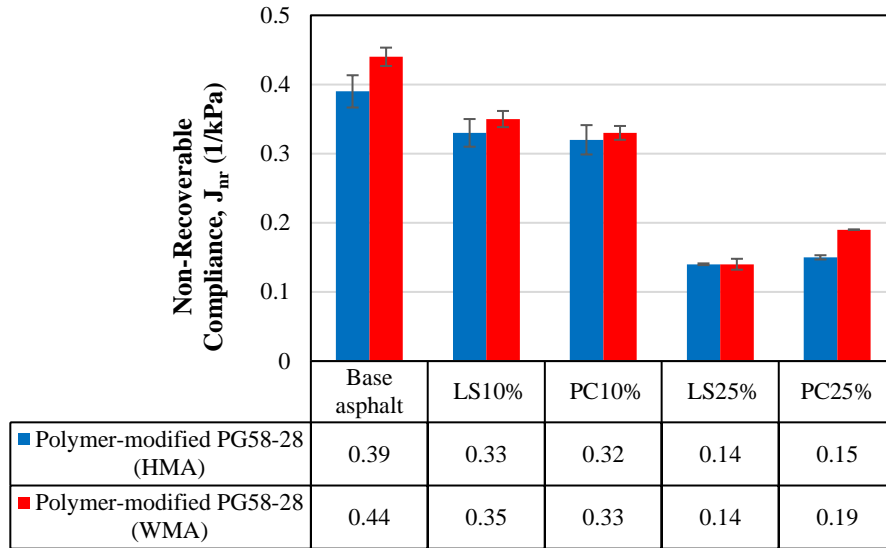


**Figure 4.18:  $J_{nr}$  for RTFO Aged HMA and WMA Polymer-modified PG58-28 Mastics at 58°C**

The MSCR tests for PG64-10-based and polymer-modified PG64-10-based mastics were performed at 3.2 kPa loading level and three different temperatures, 58 °C, 64 °C, and 70 °C, to have a better understanding of the effect of temperature on the elastic response of the mastics. The results are demonstrated in Figures 4.19 through 4.22. Based on the experimental results, it can be reported that an increase in temperature compromised the elastic response of the mastics, regardless of the filler type or filler volume concentration. Also, it can be observed that with increased filler volume concentration, the sensitivity for  $J_{nr}$  of the mastics to the temperature rise was reduced; i.e., (the rate of increase in the  $J_{nr}$  was reduced). This is a desirable outcome since it proves that by incorporating a higher filler volume, the negative impact of the increased temperature on the elastic response of the mastics becomes less significant. Further, it can be reported that in the case of PG64-10- based mastics, the warm-mix additive had an insignificant effect on the  $J_{nr}$  values at different temperatures, and PC-based mastics performed slightly better compared with LS-based mastics in terms of  $J_{nr}$  value. By comparing Figures 4.19 and 4.20 to Figures 4.21 and 4.22, it can be reported that the polymer modification had a drastic impact on the

improvement of the rutting resistance of the mastics. Further, it can be observed that at a lower temperature, the filler incorporation had a smaller effect on  $J_{nr}$  value of the mastics, but as the temperature increased, the difference between the  $J_{nr}$  value of the mastics and the neat binder became more paramount.

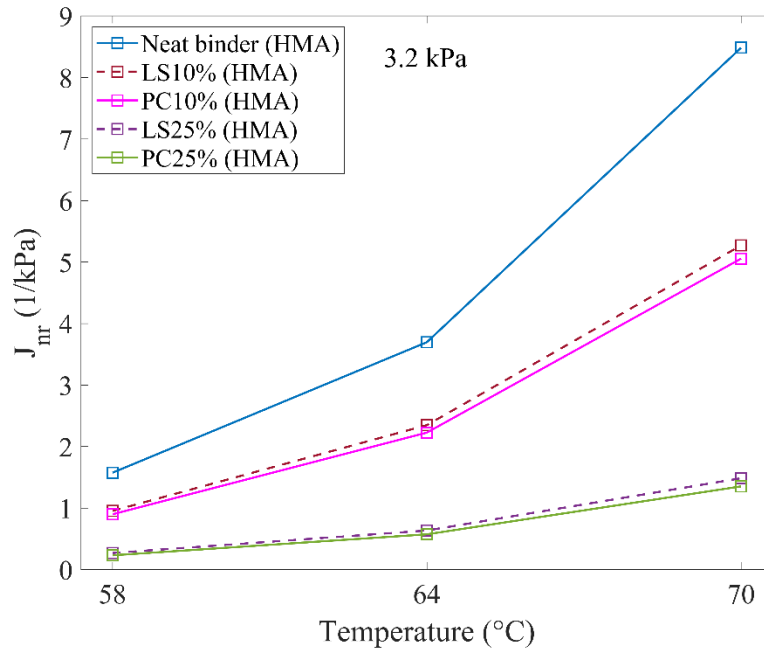


**Figure 4.19:  $J_{nr}$  for RTFO Aged HMA PG64-10 Mastics at 58°C, 64°C, and 70°C**

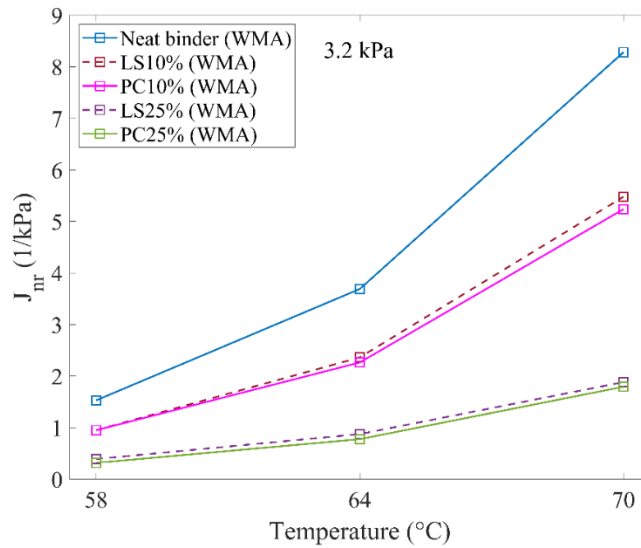


**Figure 4.20:  $J_{nr}$  for RTFO Aged WMA PG64-10 Mastics at 58°C, 64°C, and 70°C**

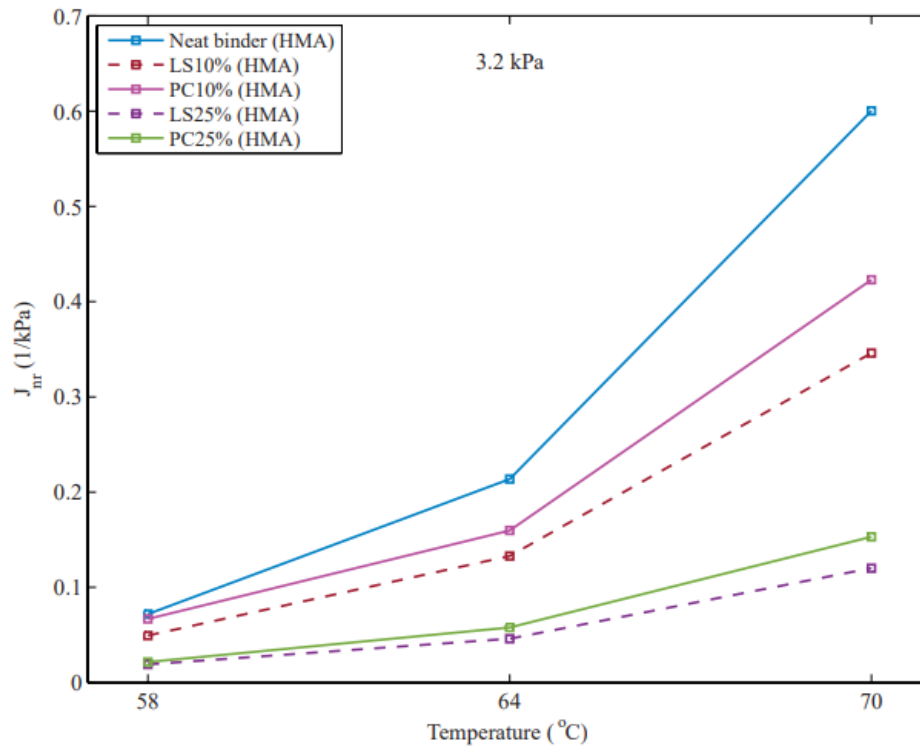


Figure 4.21: J<sub>nr</sub> for RTFO Aged HMA Polymer-modified PG64-10 Mastics at 58°C, 64°C, and 70°C

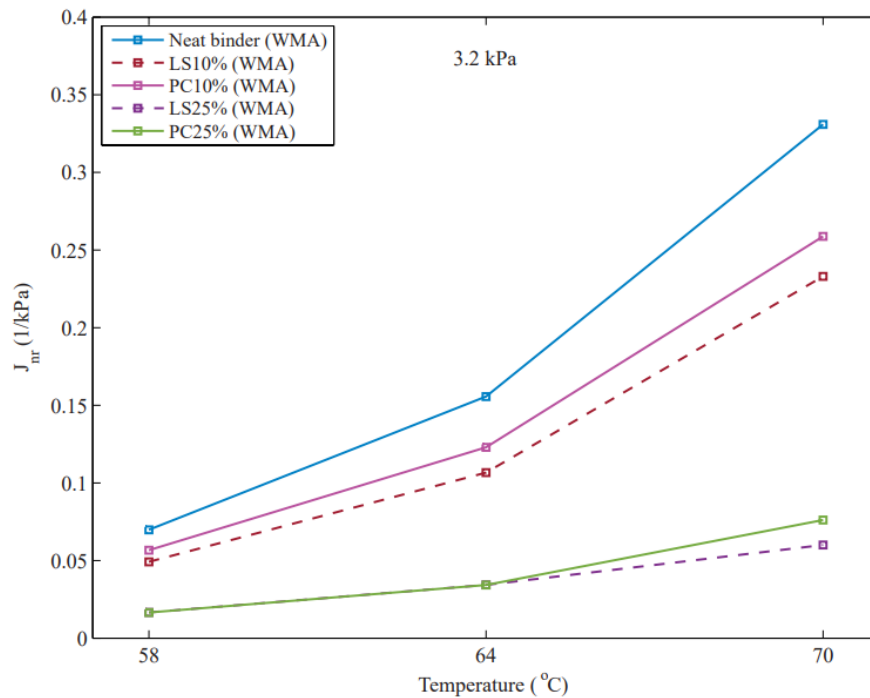


Figure 4.22: J<sub>nr</sub> for RTFO Aged WMA Polymer-modified PG64-10 Mastics at 58°C, 64°C, and 70°C

## % Recovery

The % Recovery data were also calculated from the MSCR testing at the 3.2 kPa loading level. Tables 4.23 through 4.26 report the recovery percentage on the RTFO aged HMA and WMA based on PG58-28, polymer-modified PG58-28, PG64-10, and polymer-modified PG64-10 binders, respectively. It should be noted that a higher recovery percentage is desirable as it describes a better elastic performance of a given binder. Based on the research results on mastics, the warm-mix additive did not change the recovery percentage of the binders; however, the polymer modification had a significant impact on the recovery of the binders. Based on the results reported in Tables 4.23 through 4.26 from the analyzed MSCR test, it can be concluded that polymer modification can drastically improve the rutting behavior and elastic performance of the binders.

**Table 4.23 Recovery percentage for RTFO Aged HMA and WMA PG58-28 at 58°C at 3.2 kPa loading level**

	PG58-28 (HMA)	PG58-28 (WMA)
Test Temp (°C)	58	58
Percent Recovery (%)	1.15	1.25

**Table 4.24: Recovery percentage for RTFO Aged HMA and WMA Polymer-modified PG58-28 at 58°C at 3.2 kPa loading level**

	Polymer-modified PG58-28 (HMA)	Polymer-modified PG58-28 (WMA)
Test Temp (°C)	58	58
Percent Recovery (%)	52.30	46.80

**Table 4.25: Recovery percentage for RTFO Aged HMA and WMA PG64-10 at 64°C at 3.2 kPa loading level**

	PG64-10 (HMA)	PG64-10(WMA)
Test Temp (°C)	64	64
Percent Recovery (%)	2.2	1.50

**Table 4.26: Recovery percentage for RTFO Aged HMA and WMA Polymer-modified PG64-10 at 64°C at 3.2 kPa loading level**

	Polymer-modified PG64-10 (HMA)	Polymer-modified PG64-10 (WMA)
Test Temp (°C)	64	64
Percent Recovery (%)	48.5	47

The percent recovery results were obtained by analyzing MSCR test data for the investigated mastics as reported in Figures 4.23 through 4.26. As represented by the figures, the addition of a warm-mix modifier did not affect the percent recovery values of investigated mastics. Further, it can be observed that the incorporation of filler/reactive powder resulted in an increase in the percent recovery of PG58-28 and PG64-10 and polymer-modified PG64-10 mastics, which is desirable in terms of elastic response. Based on the Figures 4.17 through 4.26, which are plotted by analyzing the MSCR test data, it can be concluded that adding fillers into asphalt binders improves the rutting resistance and the elastic response of the mastics by reduction of  $J_{nr}$  values and increasing percent recovery values.

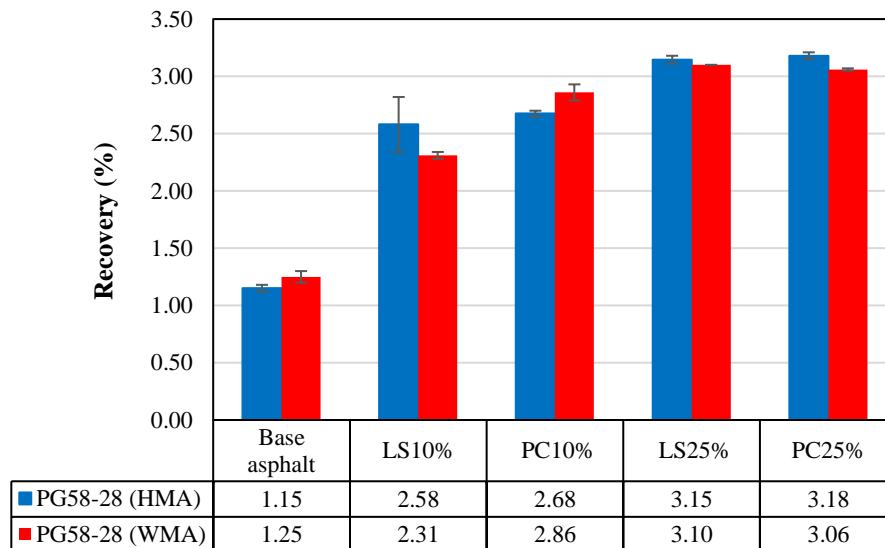


**Figure 4.23: Percent Recovery for RTFO Aged HMA and WMA PG58-28 Mastics at 58°**

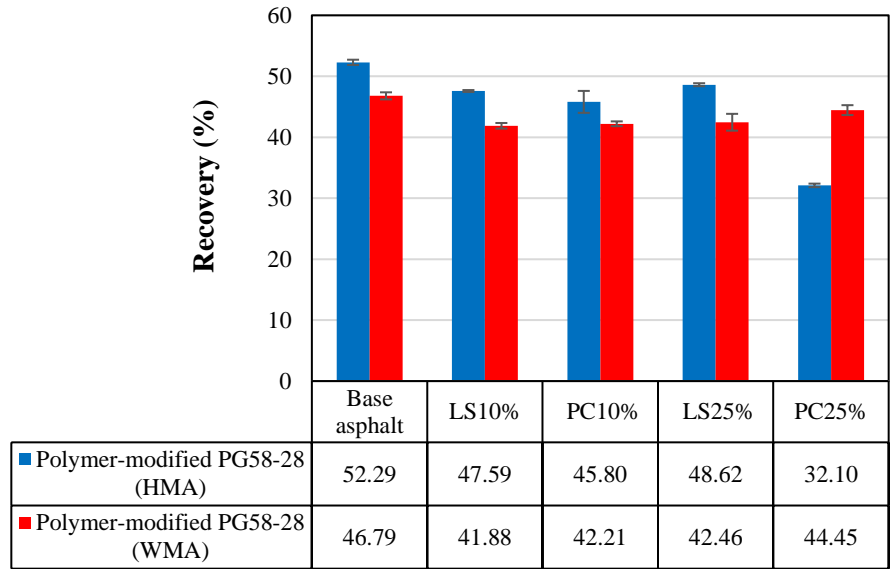


**Figure 4.24: Percent Recovery for RTFO Aged HMA and WMA Polymer-modified PG58-28 Mastics at 58°C**

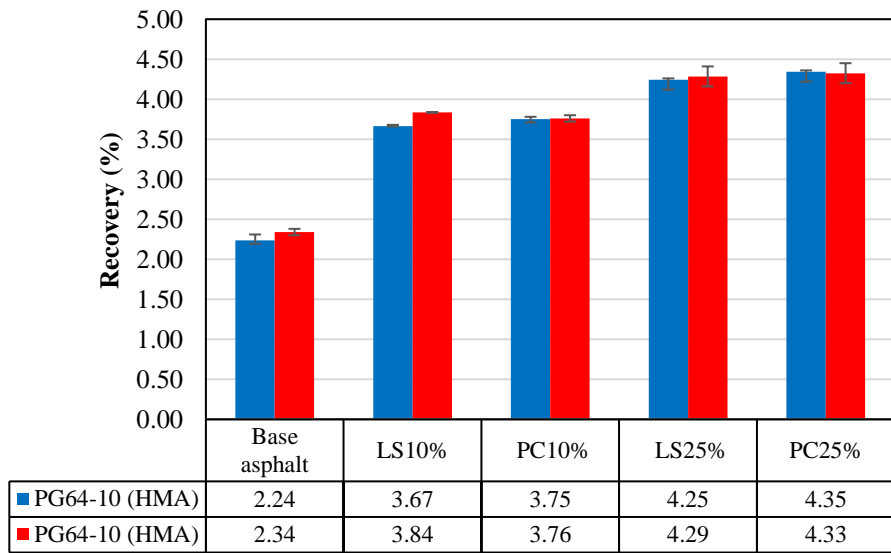


**Figure 4.25: Percent Recovery for RTFO Aged HMA and WMA PG64-10 Mastics at 64°C**

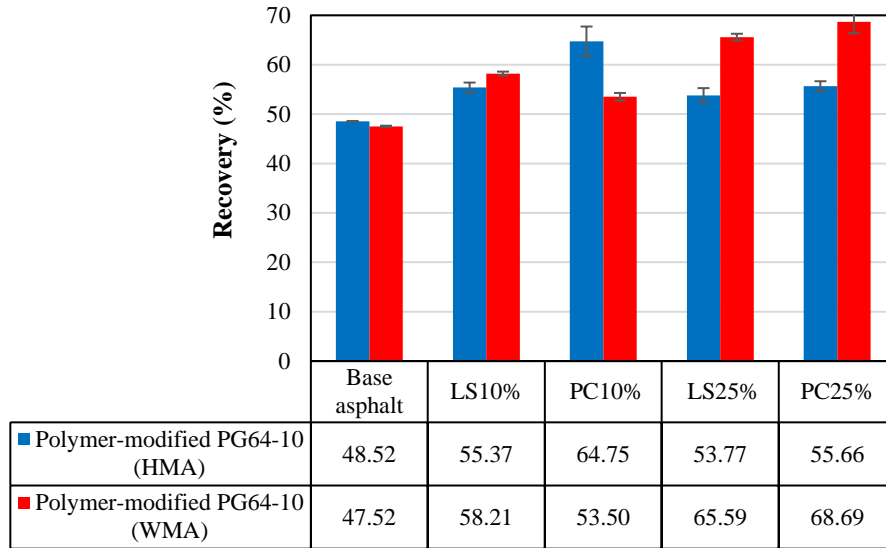


**Figure 4.26: Percent Recovery for RTFO Aged HMA and WMA Polymer-modified PG64-10 Mastics at 64oC**

#### 4.5 Fatigue Resistance

A fatigue resistance test was performed following AASHTO T315 using the DSR machine to assess the fatigue factor  $G^* \sin(\delta)$  at intermediate temperatures ( $19^\circ\text{C}$  for PG58-28 and  $31^\circ\text{C}$  for PG64-10). Fatigue cracking in asphalt binders occurs due to repeated loads at a typical service temperature over the service life of the pavement. The Superpave® specifications require that the asphalt binder be evaluated under intermediate temperature conditions using the been long-term aged (PAV aged) asphalt material. The fatigue factor  $G^* \sin(\delta)$  is assessed by applying an oscillating load at a low shear strain which is measured in the linear viscoelastic region. The Superpave® specifications also require that  $G^* \sin(\delta)$  be less than or equal to 5 MPa. Low values of  $G^* \sin(\delta)$  are desirable as this indicates a better resistance to fatigue deformation. The results for fatigue resistance of PAV-aged plain and polymer-modified binders are reported in Tables 4.27 through 4.31. It can be concluded that all the binders meet the criteria of Superpave® specifications for  $G^* \sin(\delta)$ , demonstrating fatigue resistance of less than 5 MPa. In the case of PG58-28-based

binders, polymer modification enabled a reduction of the  $G^*\sin(\delta)$  value of the binders; hence the fatigue resistance improved. However, polymer modification led to a reduction in the fatigue performance of PG64-10- based binders. Moreover, a warm-mix additive decreased the  $G^*\sin(\delta)$  value for all the long-term-aged binders, so it can be concluded that warm-mix modification enhances the fatigue performance of asphalt binders.

**Table 4.27:  $G^*\sin(\delta)$  for PAV Aged HMA and WMA PG58-28 at 19°C**

	PG58-28 (HMA)	PG58-28 (WMA)
Test Temp (°C)	19	19
$G^*\sin(\delta)$ (MPa) < 5 MPa	1.18	1.06

**Table 4.28:  $G^*\sin(\delta)$  for PAV Aged HMA and WMA Polymer-modified PG58-28 at 19°C**

	Polymer-modified PG58-28 (HMA)	Polymer-modified PG58-28 (WMA)
Test Temp (°C)	19	19
$G^*\sin(\delta)$ (MPa) < 5 MPa	0.83	0.79

**Table 4.29:  $G^*\sin(\delta)$  for PAV Aged HMA and WMA PG64-10 at 31°C**

	PG64-10 (HMA)	PG64-10 (WMA)
Test Temp (°C)	31	31
$G^*\sin(\delta)$ (MPa) < 5 MPa	0.39	0.38

**Table 4.30:  $G^*\sin(\delta)$  for PAV Aged HMA and WMA Polymer-modified PG64-10 at 31°C**

	Polymer-modified PG64-10 (HMA)	Polymer-modified PG64-10 (WMA)
Test Temp (°C)	31	31
$G^*\sin(\delta)$ (MPa) < 5 MPa	1.25	1.10

Figures 4.27 through 4.30 demonstrate the fatigue resistance of investigated PAV-aged HMA and WMA mastics. As can be observed from the figures below, all the mastics met the criteria of Superpave specification, demonstrating  $G^*\sin(\delta)$  below 5 MPa. Similar to the results for fatigue

resistance of binders, it was observed that a warm mix modification could improve the  $G^*\sin(\delta)$  value of the mastics, regardless of the type of binder, type of incorporated filler, and filler volume concentration. Further, it is demonstrated that the incorporation of filler results in a reduction in fatigue resistance vs. a corresponding binder. This is expected due to the stiffening effect of the fillers. Additionally, except for the HMA Polymer-modified PG64-10- based mastics with 25% filler volume concentration, it can be concluded that PC-based mastics had a better fatigue performance compared with LS-based mastics at a similar powder volume concentration. This result can be attributed to the physiochemical interaction of cement particles with the binders.

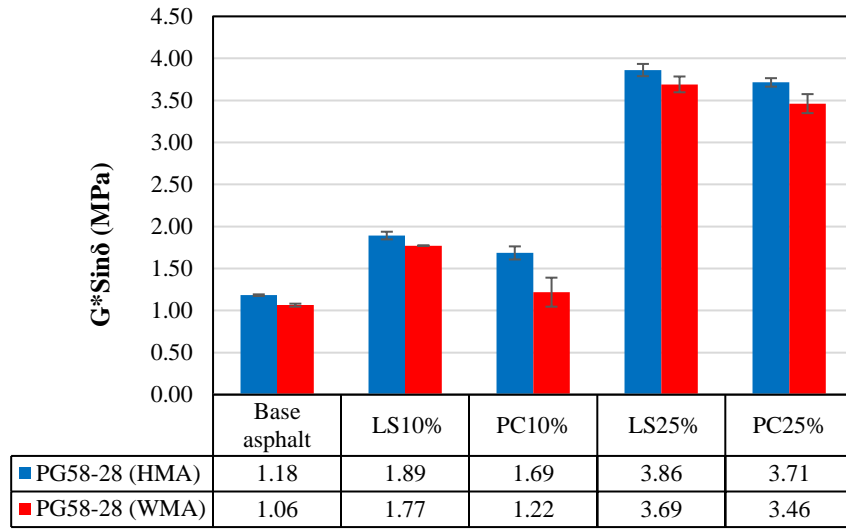


**Figure 4.27: Fatigue Performance for PAV-Aged HMA and WMA PG58-28 Mastics at 19°C**

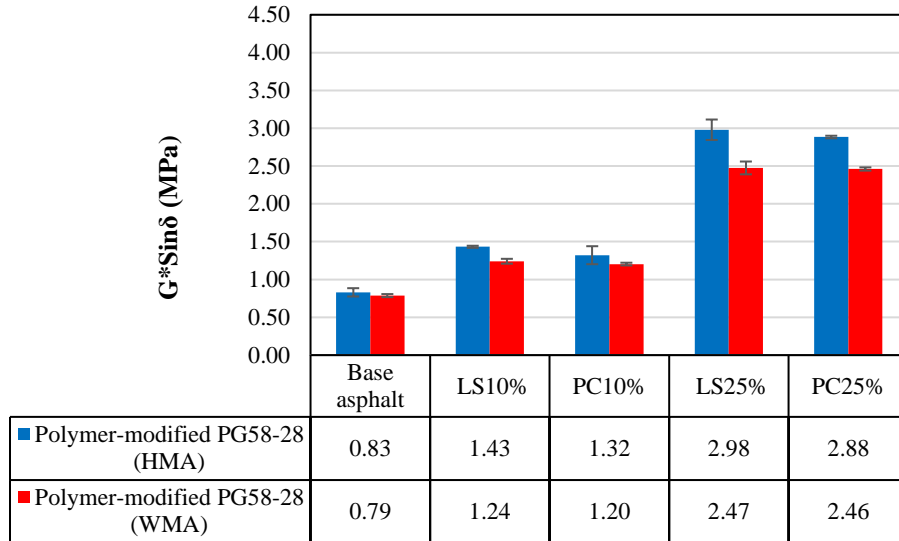


**Figure 4.28: Fatigue Performance for PAV-Aged HMA and WMA Polymer-modified PG58-28 Mastics at 19°C**

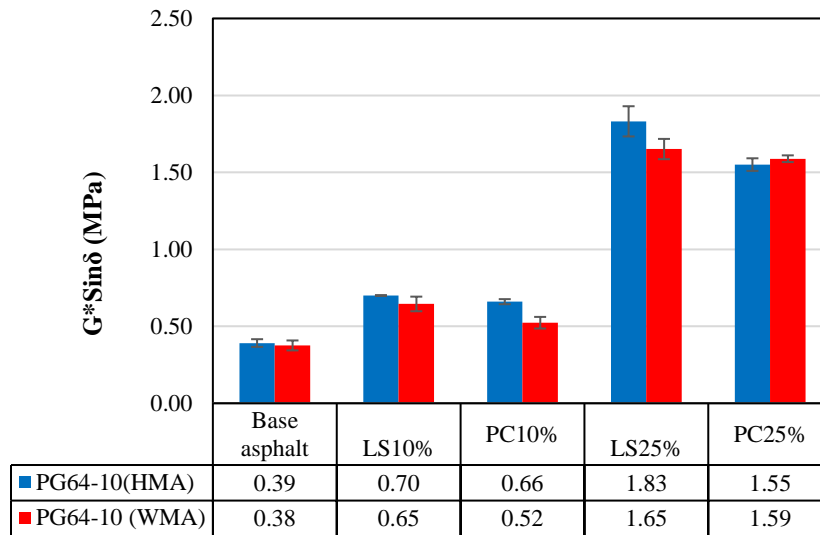


**Figure 4.29: Fatigue Performance for PAV-Aged HMA and WMA PG64-10 Mastics at 31°C**

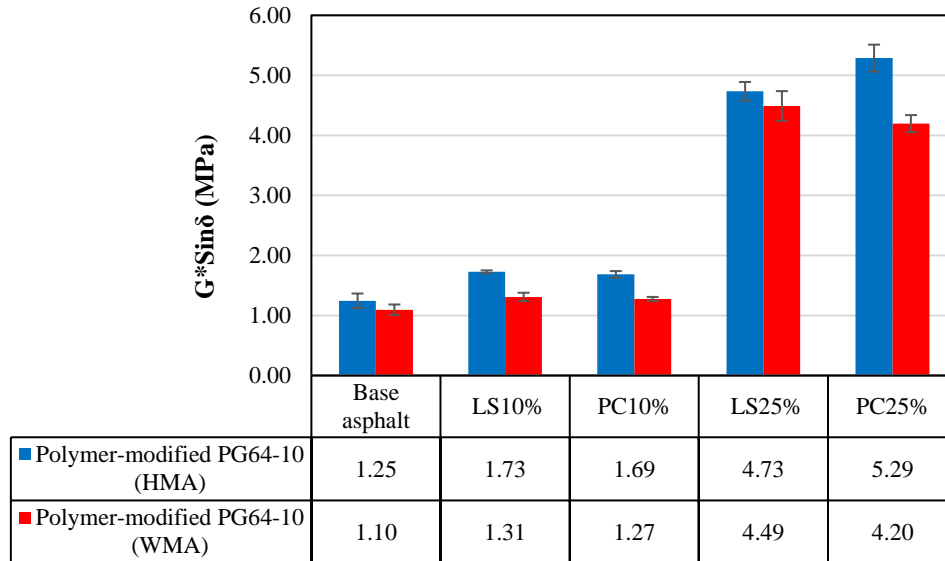


**Figure 4.30: Fatigue Performance for PAV-Aged HMA and WMA Polymer-modified PG64-10 Mastics at 31°C**

#### 4.6 Thermal-Cracking Resistance

Thermal cracking of pavements is an important parameter to evaluate, especially in cold climates, because this failure is induced by non-load-associated cracks (but still can be combined with excessive loadings). Thermal cracks are intermittent transverse cracks that form when the asphalt binder shrinks or contracts due to low temperatures. During this excessive shrinkage deformation, the tensile stresses within the asphalt layer exceed the tensile capacity of the material. These cracks typically form in aged material, and for this reason, the testing performed for thermal-cracking resistance uses PAV-aged to mimic the field conditions.

Thermal-cracking resistance testing was evaluated according to AASHTO T313 for PAV-aged materials using a Bending Beam Rheometer (BBR). This test was performed to determine the creep stiffness  $S(t)$  and  $m$ -value. Creep stiffness is the measurement of thermal stresses that result from the thermal contraction of the asphalt binder. Lower values of  $S(t)$  are desirable as they indicate a more elastic material that can reduce thermal cracking. According to Superpave® specifications,  $S(t)$  is required to be less than 300 MPa. The  $m$ -value is the rate at which the asphalt binder relieves stresses

through plastic flow, which is essentially the slope of the creep stiffness curve. Higher values of  $m$ -value are desirable as they indicate a less brittle material that can relax thermal stresses. Superpave specifications require that the  $m$ -value is a minimum of 0.3. Thermal-cracking resistance testing was evaluated at the low PG temperature plus 10°C (-18°C for PG58-28 and 0°C for PG64-10). Aside from the BBR test, Dynamic Mechanical Analysis (DMA) test was performed on a subset of investigated mastics. The mastics with 10% filler volume concentration were not included in the DMA testing. The parameters that were evaluated in this test were creep compliance and relaxation modulus. Creep compliance denotes the continuous flexural deformation of a given material under static loading. Lower shear stress represents a more elastic behavior at lower temperatures which is a desirable characteristic. Further, the relaxation modulus is the ability of a given polymer to reduce the applied stresses under a constant strain. In this regard, a higher relaxation modulus indicates a better performance of the mastic at low temperatures. To match the BBR testing, PG58-28-based and PG64-10-based mastics underwent DMA testing at -18°C and 0°C, respectively.

Figures 4-31 and 4-32 report the results for creep stiffness of HMA and WMA mastics based on PAV-aged PG58-28 and polymer-modified PG58-28 binders. The results indicate that higher filler content results in a higher creep stiffness, hence a more brittle mastic at low temperatures. However, adding a warm-mix modifier leads to a reduction in creep stiffness of a given mastic, which is a desirable outcome. Further, polymer-modified PG58-28-based mastic did not demonstrate higher stiffness than the companion non-polymer-modified mastics. This is also desirable since it indicates that material can be designed with higher stiffness due to polymer modification while retaining excellent performance at low temperatures. It should be noted that the 300 MPa benchmark, which is introduced as an acceptance criterion in Superpave® specification, is set for binders, not mastics. So, the low-temperature performance of mastics can deviate from the binder criteria indicated in the specification.

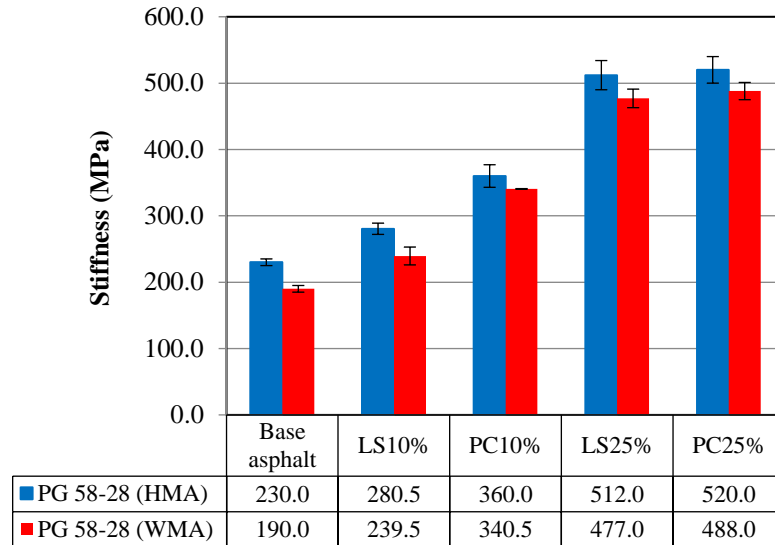


**Figure 4.31: Stiffness of PAV-Aged HMA and WMA PG58-28 Mastics at -18°C**

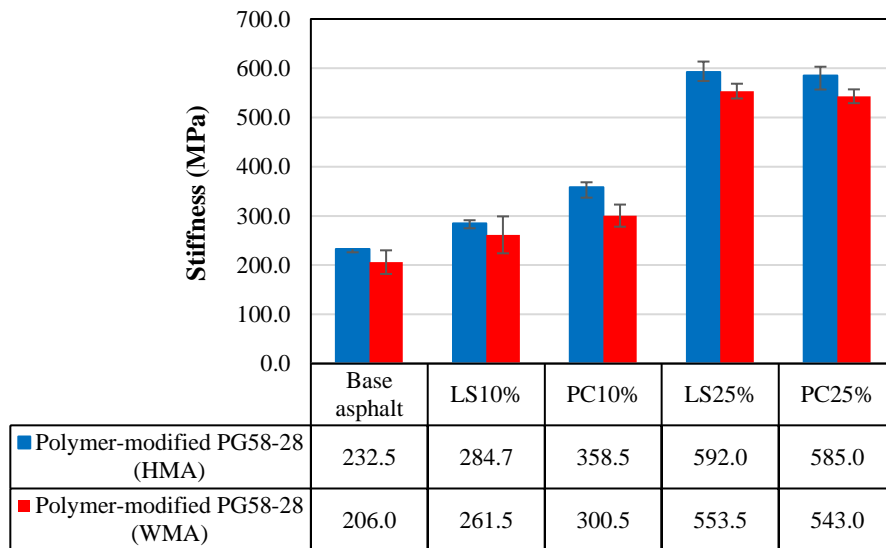


**Figure 4.32: Stiffness of PAV-Aged HMA and WMA Polymer-modified PG58-28 Mastics at -18°C**

Figures 4-33 and 4-34 report the result for creep stiffness performance of HMA and WMA PAV-aged mastics based on PG64-10 and polymer-modified PG64-10 binders at 0°C. The results indicate that higher filler volume concentrations increase the brittleness of a given mastic, especially for an LS filler. However, incorporation of a warm-mix modifier helps to reduce the

stiffness of mastics at low temperatures. It should be noted that polymer-modification led to a substantial increase in the stiffness of the mastics due to the high content of SBS polymer within the polymer-modified PG64-10 binder, which can result in a more brittle response at low temperatures. Moreover, it can be noted that HMA and WMA mastics based on PG64-10 and polymer-modified PG64-10 binders had a smaller stiffness than the companion mastics based on PG58-28 and polymer-modified PG58-28 binders. This outcome is predictable since PG64-10 is a softer bitumen than PG58-28 bitumen.

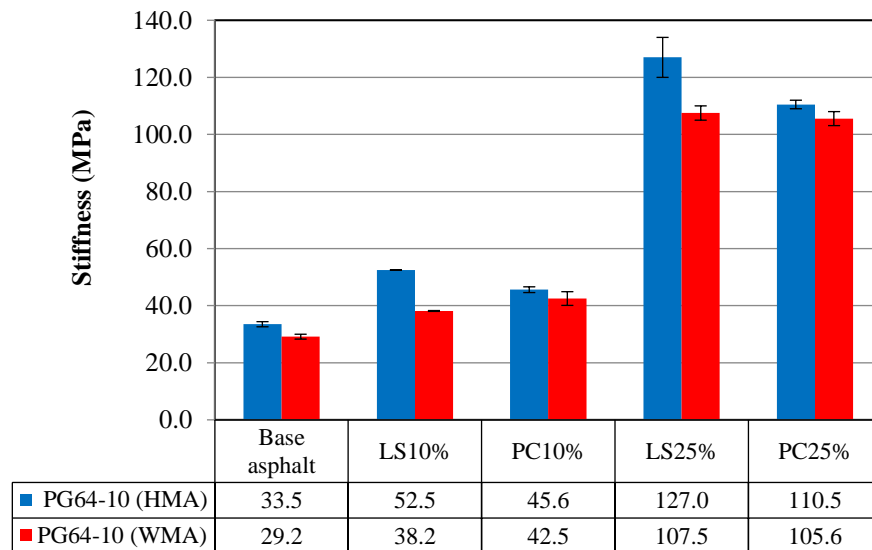


**Figure 4.33: Stiffness of PAV-Aged HMA and WMA PG64-10 Mastics at 0°C**

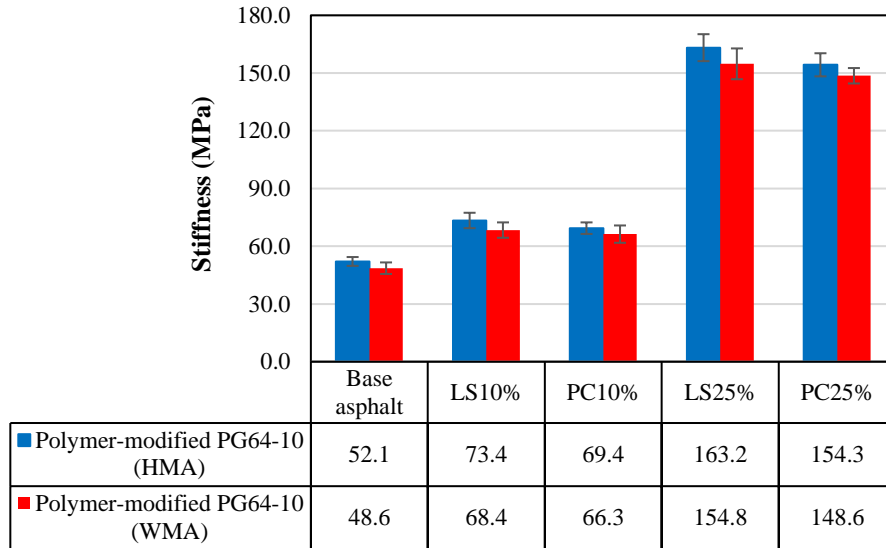


**Figure 4.34: Stiffness of PAV-Aged HMA and WMA Polymer-modified PG64-10 Mastics at 0°C**

Figures 4.35 through 4.38 report on the m-value of PVA-aged investigated mastics based on BBR testing. As it can be observed, the incorporation of a filler/reactive powder into an asphalt binder reduced the m-value of the mastics; however, the mastics containing PC reactive powder had a higher m-value than those containing LS filler, demonstrating a better performance at low temperature. Further, the incorporation of warm-mix additives resulted in a higher m-value when compared with the companion HMA mastics, which is a promising outcome. It should be noted that adding polymer modification led to a relatively higher m-value in the HMA and WMA mastics based on PG58-28 and polymer-modified PG58-28 binders.

As can be observed in Figures 4-37 and 4-38, the incorporation of warm-mix additives into asphalt mastics resulted in an increase in the m-value of the mastics based on PG64-10 and polymer-modified PG64-10 binders. However, polymer modification led to a substantial increase in the m-value of the mastics; this can be attributed to the high content of SBS polymer within the polymer-modified PG64-10 binder, which can result in a more brittle response at low temperatures. Further, by comparing the reported results in Figures 4-25 and 4-36 with those in Figures 4-37 and 4-38, it

can be concluded that the mastics based on PG64-10 and polymer-modified PG64-10 binders had higher m-value than the mastics based on PG58-28 and polymer-modified PG58-28 binders. This is due to the softer nature of PG64-10 binders, leading to better performance at low temperatures.

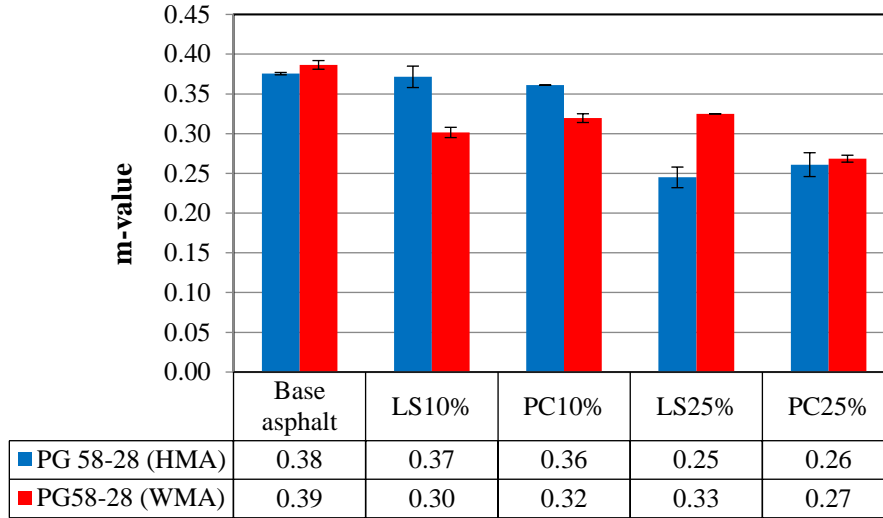


**Figure 4.35: m-value of PAV-Aged HMA and WMA PG58-28 Mastics at -18°C**

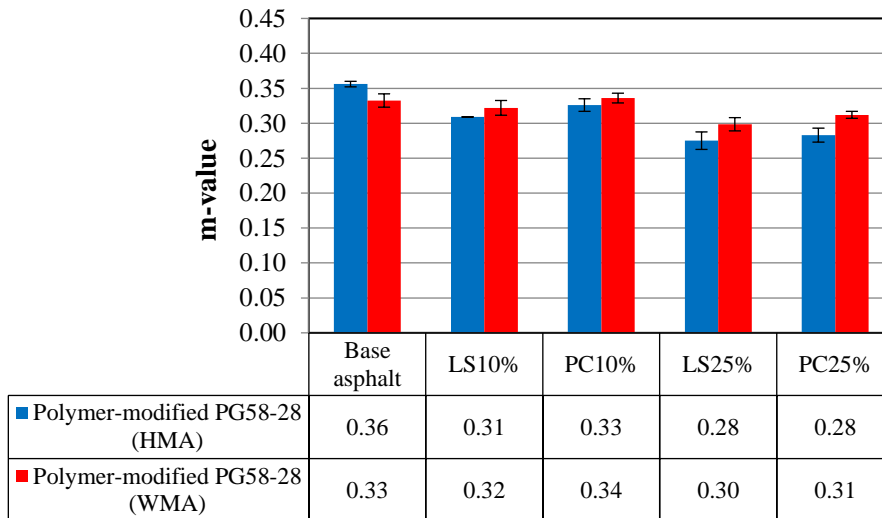


**Figure 4.36: m-value of PAV-Aged HMA and WMA HMA and WMA Polymer-modified PG58-28 Mastics at -18°C**

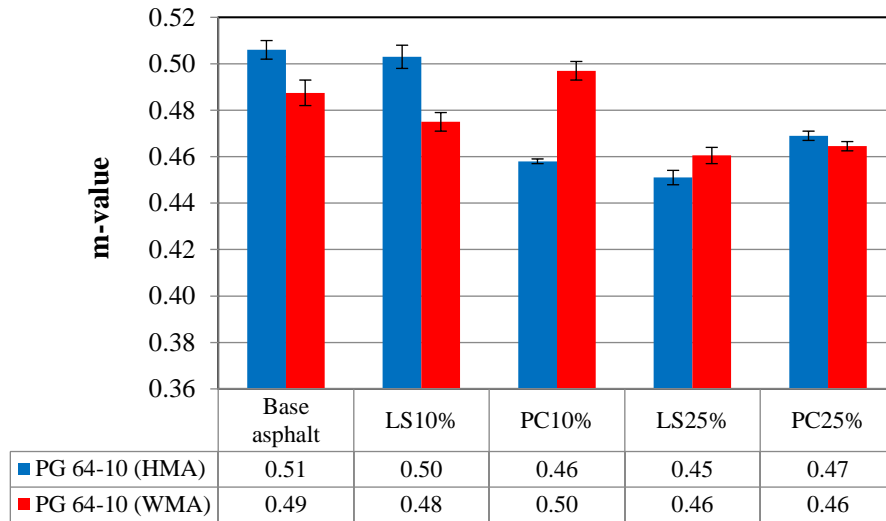


**Figure 4.37: m-value of PAV-Aged HMA and WMA PG64-10 Mastics at 0°C**

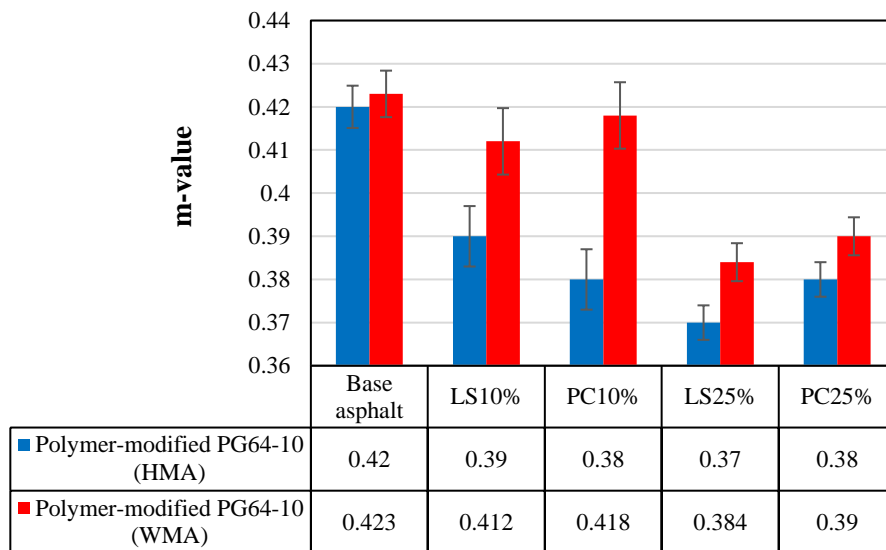


**Figure 4.38: m-value of PAV-Aged HMA and WMA Polymer-modified PG64-10 Mastics at 0°C**

Figures 4-39 and 4-40 report on the result for creep compliance of HMA and WMA PAV-aged mastics based on PG58-28 and polymer-modified PG58-28-based binders at -18°C. The results indicate that the incorporation of fillers leads to a smaller creep compliance, hence formation of a less elastic mastic at low temperatures. Moreover, adding a warm-mix modifier leads to a slight increase in creep stiffness for most of the investigated mastics, helping a given mastic to have a more elastic performance, which

can be beneficial for application in cold climates. Further, polymer-modified PG58-28-based mastics had relatively the same creep compliances as their respective non-polymer-modified mastics. This is a promising outcome, as it indicates that polymer-modification of PG58-28 would not result in a reduction of elastic performance at low temperatures.

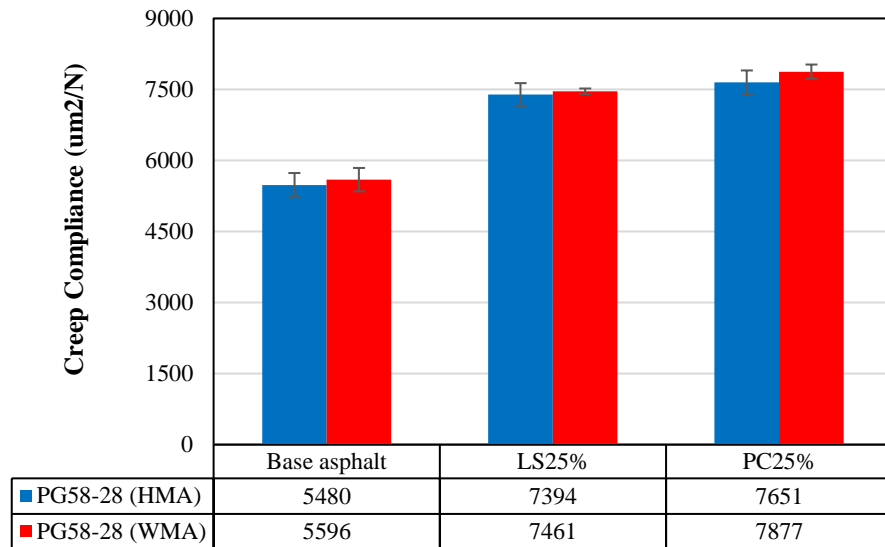


**Figure 4.39: Creep Compliance of PAV-Aged HMA and WMA PG58-28 Mastics at -18°C**

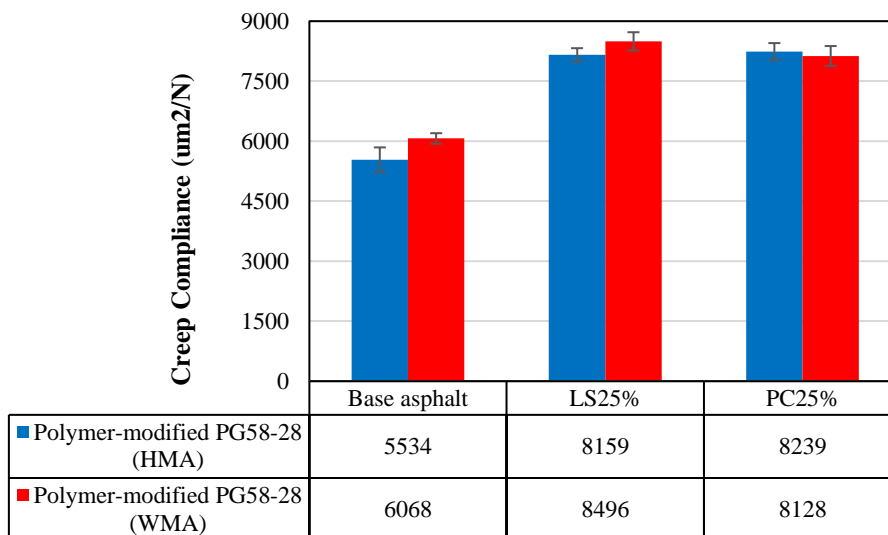


**Figure 4.40: Creep Compliance of PAV-Aged HMA and WMA Polymer-modified PG58-28 Mastics at -18°C**

Figures 4-41 and 4-42 report on the result for creep compliance of HMA and WMA PAV-aged mastics based on PG64-10 and polymer-modified PG64-10 binders at 0°C. The results indicate that increased filler content leads to a less elastic behavior of a given mastic. Also, polymer-modification increases the creep compliance of a mastic compared with the corresponding non-polymer-modified mastic, which is not desirable in terms of low-temperature performance. While the introduction of warm-mix additives did not have a significant effect on the creep compliance of mastics based on the plain and polymer-modified PG64-10 binders, polymer-modification led to an increase in the creep compliance of the mastics.

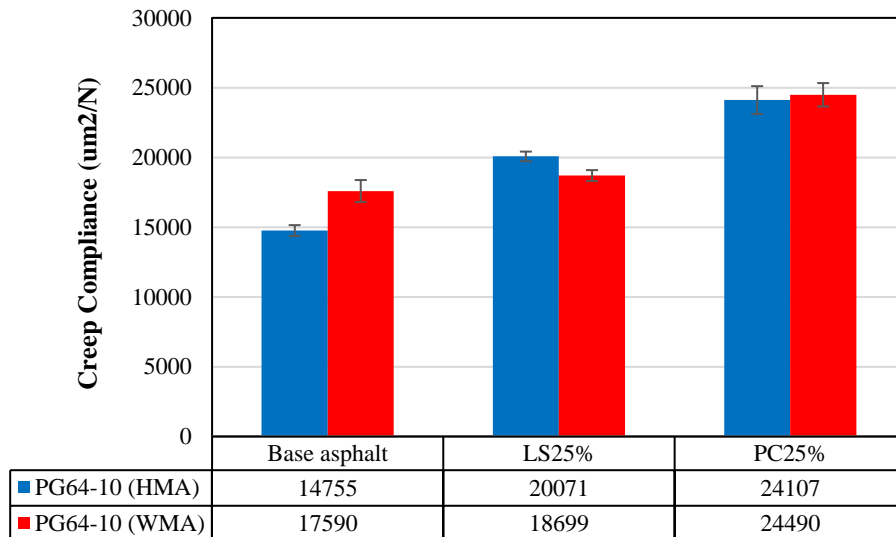


**Figure 4.41: Creep Compliance of PAV-Aged HMA and WMA PG64-10 Mastics at 0°C**

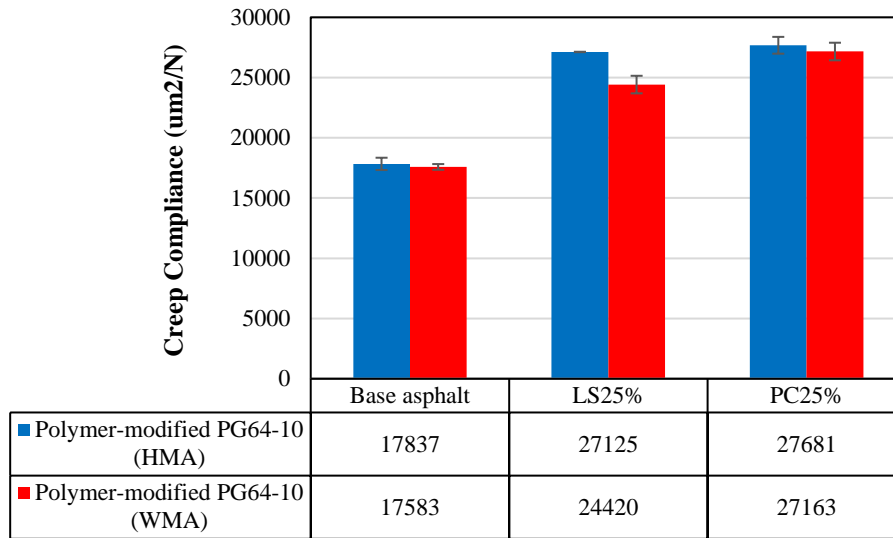


**Figure 4.42: Creep Compliance of PAV-Aged HMA and WMA Polymer-modified PG64-10 Mastics at 0°C**

Based on the reported result on the stiffness from the BBR test and creep compliance from the DMA test, Figures 4-43 and 4-44 demonstrate the trend line of the investigated mastics. In these figures, the X axis corresponds to the creep compliance values of a given mastic, which is obtained from the DMA test, while the Y axis corresponds to the stiffness of a given mastic obtained from the BBR test. In each data series, data dots with higher X and Y values belong to the filler-incorporated mastics.

As can be observed in Figure 4.43, the trend line for mastics based on PG58-28 binders is similar to the trend line for mastics based on polymer-modified PG58-28 binders. This proves that the investigated mastics demonstrate similar behavior at low temperatures under different test configurations. However, as indicated in Figure 4.44, the mastics based on the PG64-10 binder have a different trend from those mastics based on the polymer-modified PG64-10 binder. It is suspected that this difference is due to the high SBS content of the polymer-modified PG64-10 binder, making it very stiff at low temperatures, hence showing an unexpected response.

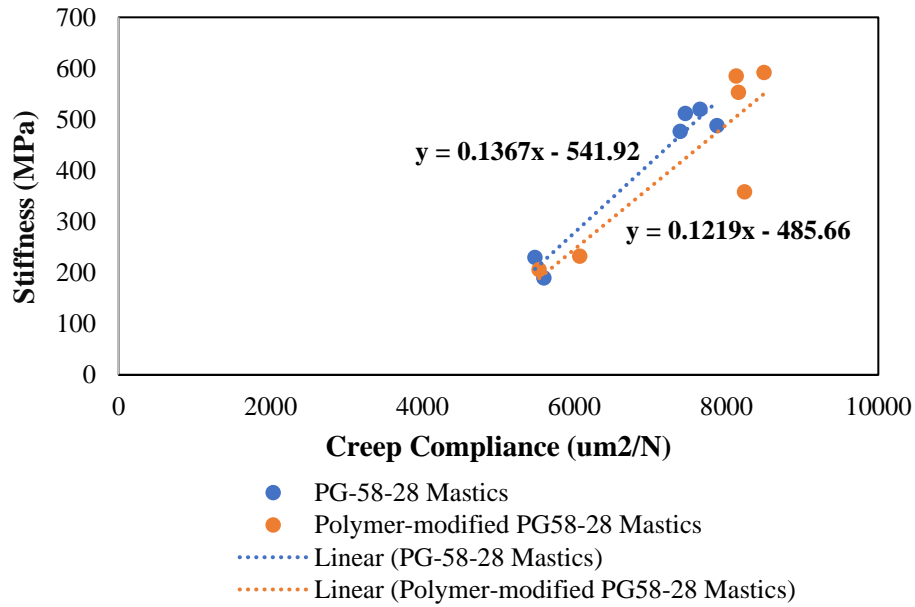


**Figure 4.43: Creep Compliance vs Stiffness of PAV-Aged HMA and WMA mastics Based on Plain and Polymer-modified PG58-28 Mastics at -18°C**

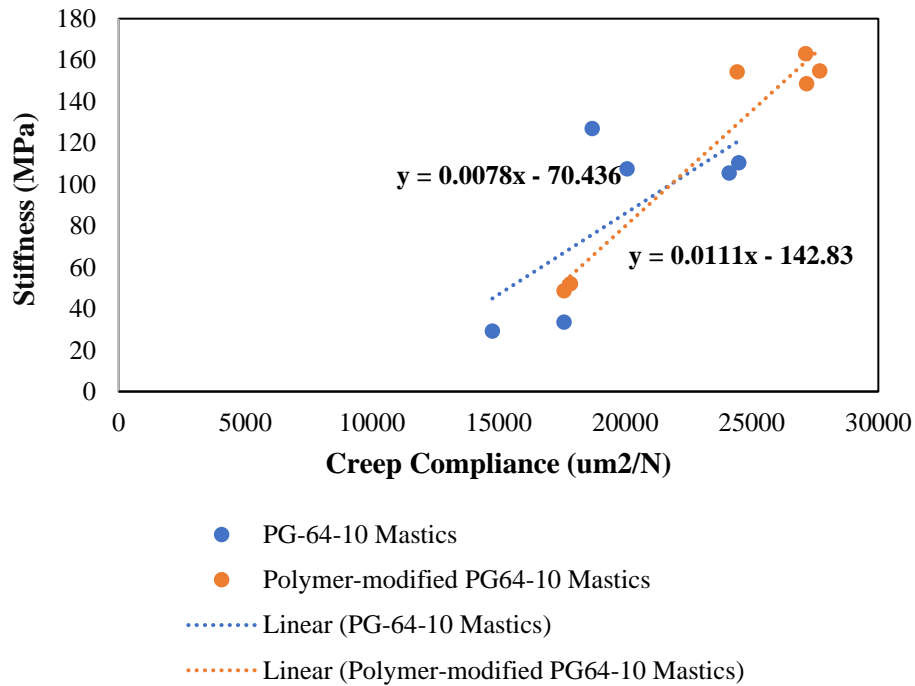


**Figure 4.44: Creep Compliance vs Stiffness of PAV-Aged HMA and WMA mastics Based on Plain and Polymer-modified PG64-10 Mastics at 0°C**

Figures 4.45 through 4.48 demonstrate the results for the relaxation modulus of PAV-aged HMA and WMA mastics based on PG58-28, and polymer-modified PG58-28, PG64-10, and polymer-modified PG64-10 binders under DMA testing. It can be concluded that polymer modification and filler incorporation lead to a reduced relaxation modulus; that is, such mastics have a smaller ability to reduce the applied stresses and a constant strain ratio, which is a non-favorable performance at low temperatures. In a reference system based on the PG58-28 binder, the use of the WMA additive leads to a significant reduction of the relaxation modulus (77%); however, this trend was not observed in all the investigated mastics and binders with the exception of polymer-modified PG58-10 LS 10. As indicated in Figures 4-47 and 4-48, the warm mix modification did not have a particular trend on the relaxation modulus of mastics based on plain and polymer-modified PG64-10 binders.

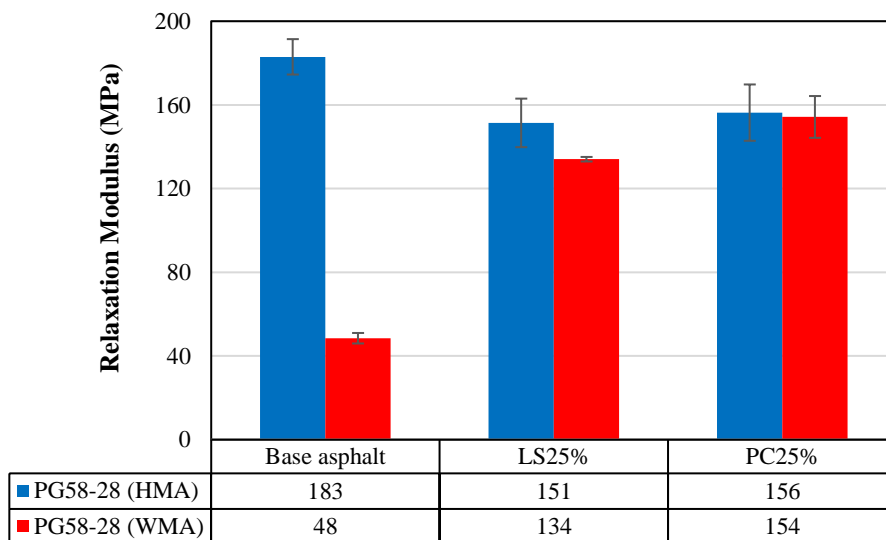


**Figure 4.45: Relaxation Modulus of PAV-Aged HMA and WMA PG58-28 Mastics at -18°C**

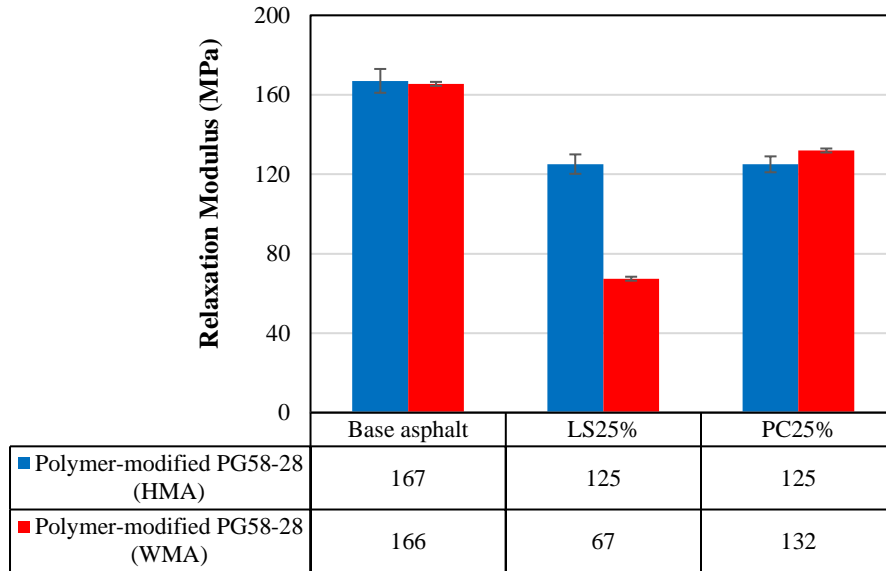


**Figure 4.46: Relaxation Modulus of PAV-Aged HMA and WMA Polymer-modified PG58-28 Mastics at -18°C**

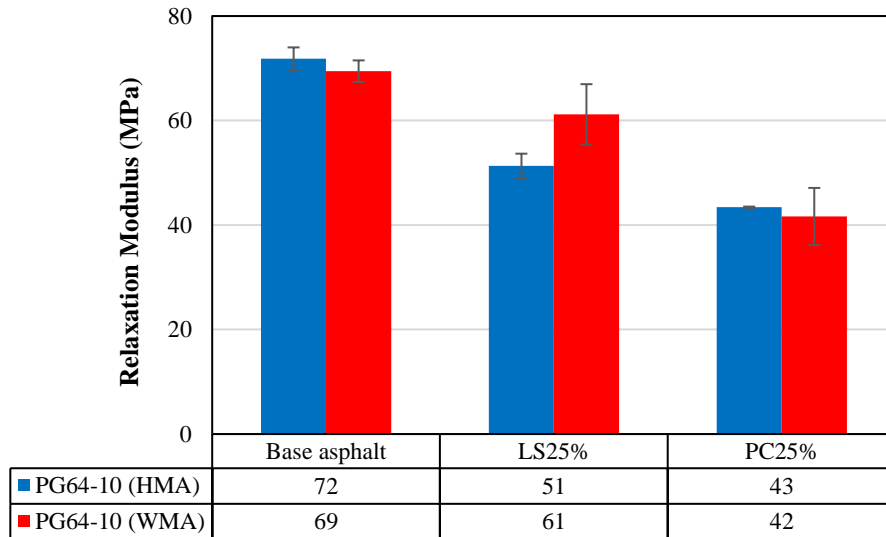


**Figure 4.47: Relaxation Modulus of PAV-Aged HMA and WMA PG64-10 Mastics at 0°C**

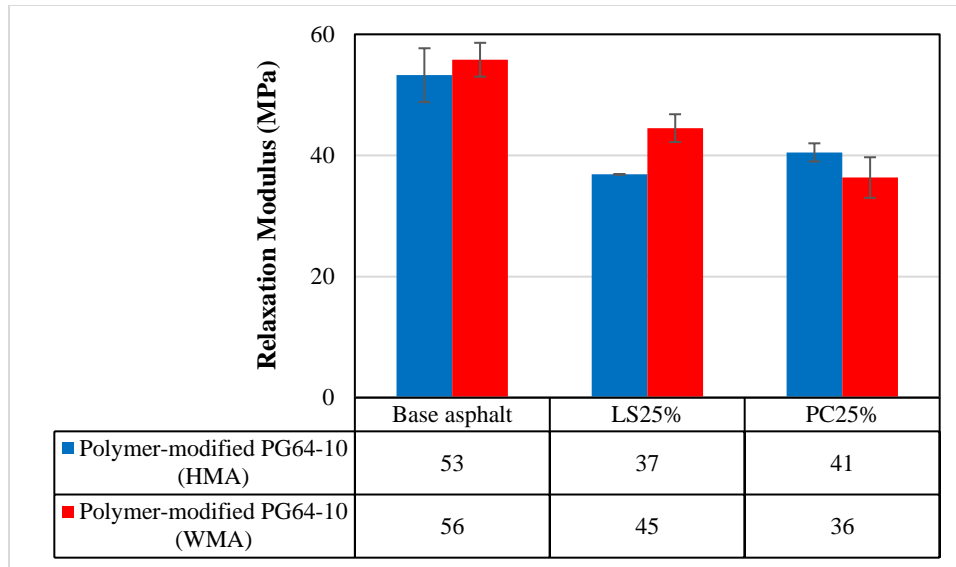


**Figure 4.48: Relaxation Modulus of PAV-Aged HMA and WMA Polymer-modified PG64-10 Mastics at 0°C**

Based on the performance of PAV-aged mastics at intermediate and high service temperatures, it can be concluded that adding a warm-mix modifier results in better behavior at such temperatures for almost all of the mastics due to the softening effect of the warm-mix agent. In the case of PG58-28-based mastics, it can be observed that the polymer modification resulted in a similar performance compared with non-polymer-modified mastics, which is a very promising outcome, indicating that the polymer-modified mastics in addition to superior performance at high-temperatures, can serve well at an extended range of temperatures. However, the polymer modification did not yield better performance for PAV-aged PG64-10-based mastics at intermediate and low service temperatures. This outcome can be explained by mentioning that PG64-10 binder was polymer-modified in the lab at a relatively high 4% of SBS, which may have made such a binder over-polymer-modified, while the polymer-modified PG58-28 binder was commercially available. Further, filler incorporation negatively affected the low-temperature performance of PAV-aged mastics, regardless of the binder type. This was expected, as filler

incorporation has a stiffening effect on the mastics. Here, the enhancement of low-temperature performance still needs an innovative solution.

## CHAPTER 5: PERFORMANCE OF MIXTURES

After characterizing the behavior of mastics at high, intermediate, and low temperatures, and evaluating the effect of the asphalt binder PG grade, polymer and warm-mix modification, and the type of reactive powder, this chapter focuses on evaluating the behavior of asphalt concrete mixtures at working temperatures. To do this, eight (8) asphalt concrete mixtures were designed, produced, and characterized: 1) WMA PG58-28 S based on a regular PG58-28 binder, warm-mix modifier and no fillers, 2) WMA PG58-28 S LS40 containing PG58-28 binder, warm-mix modifier and 40% (by volume) replacement of the binder with LS filler, 3) WMA PG58-28 S PC40 containing a regular PG58-28 binder, a warm-mix modifier and 40% (by volume) replacement of binder with PC reactive powder, 4) WMA PG58-28 P containing polymer-modified PG58-28 binder, warm-mix modifier and no fillers, 5) WMA PG58-28 P LS40 containing a polymer modified PG58-28 binder, a warm-mix modifier and 40% (by volume) replacement of the binder with LS filler, 6) WMA PG58-28 P PC40 containing a polymer modified PG58-28 binder, a warm-mix modifier and 40% (by volume) replacement of the binder with PC reactive powder, 7) WMA PG64-10 P containing a lab grade polymer-modified PG64-10 binder, a warm-mix modifier with no fillers, and 8) WMA PG64-10 P PC40 containing a lab grade polymer modified PG64-10 binder, a warm-mix modifier and 40% (by volume) replacement of binder with PC reactive powder by volume. The 40% volume replacement was chosen to make the most use of replacing asphalt binder with filler/reactive powder particles, which are still cheaper and more sustainable materials. The following section provides an assessment of mixtures based on several criteria, including aggregate coating, constructability, moisture damage resistance, fatigue resistance, and low-temperature thermal-cracking resistance. To evaluate the aggregate coating, workability, and aging, six replicates were produced and compared. For the remaining criteria, including moisture

damage resistance, fatigue resistance, and low-temperature thermal-cracking resistance, two replicates were produced and tested. Detailed descriptions of the experimental testing methods are provided by the subsequent sections.

### **5.1 Asphalt Mixtures**

To conduct the mixture testing, PC reactive powder and LS filler particles were incorporated into the asphalt mix, replacing 40% of the binder by volume. The mixtures were prepared using a job mix formula (JMF) approved by the Wisconsin DOT and had a nominal maximum aggregate size (NMAS) of 12.5 mm. Three types of binders were utilized for these mixtures: WMA PG58-28, WMA polymer-modified PG58-28, and WMA polymer-modified PG64-10. The 4-MT WMA control mixtures were designed with an optimum asphalt content of 6.1%. However, due to the incorporation of PC and LS materials at 40% by binder volume replacement, the asphalt content was reduced to only 3.5%. It should be noted that the LS filler and the PC reactive powder were treated as a part of the binder phase rather than as an aggregate component. To evaluate the impact of the added fillers/reactive powder on the performance indicators of mixtures, a control mixture (mixed without replacement of bitumen with filler particles) was used for comparison purposes.

### **5.2 Aggregate Blends**

Table 5.1 presents the aggregate JMF (Job Mix Formula) combinations along with their respective blend percentages, which were utilized in the development of the mixtures. It is noteworthy to mention that although the use of RAP (reclaimed asphalt pavement) was suggested in JMF, it was not used in this study in order to omit the affecting parameters other than the type of incorporated powders on the performance of investigated asphalt mixtures.

**Table 5.1: The 4-MT Job Mix Formula Determining Combination of Aggregates (by WisDOT)**

Aggregate Type	Combination (%)
5/8" Chips	17.95
3/8" Chips	10.26
Manufactured Sand	34.61
Natural Sand	36.54
Dust	0.64

Table 5.2 presents the values for particle size distributions (PSD) of different types of aggregates. Meanwhile, Figure 5.1 illustrates the actual PSD curves for each of these aggregate types. Table 5.2 and Figure 5.1 depict the particle size distribution of the Job Mix Formula (JMF), which was determined using the specific blend percentages provided in Table 5.1.

**Table 5.2: Particle Size Distribution (PSD) for All Aggregate Types**

Sieve		5/8" Chips	3/8" Chip	Manufactured Sand	Natural Sand	Limestone Dust	JMF
(std)	(mm)						
1 1/2"	37.5	100	100	100	100	100	100
1"	25	100	100	100	100	100	100
3/4"	19	100	100	100	100	100	100
1/2"	12.5	80	100	100	100	100	96.4
3/8"	9.5	28	100	100	100	100	84.8
#4	4.75	3	30	97	94	100	72.2
#8	2.36	2	6	66	84	100	51.2
#16	1.18	2	4	35	73	100	40.2
#30	0.6	2	4	17	58	100	28.5
#50	0.3	2	4	7	22	100	11.9
#100	0.15	2	4	3	2	100	3.2
#200	0.075	1.8	3.6	1.9	1	100	2.4

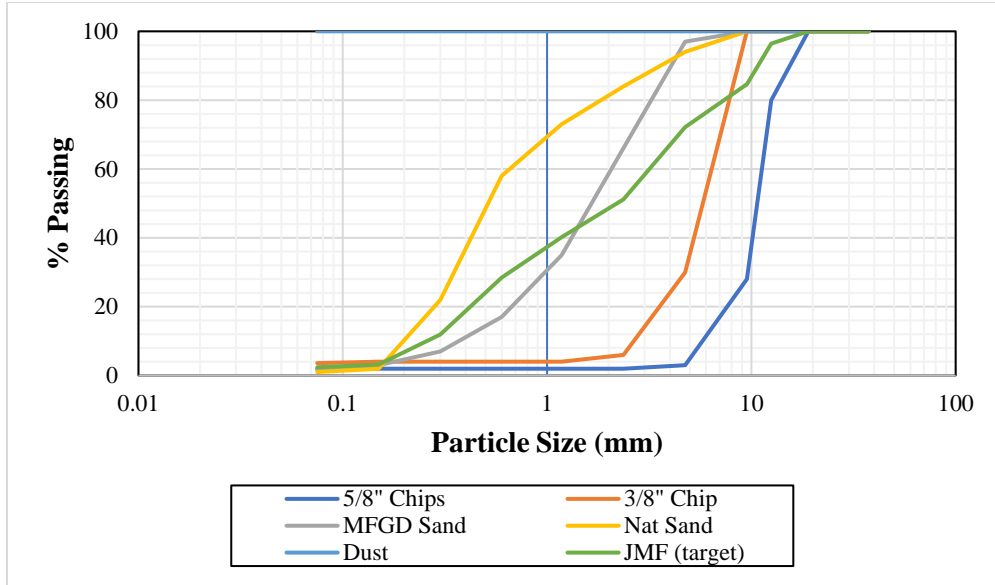


**Figure 5.1: Aggregate Particle Size Distribution Graphs**

The PSD curve of the JMF mixture was utilized to compare against the 0.45 power curve based on the maximum aggregate size incorporated in the mixture. Figure 5.2 depicts that the composite curve of JMF closely resembles the 0.45 power curve, thereby indicating an ideal aggregate configuration.

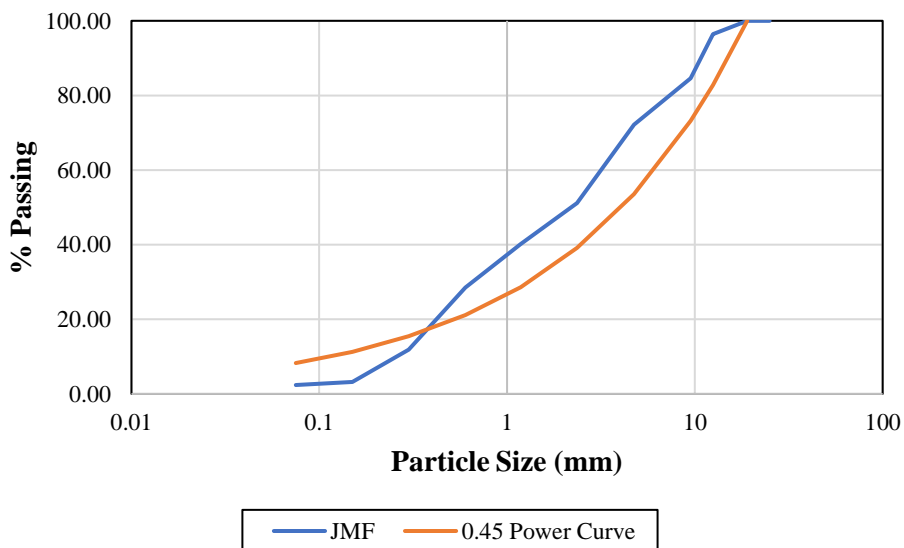


**Figure 5.2: JMF vs. 0.45 Power Curve Particle Size Distribution Graph**

Although the particle size distribution of JMF appeared similar to the 0.45 power curve, it was imperative to assess its adherence to the Superpave® gradation limits. The gradation limits with JMF's combination particle size distribution are depicted in Figure 5.3. It can be observed that the 0.45 power curve corresponds to the maximum density line where the particles can be arranged (and re-arranged during compaction) in the densest possible configuration. The JMF particle size distribution line adheres to all control points, which is essential since these points represent the extremities for the gradation to pass through. Furthermore, the JMF combination curve does not intersect the restricted zone, implying that the mixture is not over-sanded.

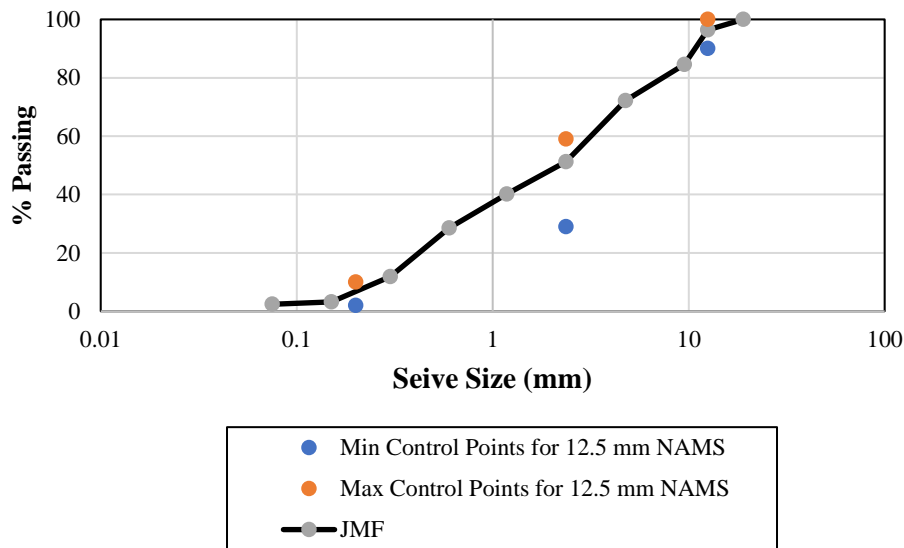


**Figure 5.3: Superpave® Gradation Limitations**

### 5.3 Aggregate Coating

The assessment of appropriate aggregate coating for all the investigated mixtures involved the evaluation of asphalt film thickness. This parameter was deemed crucial, given that mixtures containing LS filler and PC reactive powder involved an extremely high 40% binder replacement by volume, which reduces the available binder for coating the aggregates. Asphalt film thickness is a measure of the average thickness of the asphalt layer surrounding the aggregate particles and

has been directly linked to the durability of the mixture. Inadequate thickness of the asphalt film may result in easy air transport through the material, leading to oxidation of the binder, which may subsequently cause the asphalt to become brittle and fracture. Additionally, insufficient film thickness results in the ingress of water through the binder layer, allowing it to saturate the aggregate particles, leading to moisture damage, binder separation, weakening of the contact zone, and causing issues such as rutting, raveling, and freeze-thaw damage.

Although Superpave® design requirements do not include evaluation of asphalt film thickness, evaluating aggregate coating was deemed crucial. Studies have reported that asphalt film thickness should typically fall within the range of 6 to 11  $\mu\text{m}$  (Hmoud 2011). This thickness range is considered optimal for establishing a sufficiently thick coating around the aggregate particles, preventing rapid oxidation and moisture damage.

Table 5.3 presents the surface area factors, percent passing values of the asphalt mixtures, and surface area measurements of aggregates. It is evident from the table that the cumulative surface area of aggregates incorporated in all WMA mixtures was approximately 4.52  $\text{m}^2/\text{kg}$ .

**Table 5.3: Calculated Surface Area of Aggregates**

Sieve Size	Surface Area Factors	Percent Passing	Surface Area ( $\text{m}^2/\text{kg}$ )
Maximum (19.0mm)	2	100	0.41
No.4 (4.75mm)	2	72.2	0.3
No.8 (2.36mm)	4	51.2	0.42
No. 16 (1.18mm)	8	40.2	0.66
No. 30 (0.6)	14	28.5	0.82
No. 50 (0.3)	30	11.9	0.73
No. 100 (0.15)	60	3.2	0.39
No. 200 (0.075mm)	160	2.4	0.79
		SUM	4.52

**Table 5.4: Asphalt Film Thickness for Investigated Mixtures**

Sieve Size	Control Mixture	40% LS-based Mixture	40% PC-based Mixture
Surface Area of Aggregates (m <sup>2</sup> /kg)/ (ft <sup>2</sup> /lb)	4.52/ 22.07	4.52/ 22.07	4.52/ 22.07
Bulk Specific Gravity of Aggregates	2.668	2.668	2.668
Effective Specific Gravity of Aggregates	2.742	2.742	2.742
Asphalt Specific Gravity	1.017	1.017	1.017
Asphalt Content (%)	6.1	3.5	3.5
Total Weight of Aggregates (g)	4700	4700	4700
Asphalt Volume (mL)	277.75	161.75	161.75
Asphalt Absorbed (by weight of aggregates)	0.966	0.993	0.993
Weight of Absorbed Asphalt (g)	45.15	46.67	46.67
Volume of Absorbed Asphalt (mL)	44.64	45.89	45.89
Effective Volume of Asphalt (mL)	233.11	115.86	115.86
Film Thickness (FT) (microns)	12.03	5.93	5.93

The observed film thickness in the control mixtures is slightly higher than the expected range, due to the relatively high binder volume used, whereas for the 40% Ls-based mixtures and 40% PC-based mixtures, the film thickness falls slightly below the anticipated range. However, these findings are deemed acceptable given the significant quantity of asphalt that is substituted with fillers.

#### **5.4 Constructability**

To assess the workability, the densification curves of the control mixtures were compared with those containing LS filler, and also mixtures with PC reactive powder were compared. The workability of the mixtures was assessed through the compaction data for short-term aged materials, as this reflects the physical state of the material during mixing, placement, and compaction in real-world conditions. In this context, lower compaction efforts were indicative of better workability characteristics. The PG58-28-based and polymer-modified PG58-28-based mixtures were mixed at a temperature of 120°C and compacted at 115°C, while the polymer-

modified PG64-10-based mixtures, due to their high viscosity, were mixed at an evaluated temperature of 150°C and compacted at 145°C.

Figures 5.4, 5.5, and 5.6 depict the workability results for WMA PG58-28-based, polymer-modified WMA PG58-28-based, and polymer-modified PG64-10-based mixtures, respectively. The specimens were compacted to 100 gyrations to evaluate the material behavior over a wide range of gyrations while maintaining a critical parameter of approximately 96-97%  $G_{mm}$  (3-4% air voids) in accordance with Superpave® compaction requirements. Regarding WMA PG58-28-based and polymer-modified PG58-28-based mixtures, it can be reported that mixtures containing 40% PC reactive powder outperform the control mixtures and mixtures containing LS filler in terms of compaction effort since smaller numbers of gyration are required for PC-based mixtures to get to the same  $G_{mm}$ %. As an example, WMA PG58-28 S PC40 reached to 92%  $G_{mm}$  at 25 gyrations, while WMA PG58-28 S and WMA PG58-28 S LS40 reached to the same  $G_{mm}$  at 31 and 28 gyrations, respectively. This is a desirable outcome. Although the binder content, that acts as a lubricating agent in the mixing process, was reduced from 6.1% to 3.5%, and still less compaction effort was required to reach the desired  $G_{mm}$ %. Further, it was indicated that PC particles, surrounded by the bitumen phase, can greatly fit into the voids between the aggregates, resulting in a denser and more stable particle-reinforced matrix. However, the compaction effort for the WMA PG64-10 P PC40 was higher than that for WMA PG64-10 P. It should be mentioned that during the experimental phase, attempts were made to mix WMA PG64-10 P LS 40, but the mix did not reach to 93%  $G_{mm}$  after 115 gyrations, so the mix was excluded from the remaining tests.

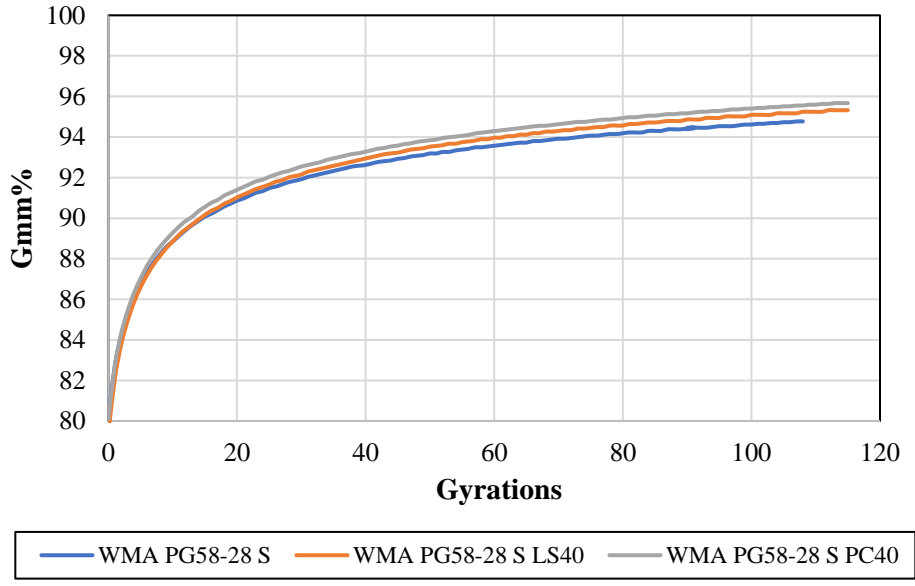


**Figure 5.4: Densification Curves for WMA PG58-28 Mixtures**

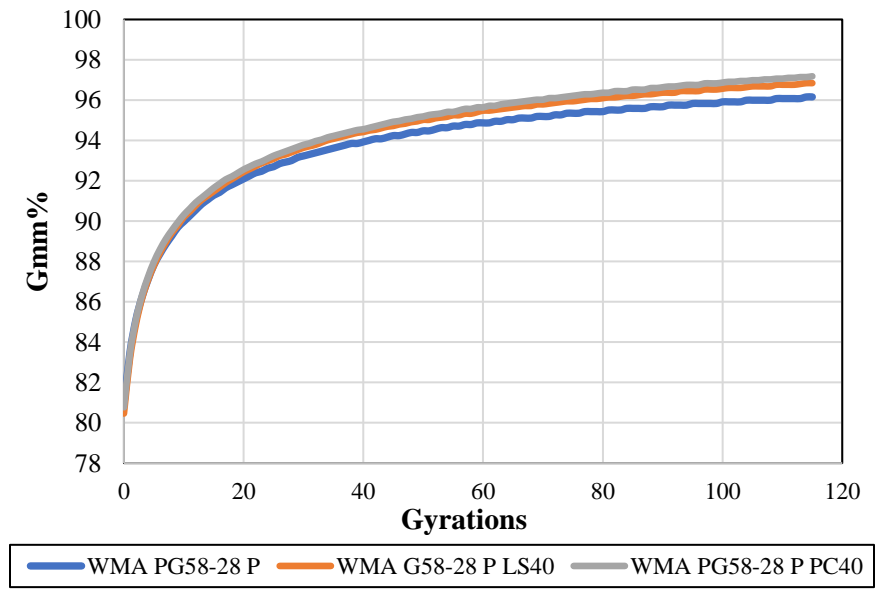


**Figure 5.5: Densification Curves for Polymer-modified WMA PG58-28 Mixtures**

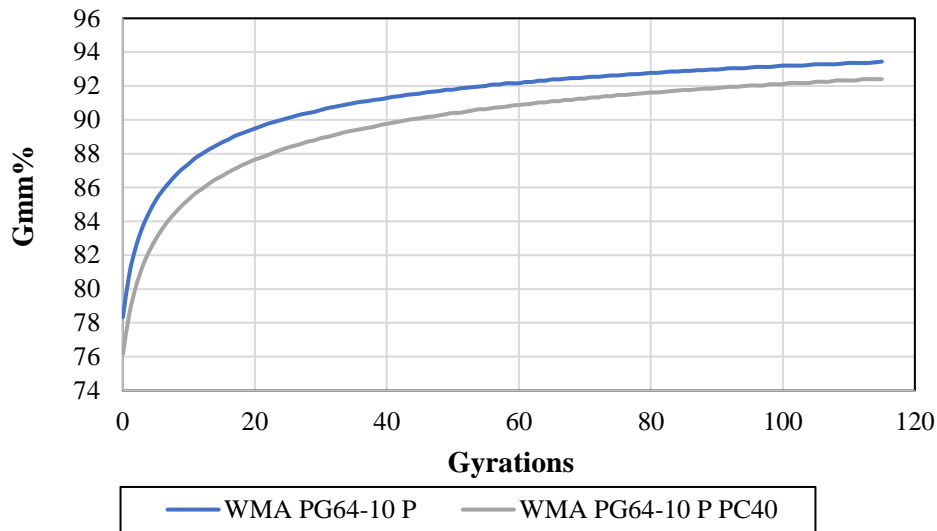


**Figure 5.6: Densification Curves for Polymer-modified WMA PG64-10 Mixtures**

The compaction volumetrics were analyzed to figure out the dissimilarities between the control mixtures and the LS-based and PC-based mixtures containing 40% powder. Tables 5.5, 5.6, and 5.7 illustrate the mixture volumetrics for the WMA PG58-28 S, WMA PG58-28 P, and WMA PG64-10 P mixtures, respectively. It can be observed from the reported data that both the bulk specific gravity ( $G_{mb}$ ) and the maximum specific gravity ( $G_{mm}$ ) increased with the addition of the LS filler and the PC reactive powder. This increase is attributable to the higher specific gravity of the powders (LS, 2.85; PC, 3.15) in comparison with the specific gravity of the asphalt binder (1.017). As 40% of the binder was replaced with the fillers (by volume), the bulk and mix-specific gravities increased proportionally.

Based on Table 5.5, it can be reported that VMA, VFA, and the dust-to-binder ratio for the PG58-28-based mixtures were within the specified ranges. For polymer-modified PG58-28 mixtures, by analyzing the results in Table 5.6, it can be concluded that the VMA and dust-to-binder ratio are within the range, but VFA (volume of voids in the aggregates filled by asphalt) for

the mixtures containing fillers, exceeds the upper limit (78%). This approach can be justified based on the consideration of LS and PC as components of the binder phase rather than of the aggregate phase. The replacement of the binder with a filler was conducted on a volume basis rather than on a mass basis. As the specific gravity of the fillers was found to be greater than that of the asphalt binder, more binder and filler by mass were incorporated into the mix design. This, in turn, resulted in the filling of more voids within the aggregates. Therefore, the resulting increase in the bulk specific gravity and maximum specific gravity values observed in the mix design may be attributed to the additional mass of the binder and filler that was included in the design, leading to a more densely packed mix with a reduced level of voids. Based on the results indicated in Table 5.7 for polymer-modified PG64-10 mixtures, it can be reported that VMA and the dust-to-binder ratio parameters are within the range, but VFA is smaller than the lower limit (65%). This is attributed to the fact that the polymer-modified PG64-10 binder was highly viscous, even at the mixing temperature of 150°C, so the binder with aggregates mixing was challenging, leading to the formation of a less optimal structure.

**Table 5.5: The Volumetrics of WMA PG58-28 Asphalt Mixture**

Mixture	WMA PG58-28 S	WMA PG58-28 S LS40	WMA PG58-28 S PC40
$G_{mm}$	2.465	2.486	2.587
$G_{mb}$	2.339	2.440	2.475
$G_{sb}$	2.668	2.668	2.668
$G_{se}$	2.742	2.742	2.742
$G_b$	1.017	1.017	1.017
Design P(%)	6.1	3.5	3.5
$P_{ba}$ (%)	0.966	0.993	0.993
$P_s$ (%)	93.9	89.8	89.2
$P_{be}$ (%)	5.19	2.61	2.61
VMA (%) > 14%	17.68	17.87	17.25
$V_a$ (%) at 100 Gyrations	5.38	4.91	4.60
VFA (%) (65-78)	69.57	72.52	73.33
Dust-to-Binder Ratio < 1.2	0.45	0.90	0.90

**Table 5.6: The Volumetrics of Polymer-modified WMA PG58-28 Asphalt Mixture**

Mixture	WMA PG58-28 P	WMA PG58-28 P LS40	WMA PG58-28 P PC40
G <sub>mm</sub>	2.409	2.471	2.502
G <sub>mb</sub>	2.316	2.393	2.432
G <sub>sb</sub>	2.668	2.668	2.668
G <sub>se</sub>	2.742	2.742	2.742
G <sub>b</sub>	1.017	1.017	1.017
Design P(%)	6.1	3.5	3.5
P <sub>ba</sub> (%)	0.966	0.993	0.993
P <sub>s</sub> (%)	93.9	89.8	89.2
P <sub>be</sub> (%)	5.19	2.61	2.61
VMA (%)> 14%	18.48	19.46	18.69
V <sub>a</sub> (%) at 100 Gyrations	4.08	3.43	3.12
VFA (%) (65-78)	77.92	82.37	83.33
Dust-to-Binder Ratio <1.2	0.45	0.90	0.90

**Table 5.7: The Volumetrics of Polymer-modified WMA PG64-10 Asphalt Mixture**

Mixture	WMA PG64-10 P	WMA PG58-28 P PC40
G <sub>mm</sub>	2.472	2.601
G <sub>mb</sub>	2.311	2.387
G <sub>sb</sub>	2.668	2.668
G <sub>se</sub>	2.742	2.742
G <sub>b</sub>	1.017	1.017
Design P(%)	6.1	3.5
P <sub>ba</sub> (%)	0.966	0.993
P <sub>s</sub> (%)	93.9	89.2
P <sub>be</sub> (%)	5.19	2.61
VMA (%)> 14%	18.66	20.19
V <sub>a</sub> (%) at 100 Gyrations	6.55	7.98
VFA (%) (65-78)	64.89	60.47
Dust-to-Binder Ratio <1.2	0.45	0.90

### 5.5 Moisture Susceptibility

The durability of asphalt pavements was assessed by using moisture susceptibility as a parameter. Asphalt specimens were subjected to testing under various environmental conditions to determine the effects of moisture on the performance. The testing involved the use of dry, saturated, and

conditioned environments. The dry samples were enclosed in a leak-proof plastic bag and submerged in a water bath at a temperature of  $25 \pm 0.5^\circ\text{C}$  for a duration of 2 hours  $\pm$  10 minutes, after which the samples were tested using the Indirect Tensile (IDT) test method. The saturated and conditioned specimens were vacuum-saturated to a degree of saturation of 70 to 80%, with the saturated specimens also being placed in a water bath at a temperature of  $25 \pm 0.5^\circ\text{C}$  for a duration of 2 hours  $\pm$  10 minutes prior to being tested using the IDT method. The conditioned samples, on the other hand, were immersed in a water bath at a temperature of  $60 \pm 1^\circ\text{C}$  for a duration of  $24 \pm 1$  hours, followed by exposure in a water bath at a temperature of  $25 \pm 0.5^\circ\text{C}$  for 2 hours  $\pm$  10 minutes prior to being subjected to testing using the IDT method.

Table 5-8 through 5-10 present the results of the Indirect Tensile Test (IDT) conducted on dry and conditioned asphalt samples for PG58-28-based, polymer-modified PG58-28-based, and polymer-modified PG64-10-based mixtures, respectively. Based on the results reported in Tables 5.5 and 5.6, PC reactive powder mixtures for both WMA PG58-28 and polymer-modified WMA PG58-28 mixes demonstrated higher strengths when compared with the control mixture and LS-based mixtures, but at the expense of a reduced flow (displacement) in most instances. It is worth noting that load and displacement tend to have an inverse relationship, implying that a rise in the maximum load would lead to a decrease in the maximum flow. Specifically, for the dry polymer-modified WMA PG58-28 samples, the PC40 mixture demonstrated the highest ultimate strength of 10.67 kN, while the polymer-modified PG58-28 control mixture exhibited the lowest ultimate load of 7.26 kN. Additionally, the polymer-modified WMA PG58-28 control samples had the highest flow (displacement) of 2.08 mm, while the WMA PG58-28 P PC40 samples demonstrated the lowest flow of 1.81 mm, thereby highlighting the inverse relationship between the load and deformation. In the case of dry WMA PG58-28 samples, the PC mixture had the highest ultimate

strength of 11.31 kN, while the control mixture exhibited the lowest strength of 8.89 kN. Notably, the WMA PG58-28 S PC40 samples had the average lowest flow of only 1.21 mm, whereas the WMA PG58-28 S samples had the average highest flow of 2.33 mm. Additionally, it can be observed that conditioning the samples reduces the maximum load due to moisture damage; however, the rate of reduction is smaller when polymer modification is incorporated. Particularly, conditioned WMA PG58-28 S PC 40 samples experienced a 7% reduction of maximum load when compared with dry samples, while the conditioned WMA PG58-28 P PC40 samples had only a 3% reduction in the maximum load compared with the dry samples.

**Table 5.8: Moisture Damage Load and Flow Results for WMA PG58-28 Mixtures**

Sample	Environment	Max Load (kN)	Max Flow (mm)
WMA PG58-28 S	Dry	8.89	2.33
	Conditioned	8.520	2.21
WMA PG58-28 S LS40	Dry	10.42	1.54
	Conditioned	8.99	1.00
WMA PG58-28 S PC40	Dry	11.31	1.45
	Conditioned	10.50	1.21

**Table 5.9: Moisture Damage Load and Flow Results for WMA Polymer-modified PG58-28 Mixtures**

Sample	Environment	Max Load (kN)	Max Flow (mm)
WMA PG58-28 P	Dry	7.26	2.08
	Conditioned	7.13	2.01
WMA PG58-28 P LS40	Dry	7.43	1.84
	Conditioned	7.08	1.75
WMA PG58-28 P PC40	Dry	10.67	1.81
	Conditioned	10.34	1.21

Based on the results in Table 5.10 it can be reported that the PC-based polymer modified PG64-10 mixture had a lower average maximum load compared with the control mixture due to its less dense structure and the presence of more air voids. Moreover, the rate of decrease in maximum

load after sample conditioning for the control mixture is lower than that of the PC-based mixture. While the WMA PG64-10 P experienced only a 6% reduction in the maximum load, WMA PG64-10 P PC40 had a 12% reduction in the maximum load. This also can be attributed to the less dense structure with more air voids in the PC-based polymer-modified PG64-10 mixture, which allows water to penetrate through the air voids.

**Table 5.10: Moisture Damage Load and Flow Results for WMA Polymer-modified PG64-10 Mixtures**

Sample	Environment	Max Load (kN)	Max Flow (mm)
WMA PG64-10 P	Dry	17.37	1.33
	Conditioned	16.27	1.22
WMA PG64-10 P PC40	Dry	11.05	1.54
	Conditioned	9.68	0.96

Figures 5-7 through 5-9 depict the horizontal tensile stress, which correlates with the maximum load results presented in Tables 5-8 through 5-10. The results demonstrate that in the case of WMA PG58-28 and polymer-modified WMA PG58-28, the maximum horizontal stresses for the PC reactive powder mixtures were higher than the control mixtures and LS-based mixtures under all environmental conditions. For the dry WMA PG58-28 samples, the PC mixtures exhibited the highest maximum horizontal stress at all environmental conditions. Similarly, for the polymer-modified WMA PG58-28 samples, the PC mixtures had the highest maximum horizontal stress at all environmental conditions. The observed trend suggests that as environmental exposure becomes more severe, the ultimate stress resisted by the specimen decreases. Further, it is indicated that WMA PG64-10 P mixtures had a higher resistance for horizontal stresses compared with WMA PG58-28 S and WMA PG58-28 P mixtures.

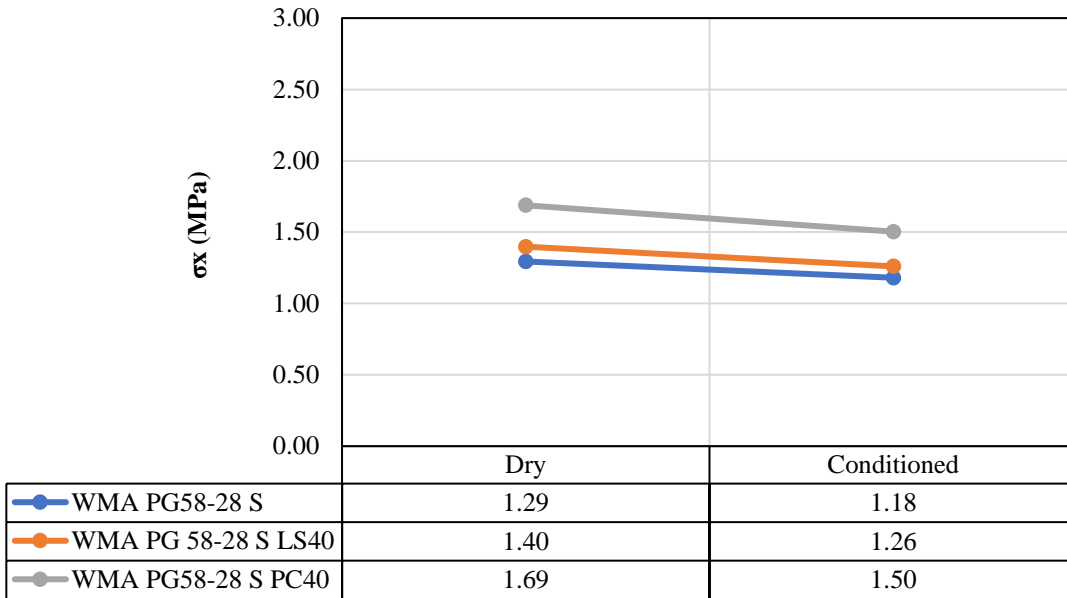


Figure 5.7: Horizontal Tensile Stress at Center of Samples for WMA PG58-28 Mixtures

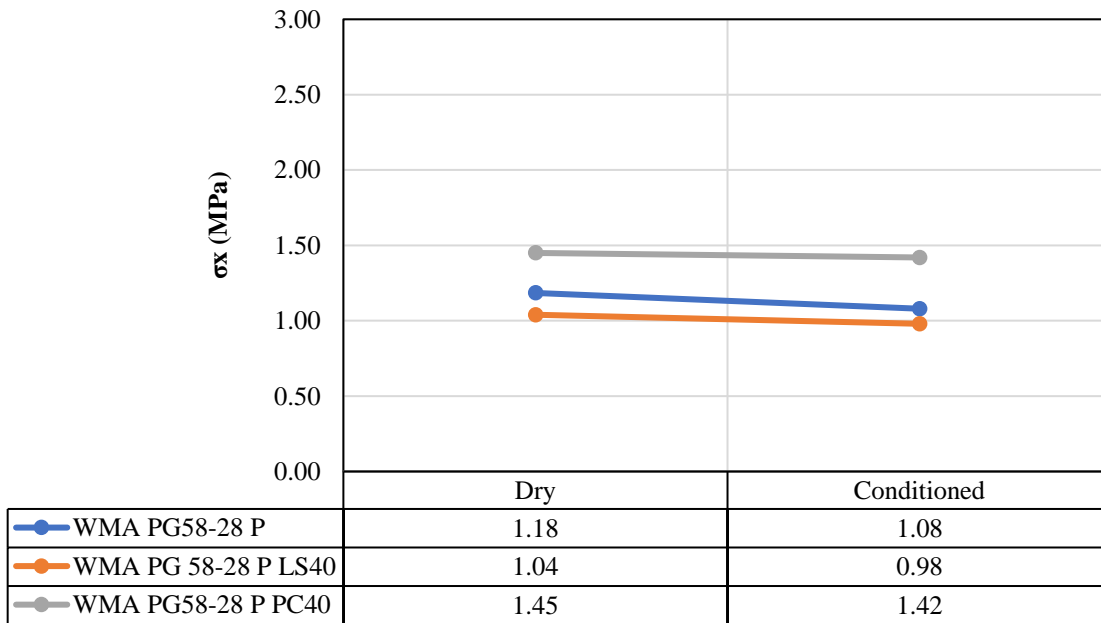
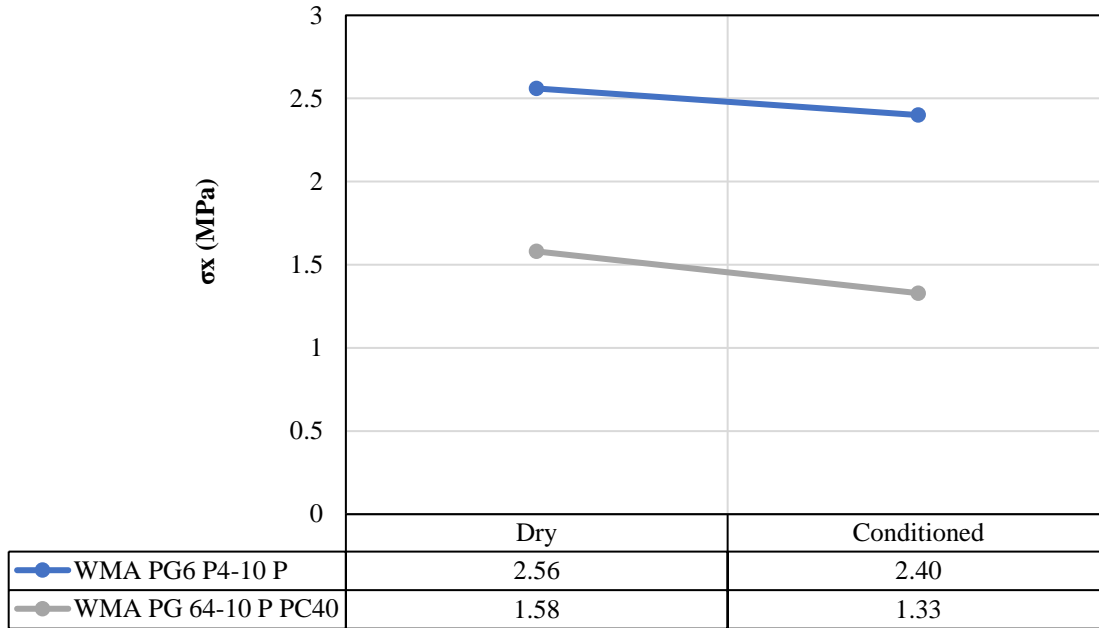
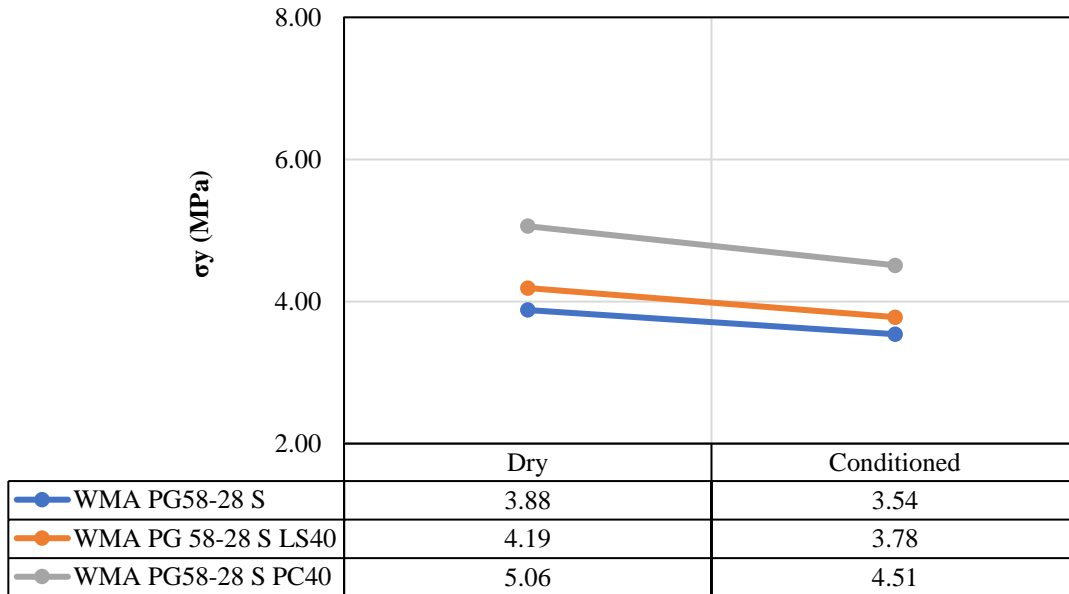


Figure 5.8: Horizontal Tensile Stress at Center of Samples for Polymer-modified WMA PG58-28 Mixtures



**Figure 5.9: Horizontal Tensile Stress at Center of Samples for Polymer-modified WMA PG64-10 Mixtures**

Figures 5-10 through 5-12 illustrate the ultimate vertical compressive stress of the mixtures, which directly correlates with the horizontal tensile stress results. The research data confirms that the maximum vertical stresses of the reactive powder mixtures based on WMA PG58-28 S and WMA PG58-28 P compositions were higher than the control and LS-based mixtures under all environmental conditions. For dry WMA PG58-28 samples, the PC 40 mixtures exhibited the highest maximum vertical stress in all environmental conditions. Similarly, for dry polymer-modified WMA PG58-28 samples, the PC reactive powder mixture displayed the highest maximum vertical stress at all environmental conditions. Comparing the reported results in Figure 5-12 with those indicated in Tables 5-10 and 5-11, it can be reported that polymer-modified WMA PG64-10 mixtures had higher ultimate vertical stresses than WMA PG58-28 and polymer-modified WMA PG58-28 mixtures; however, WMA PG64-10 P PC40 experienced lower vertical stress than WMA PG64-10 P.



**Figure 5.10: Vertical Compressive Stress at Center of Specimen for WMA PG58-28 Mixtures**

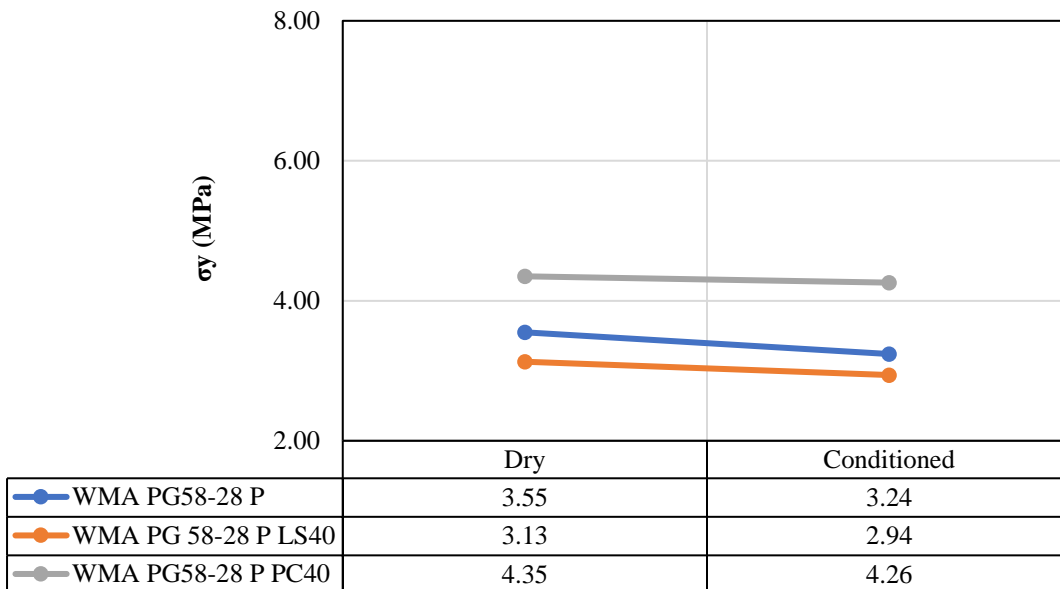


**Figure 5.11: Vertical Compressive Stress at Center of Specimen for Polymer-modified WMA PG58-28 Mixtures**

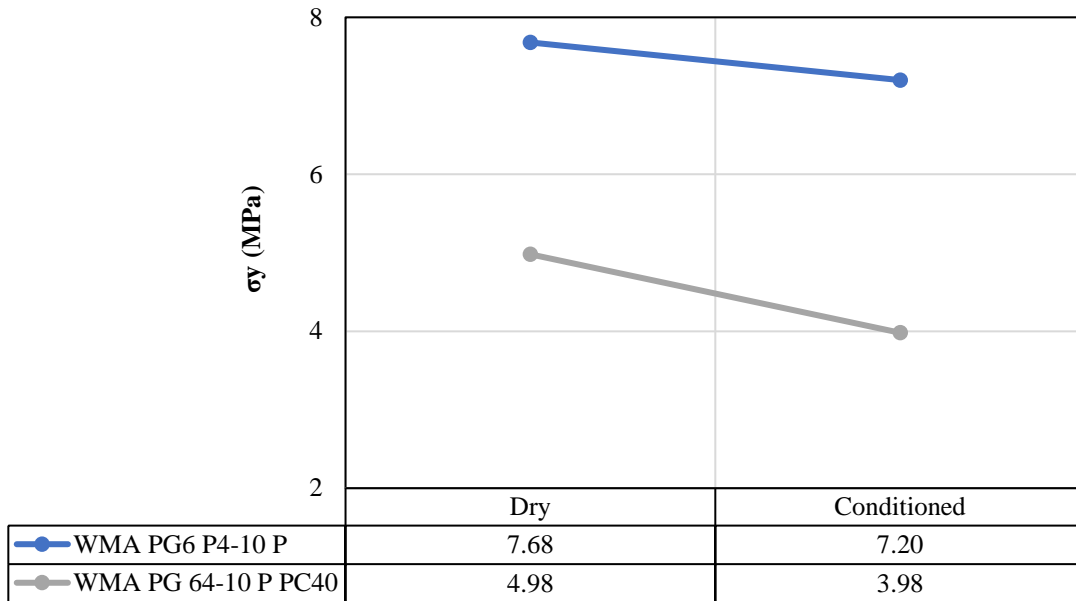


**Figure 5.12: Vertical Compressive Stress at Center of Specimen for Polymer-modified WMA PG64-10 Mixtures**

Figures 4.50 and 4.51 depict the tensile strain at failure for the WMA PG58-28 mixtures and WMA PG52-34 mixtures, respectively. These results offer a graphical representation of the maximum flow (displacement) outcomes presented in Tables 5-8 through 5-10. The research data highlights the impact of moisture damage on the deformability of asphalt pavements. For dry WMA PG58-28 samples, the control mixture displayed the highest strain at failure of 1.21 mm/mm, while the dry WMA PG58-28 S PC40 samples had an average tensile strain of 0.76 mm/mm. Comparing the reported results in Tables 5-13 and 5-14, it can be found that polymer modification resulted in a reduction in the ultimate strain of PG58-28-based mixtures. In all cases, the strain at failure was reduced for the saturated specimens when compared with the dry specimens. Based on the reported results in Table 5.15, it can be observed that the ultimate strain of polymer-modified PG64-10 is higher than that of the PC-based polymer-modified PG64-10 mixture. Based on the results reported in this section, it can be concluded that by exposing asphalt mixtures to moisture, not only the load resistance but also their deformability is reduced. However, incorporating PC reactive powder into

the mixture improves the ultimate load-bearing capacity of compositions based on plain and polymer-modified PG58-28 binders. The results for polymer-modified PG64-10 mixtures were different from the obtained results for other types of binders/mixtures.

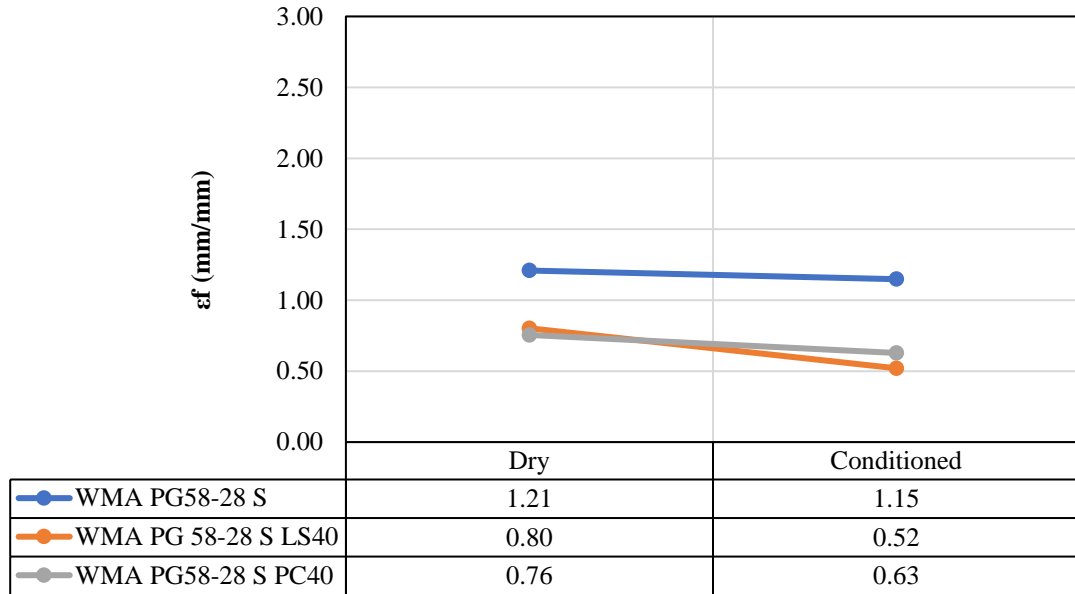


**Figure 5.13: Tensile Strain at Failure for WMA PG58-28 Mixtures**

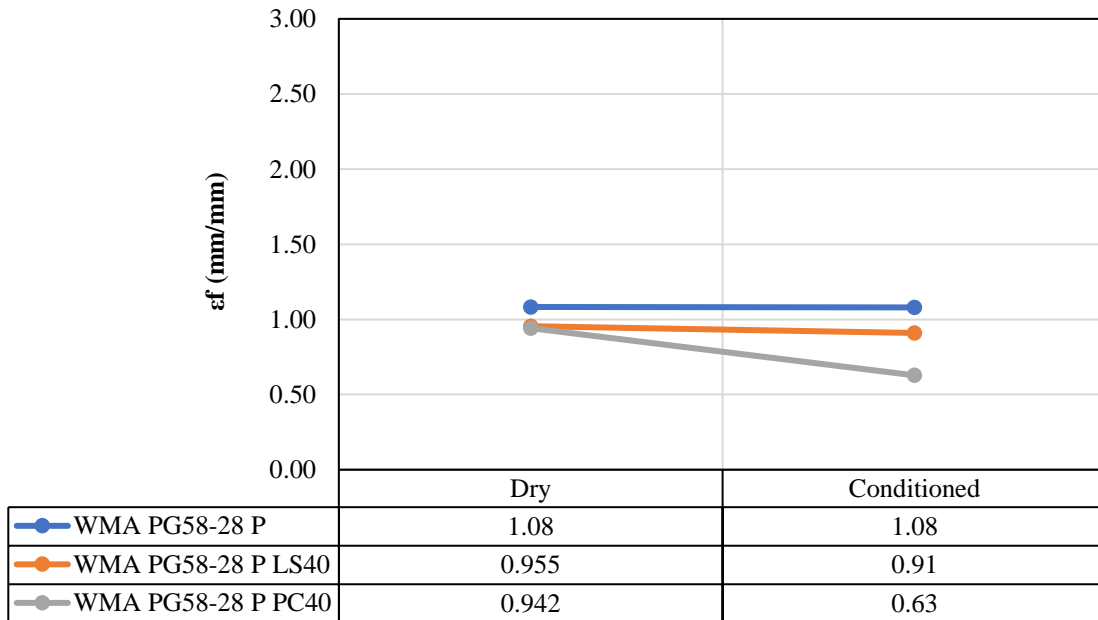


**Figure 5.14: Tensile Strain at Failure for Polymer-modified WMA PG58-28 Mixtures**

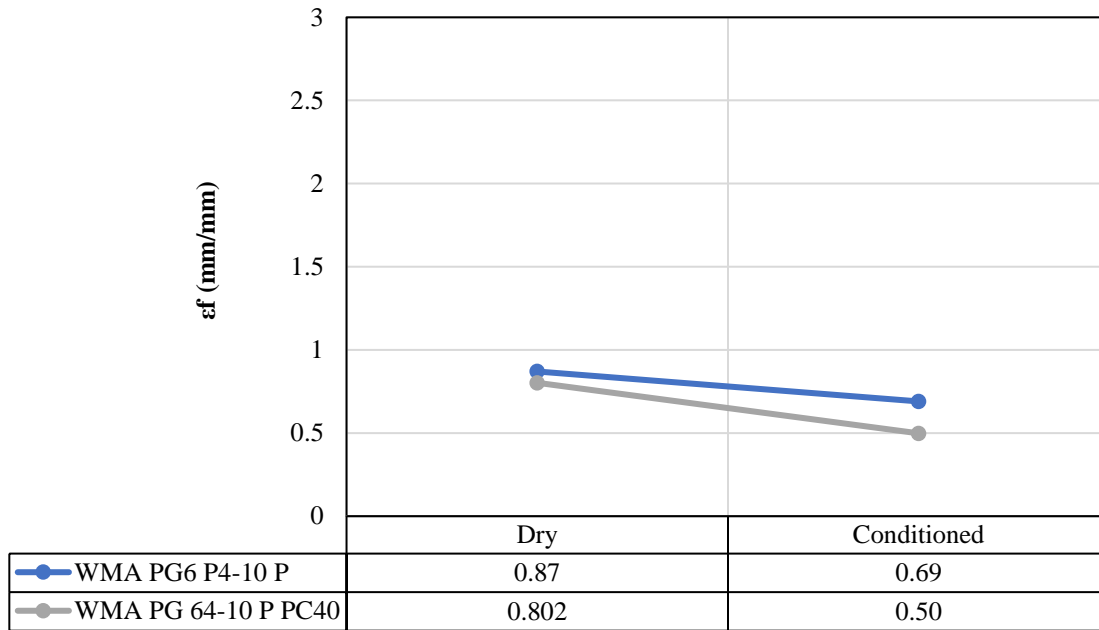


**Figure 5.15: Tensile Strain at Failure for Polymer-modified WMA PG64-10 Mixtures**

The Tensile Strength Ratio (TSR) was evaluated on the investigated asphalt mixtures under both dry and conditioned states, and the outcomes are reported in Figures 5-16 through 5-18. The results prove that all mixtures fulfilled the minimum requirement of TSR values at or above 0.80, indicating a satisfactory resistance to moisture damage. However, the control mixture exhibited better TSR values than the LS-based mixture and PC reactive powder mixtures made of WMA PG58-28 binder. Still, the differences between the control and filler-incorporated mixtures were minimal, as the control mixture only showed a TSR that was 1.1% higher than the LS-based samples and 2.2% higher than the PC-based samples for the WMA PG58-28-based specimens. In contrast, for the polymer-modified WMA PG58-28-base specimens, the mixture containing PC reactive powder had a superior performance with a TSR of that was 7.7% and 4.3% higher than that of the control mixture and LS-based mixture, respectively. In the case of polymer-modified PG64-10 mixtures, the control mixture had a TSR that was 10.6% higher than PG64-10 P PC40.

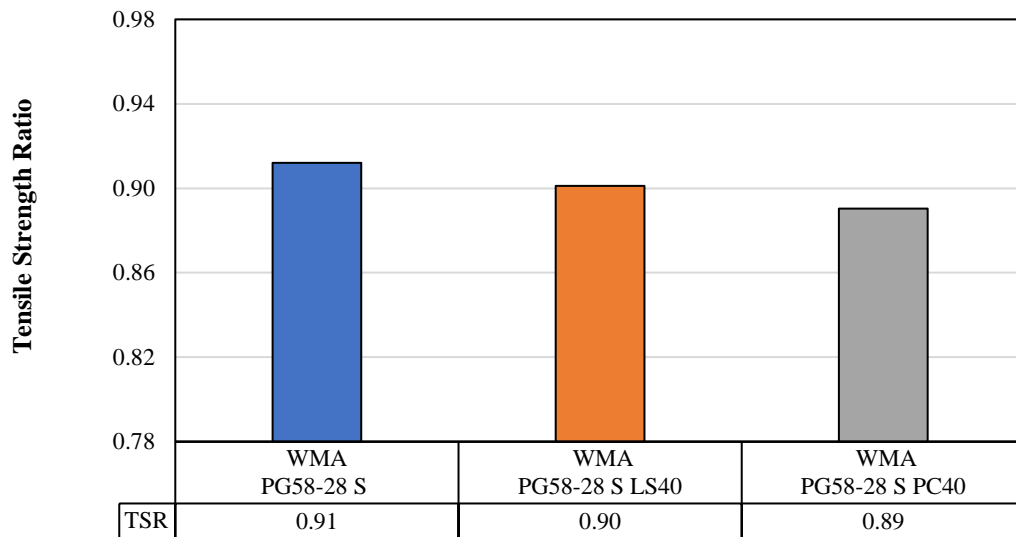


**Figure 5.16: TSR for WMA PG58-28 Mixtures**

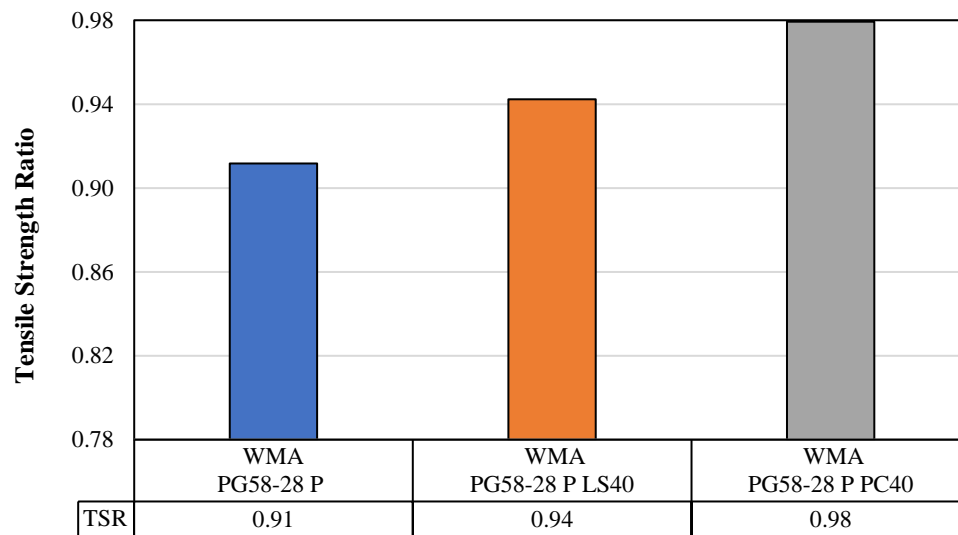


**Figure 5.17: TSR for Polymer-modified WMA PG58-28 Mixtures**

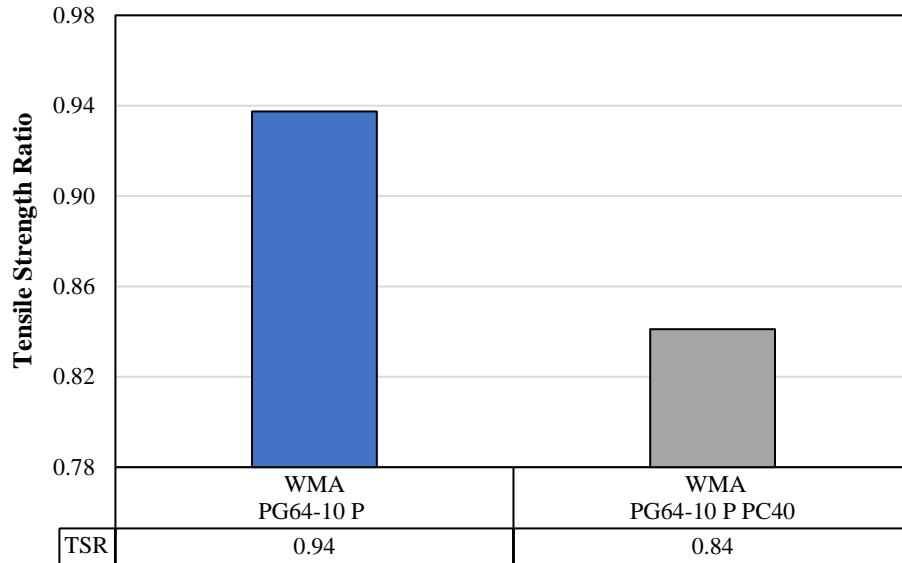


**Figure 5.18: TSR for Polymer-modified WMA PG64-10 Mixtures**

### 5.6 Fatigue Resistance

Fatigue tests were conducted on the asphalt concrete specimens to evaluate their ability to withstand a certain number of cycles before failure. This testing was achieved by determining the slope of the secondary fatigue section and identifying the failure point ( $N_f$ ), that makes the onset of the tertiary fatigue section (See Figure 3.31). It was observed that at this point, the complex modulus ( $E^*$ ) began to decrease, resulting in an increase in the slope of the deformation (strain) line. The desired asphalt pavements exhibited lower deformation rates and greater endurance to cycles until failure. Two specimens were tested for WMA PG58-28 S, WMA PG58-28 SLS40, WMA PG58-28 S PC40, WMA PG58-28 P, and WMA PG58-28 P LS40 mixtures, and one specimen was tested for WMA PG58-28 P PC40, WMA PG64-10 P, and WMAPG64-10 PC40 mixtures, due to samples' availability.

In this study, fatigue was assessed through the application of a sine wave loading condition, with a test temperature range of 20 to 25°C, a 0.1 kN pre-loading condition, a 10% ultimate loading condition, and a frequency of 10 Hz. Following evaluation of the results from the indirect tensile

test (IDT) test for dry samples, the following constant loads were applied to the specimens: 0.892 kN for WMA PG58-28 S specimens, 1.04 kN for WMA PG58-28 S LS40 specimens, 0.131 kN for WMA PG58-28 S PC40 specimens, 0.73 kN for WMA PG58-28 P specimens, 0.74 kN for WMA PG58-28 P LS40 specimens, 1.07 kN for WMA PG58-28 P PC40 specimen, 1.74 kN for WMA PG64-10 P specimen, and 1.11 kN for WMA PG64-10 P PC40 specimen. The fatigue test was conducted with a failure criterion of either the occurrence of failure in the materials under examination or the completion of 800000 cycles, whichever event occurred first.

Figures 5-19 through 5-21 report on the number of cycles that specimens could withstand before they experienced a drop in  $E^*$  (complex modulus). The observed decrease in the complex modulus ( $E^*$ ) is highly correlated with the point of failure ( $N_f$ ), which is defined in the figures. As can be observed in the figures, incorporation of filler/powder resulted in a significant increase in the life cycle of the mixtures. Particularly, incorporation of 40% replacement of the binder with a cement reactive powder resulted in a 492%, 813%, and 110% in WMA PG58-28, polymer-modified WMA PG58-28, and polymer-modified WMA PG64-10 mixtures, respectively. Moreover, it can be observed that mixtures containing PC reactive powder had a larger  $N_f$ , compared with the mixtures containing LS filler. Specifically, the  $N_f$  for WMA PG58-28 S PC40 and WMA PG58-28 P PC40 mixtures were 61% and 18% larger than that for WMA PG58-28 S LS40 and WMA PG58-28 P LS40 mixtures, respectively. In case of WMA PG64-10 P PC40, it should be noted that the specimen did not fail after 800000 loading cycles and there was one specimen available for this mixture, so 800000 was considered as the  $N_f$  for the mixture.

The reported outcome from the test is very promising since it proves that replacing a large volume (40%) of the binder with a PC reactive powder can lead to achieving a more sustainable asphalt pavement from an economical and life-cycle performance points of view.

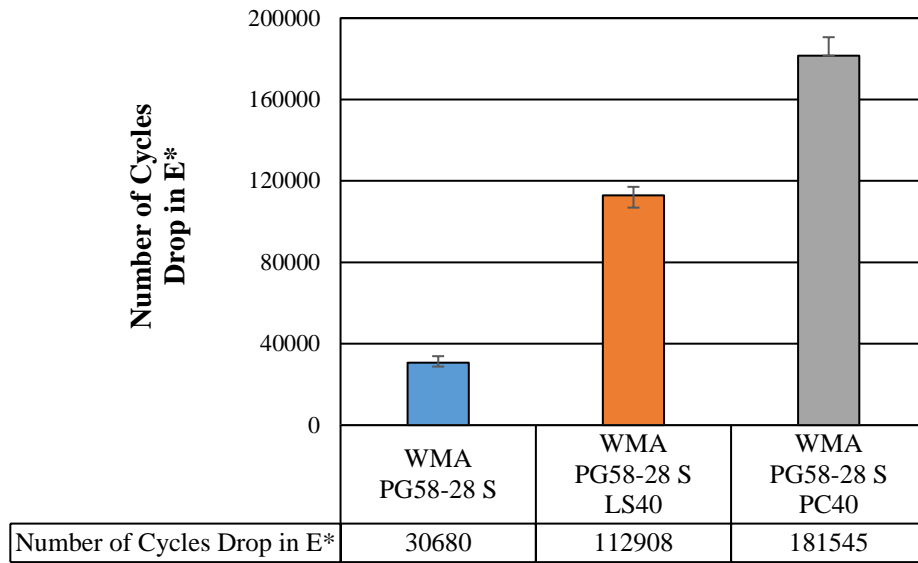


**Figure 5.19: Number of Cycles Drop in E\* for WMA PG58-28 Mixtures**

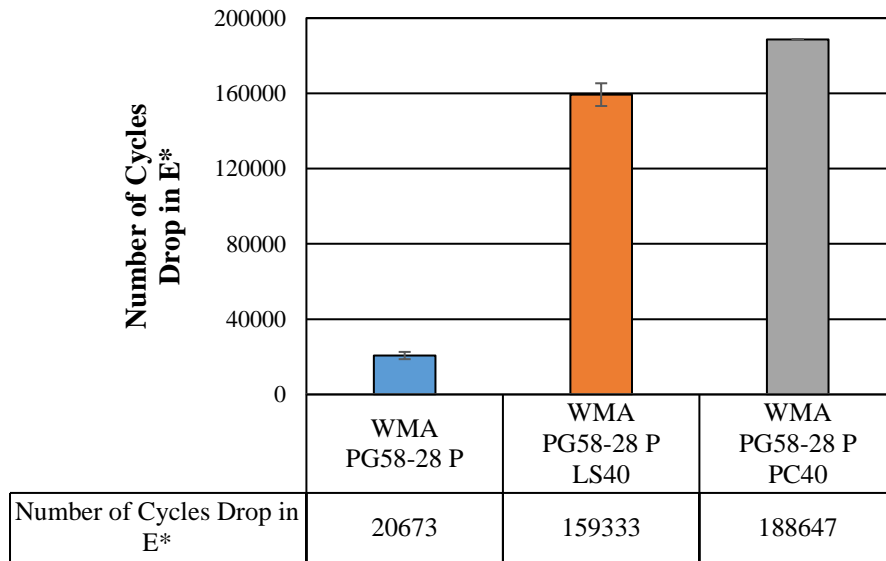


**Figure 5.20: Number of Cycles Drop in E\* for Polymer-modified WMA PG58-28 Mixtures**

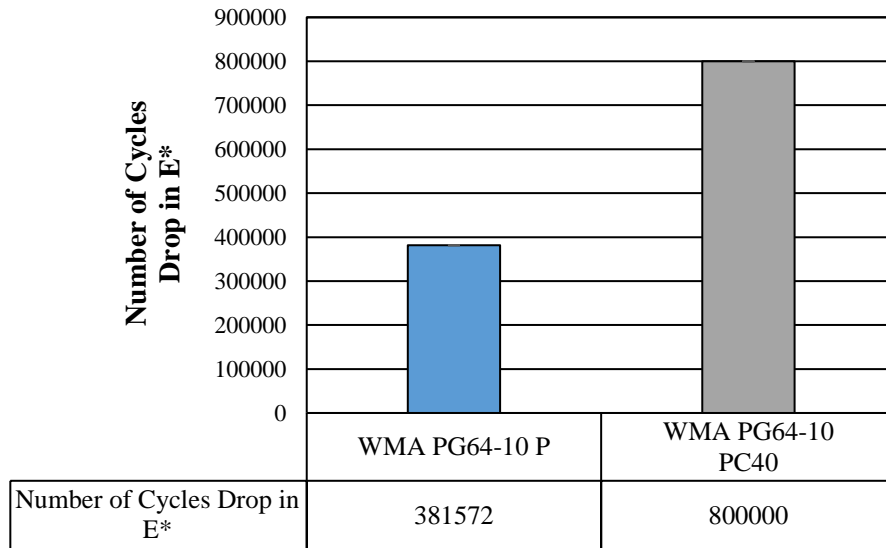


**Figure 5.21: Number of Cycles Drop in E\* for Polymer-modified WMA PG64-10 Mixtures**

The results of the actual vertical deformation for fatigue slopes from the secondary fatigue sections (See Figure 3.31) are demonstrated in Figures 5-22 through 5-24. A lower fatigue slope is considered desirable since it suggests a reduced rate of deformation when subjected to cyclic loading. It can be observed that the mixtures containing the filler/powder had a significantly smaller deformation slope, suggesting that they experience less deformation during their life cycle leading to higher durability. Further, it can be observed that mixtures containing a PC reactive powder outperformed the mixtures containing LS filler in terms of the deformation slope. As an example, the deformation slope for WMA PG58-28 S PC40 and WMA PG58-28 P PC40 mixtures were 70% and 73% smaller than that of WMA PG58-28 S LS40 and WMA PG58-28 P LS40 mixtures, respectively. It should be noted that the WMA PG64-10 P PC40 did not fail after 800000 cycles, and this cycle number and the corresponding displacement were considered for the deformation slope calculation.

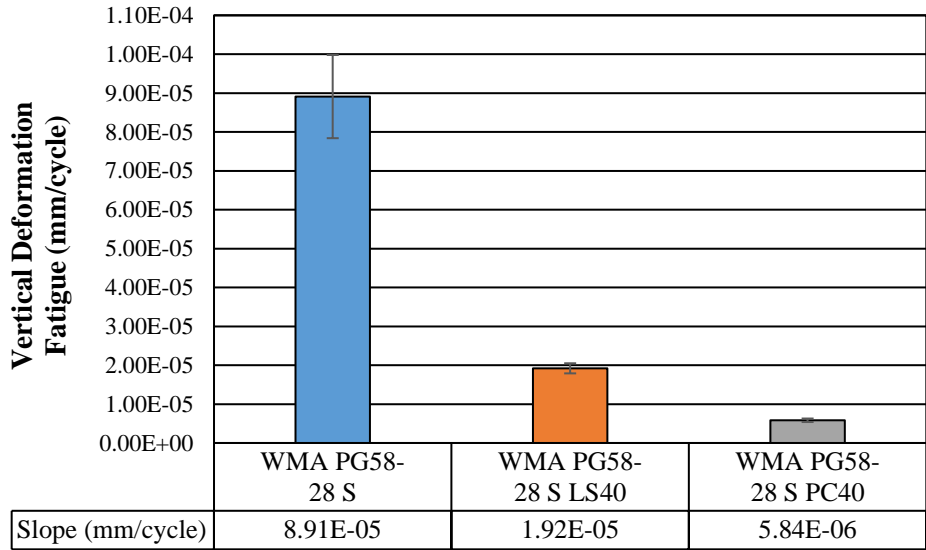


**Figure 5.22: Vertical Deformation Fatigue Slope for WMA PG58-28 Mixtures**

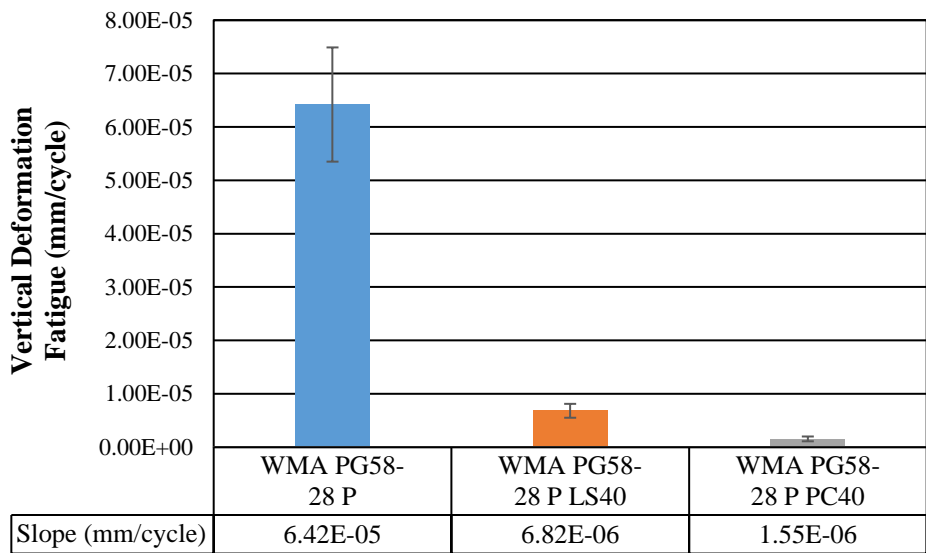


**Figure 5.23: Vertical Deformation Fatigue Slope for Polymer-modified WMA PG58-28 Mixtures**

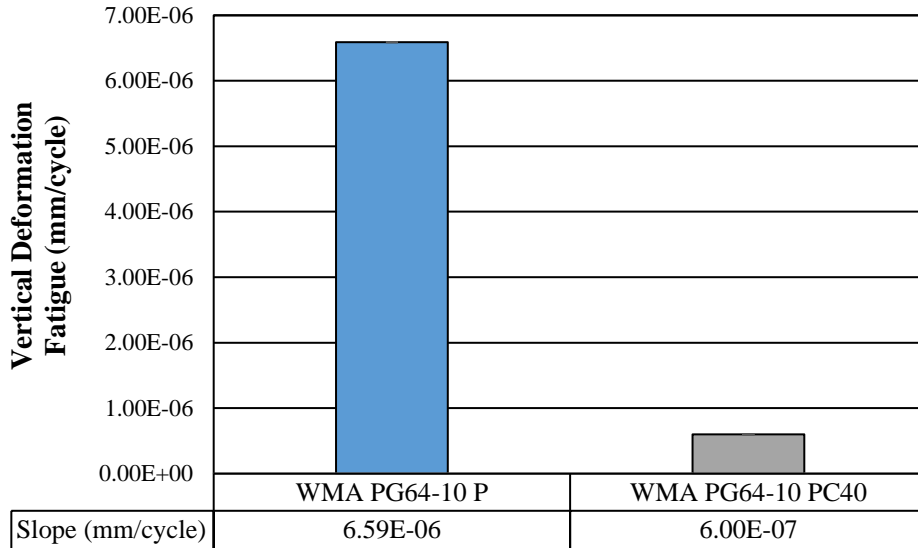


**Figure 5.24: Vertical Deformation Fatigue Slope for Polymer-modified WMA PG64-10 Mixtures**

The data obtained from the fatigue and IDT tests were plotted on a graph of fatigue life versus tensile stress, developed by (Porter and Kennedy 1975) to determine the location of the data points. The results are demonstrated in Figure 5.25. As can be observed in the figure, most of the data points were located between the data lines developed by Monismith et al. with T=68°F and Pell et al. with T=7°F. Further, for the mixtures made of PG58-28 and polymer-modified PG58-28 binder, the specimens containing the PC reactive powder have a higher tensile strength and a higher fatigue life, demonstrating the superior performance of such mixtures compared with their companion mixtures made of similar asphalt binder.

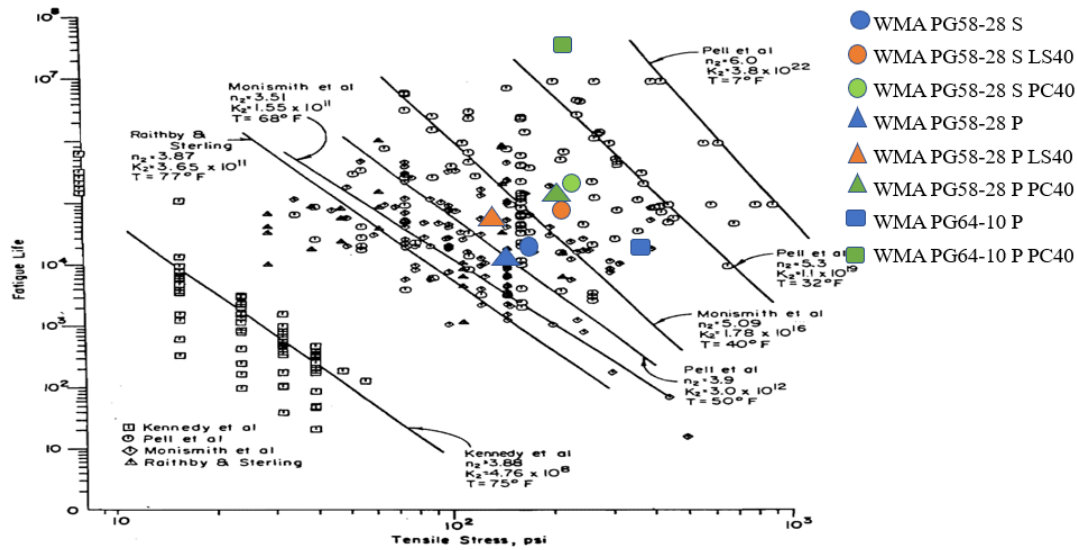


**Figure 5.25:Dispersion of Fatigue Life Data Points in Fatigue Life vs. Tensile Stress Graph Developed by (Porter and Kennedy 1975)**

In Figure 5.26, the data points obtained from the fatigue test are plotted in fatigue life vs. stress/strength ratio, developed by (Adedimila and Kennedy 1975). As the applied load for each specimen in the fatigue test was 10% of their ultimate strength at IDT test, all the data points were located in a similar vertical line in the graph. As can be seen in the figure below, all the specimens made of PG58-28 and polymer-modified PG58-28 asphalt binders, were located in 99% confidence interval for predicted fatigue life. Also, it is demonstrated that the PC-based mixtures have a higher fatigue life than their corresponding mixtures made of similar asphalt binder.

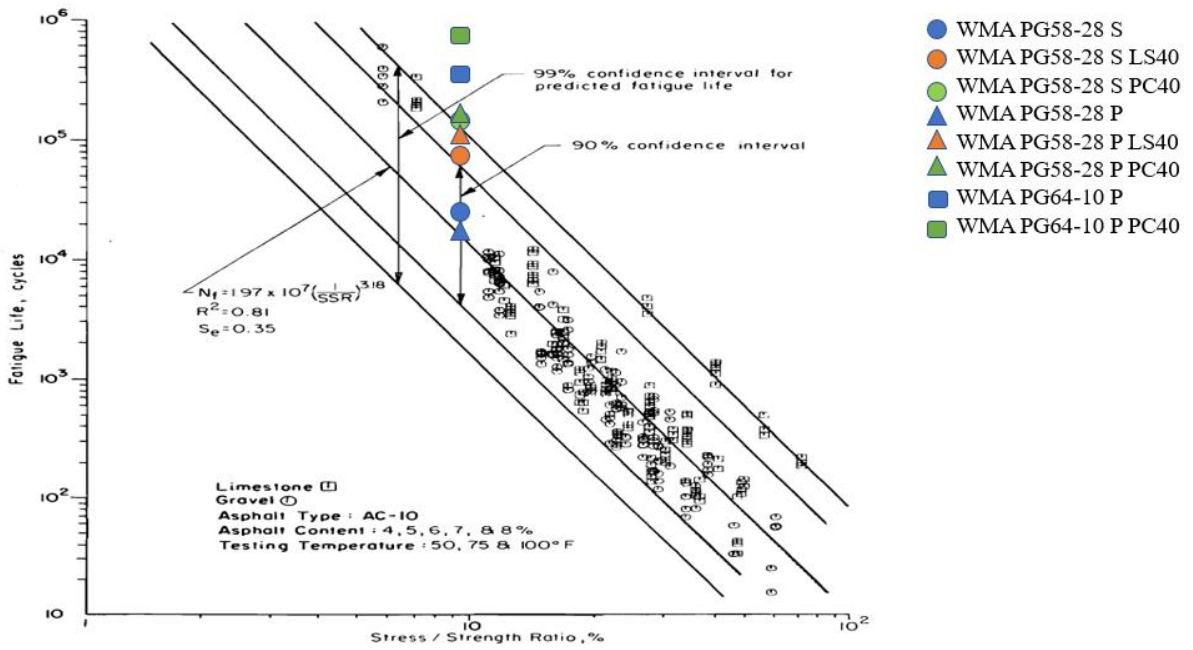


Figure 5.26: Dispersion of Fatigue Life Data Points in Fatigue Life vs. Stress/Strength Ratio Graph Developed by (Adedimila and Kennedy 1975)

## CHAPTER 6: CONCLUSIONS

This study discussed the rheological, mechanical, and durability impact of using portland cement as a reactive powder in a hybrid WMA asphalt concrete. The study was divided into two phases; the mastic phase and the asphalt concrete phase. The self-healing property of the mastics was evaluated using SEM imaging. The investigated rheological response of the mastics included viscosity using a rotational viscometer (RV), complex modulus ( $G^*$ ), phase angle ( $\delta$ ), rutting resistance, non-recoverable creep compliance ( $J_{nr}$ ) and recovery percentage, and fatigue resistance using a DSR machine, creep stiffness, and m-value using a BBR device, and relaxation modulus and creep compliance using a DMA machine. In the asphalt concrete phase, the investigated mechanical properties included constructability using an SGC machine, moisture damage resistance, and fatigue resistance using an MTS machine. The following sections summarize the research results.

### 6.1 MASTIC STUDY

- The SEM images indicate that cement-based mastics exhibit self-healing properties under moisture conditions due to the capability to self-weld cracks through cement hydration products. In contrast, SEM images of limestone-based mastics show that cracks remain unfilled as limestone powders do not possess reactive filling properties. These findings demonstrate that incorporating cement as a reactive powder in asphalt mixtures can potentially reduce costs while yielding a product with moisture-induced self-healing abilities, particularly in colder and wet climates.
- Workability was assessed by evaluating the viscosity of unaged mastics. The results demonstrated that filler/powder incorporation and polymer modification had a significant

effect on the increase in viscosity of the investigated mastics, hence reducing the workability of the mastics. However, the warm-mix additive reduced the viscosity of the mastics based on polymer-modified binders.

- Incorporation of fillers/powders and polymer modification increased the complex modulus of the unaged mastics. While this increase is desirable at high temperatures, it may result in brittle behavior at lower temperatures. However, the addition of warm-mix modifiers reduced the complex modulus of the mastics by exerting a softening effect. The findings suggest that the introduction of warm-mix modifiers to filler-incorporated or polymer-modified mastics can establish a balance between the stiffening response of the mastic and its ability to resist brittle behavior.
- Relative complex modulus  $G_r^*$  was used to identify the relationship between the neat binder and filler incorporation, warm-mix addition, and polymer modification. The results indicated that  $G_r^*$  is significantly dependent on the filler volume concentration, while the warm mix modifier reduces the relative  $G^*$  when the filler volume concentration increases, which again suggest that the softening effect of the warm mix modifier can balance the stiffening effect of the filler incorporation.
- The reported results for the relative phase angle demonstrated that the phase angle remains unaltered by filler type, filler dosage, and warm mix modification, and the relative phase angle exhibits no significant changes. However, the introduction of polymer modification significantly reduces the relative phase angle, indicating a considerable increase in elasticity of polymer-modified mastics.
- Rutting resistance was evaluated based on the rutting factor  $G^*/\sin(\delta)$  for RTFO-aged mastics. The findings indicate that an increase in filler volume concentration results in

enhanced rutting resistance of mastics due to the stiffening effect of fillers/powders. Polymer modification increased the rutting factor, while the addition of warm mix led to a reduction in the rutting factor of the mastics.

- To characterize the deformation resistance of RTFO-aged mastics, non-recoverable compliance ( $J_{nr}$ ) and percentage recovery were determined using the multiple stress creep and recovery test. For the mastics based on PG58-28 binders, the test was conducted at 58°C. However, for the mastics based on PG64-10 binders, the test was conducted at 58°C, 64°C, and 70°C. The test results showed that the incorporation of powders in the mastics leads to an increase in rutting resistance in comparison with the unfilled binder. This is because  $J_{nr}$  values decrease with an increase in powder concentration. Further, it was noted that polymer modification resulted in a significant enhancement in the elastic response of investigated mastics. For the mastics based on PG64-10 binders, it was noted that PC-based mastics had a slightly lower  $J_{nr}$  in a similar filler volume concentration at all the tested temperatures compared with LS-based mastics. Also, it was noted that an increase in temperature compromised the elastic response of the mastics; however, by incorporating a higher filler volume, the negative impact of increased temperature on the elastic response of the mastics becomes less significant.
- The results showed that the addition of warm mix did not significantly alter the recovery percentage, whereas the incorporation of fillers and polymer modification increased the recovery percentage of mastics. This improvement enables the mastics to exhibit a more elastic response at high temperatures.
- Fatigue resistance was examined for PAV-aged mastics based on Superpave® specifications for the fatigue factor  $G^*\sin(\delta)$ . The findings indicate that incorporating

fillers in the mastics reduces their fatigue resistance in comparison with the corresponding neat binder. This outcome was anticipated since the incorporation of fillers results in a stiffening effect; however, the warm mix addition improved the fatigue resistance due to its plasticizing effect. Also, it was noted that for the mastics based on PG58-28 binders, polymer modification enhanced the fatigue resistance. Further, with the exception of HMA Polymer-modified PG64-10-based mastics with 25% filler volume concentration, it was reported that PC-based mastics exhibit better fatigue performance than LS-based mastics with comparable filler volume concentration.

- Thermal cracking resistance was assessed by evaluating the creep stiffness  $S(t)$ ,  $m$ -value, creep compliance, and relaxation modulus of PAV-aged mastics through BBR and DMA tests. The findings from the BBR test demonstrated that filler incorporation led to more brittle behavior of the mastics, and polymer modification led to a relatively similar rheological response, while warm-mix additives reduced the stiffness of the investigated mastics at low temperatures. Also, it was demonstrated that the correlation between the creep stiffness (obtained from BBR) and the creep compliance (obtained from DMA) of the mastics based on PG58-28 binder is similar to that of mastics based on polymer-modified PG58-28 binders; this result proves that the investigated mastics demonstrate similar behavior at low temperatures under different test configurations.

## 6.2 MIXTURE STUDY

- Aggregate coating was used as a means of investigating the interaction between the aggregates and the asphalt binder. The results indicated that the asphalt film thickness was higher for the control mixtures, measuring 12.03  $\mu\text{m}$ , in comparison with the reactive powder mixtures, which measured 5.93  $\mu\text{m}$ . This finding can be attributed to the fact that the mixtures containing filler/ reactive powder had a binder replacement of 40% by volume, as compared with the control mixture. However, despite the reduced quantity of the binder, no significant differences were observed in terms of the quality of aggregate coating or the mixing performance between the two types of mixtures.
- The assessment of compaction efforts (WMA) mixtures containing LS filler and PC reactive powder and control was conducted by evaluating the workability of the mixtures. The degree of densification was determined based on the percentage of maximum theoretical density ( $\%G_{mm}$ ), and the resulting differences were compared between the two mixture types. It was noted that for WMA mixtures based on PG58-28 binders, the mixtures containing PC reactive powder required less compaction effort to reach a desired  $\%G_{mm}$ , meaning that such mixtures require less compaction effort at the field, although the asphalt binder content is reduced.
- The research results from the indirect tensile (IDT) test indicated that the WMA mixtures made of plain and polymer-modified PG58-28 binders and containing PC reactive powder demonstrated higher ultimate strength, while having less deformation in dry conditions when compared with the LS-based and control mixtures.
- By comparing the tensile strength ratio (ITS), which is the ratio of ultimate stress of the WMA mixtures in conditioned and dry WMA mixture specimens, it was revealed that the

mixtures made of northern bitumen containing PC reactive powder experienced similar or less moisture damage than the LS-based and control mixtures.

- Intermediate-temperature fatigue cracking analysis was evaluated based on secondary fatigue slopes and complex modulus  $E^*$ . The results reported that the WMA mixtures containing PC reactive powder showed a superior fatigue resistance compared with WMA LAS-based and control mixtures. Further, it was observed that the mixtures containing PC reactive powder had a significant smaller deformation slope, suggesting that they experience less deformation during their life cycle leading to a higher durability, when compared with the companion LS-based and control mixtures.
- Based on the reported results in the asphalt mixture study, it appears that field implementation of WMA polymer-modified PG58-28 with 25-40% replacement of the binder with portland cement can be a promising alternative used to characterize further the long-term mechanical performance of such compositions. The rationale for conducting long-term characterization of asphalt mixtures is to evaluate the potential activation of portland cement during freeze-thaw cycles, where the water penetrating through the mixture matrix could lead to a reaction. This activation may enhance the durability and mechanical performance of the mixture over time.
- Further, the results for WMA mixtures based on polymer-modified PG64-10 binders were not as expected. This can be attributed to the fact that the polymer-modified PG64-10 binder was manufactured in an asphalt laboratory with a relatively high SBS content of 4%. The binder was extremely viscous, even at 150°C. It is suggested that the mixture study be reconducted on plain and company-manufactured PG64-10 binders to evaluate the

potential use of portland cement reactive powders as a partial replacement of the binder intended for application in the U.S. states with warmer climates.

- By conducting a cost calculation for WisDOT approved mix design that was used in this study, it can be concluded that the replacement of 40% of PG58-28 asphalt binder by volume with portland cement reactive powder can lead to a 23% materials cost reduction associated with the production of asphalt concrete. This cost reduction can reach 15% when only 25% of the binder is replaced with portland cement. This cost-saving, in combination with the superior performance of portland cement-based mixture, can pave the way to achieve an environmentally sound economical and sustainable hybrid pavement material.

## REFERENCES

- Adedimila, A. S. and T. W. Kennedy (1975). Fatigue and resilient characteristics of asphalt mixtures by repeated-load indirect tensile test, University of Texas at Austin.
- Almeida-Costa, A. and A. Benta (2016). "Economic and environmental impact study of warm mix asphalt compared to hot mix asphalt." Journal of Cleaner Production **112**: 2308-2317.
- Asphalt Institute (2001). Superpave Mix Design. Superpave Series No. 2 (SP-02). Lexington, KY, Asphalt Institute.
- Association, A. A. P. (2004). National asphalt specification, The Association.
- Bahia, H. U., et al. (2001). Characterization of modified asphalt binders in superpave mix design.
- Bahia, H. U., et al. (1997). "Applicability of Superpave binder testing protocols to modified binders." Transportation research record **1586**(1): 16-23.
- Bahia, H. U., et al. (1999). "Non-linear viscoelastic and fatigue properties of asphalt binders." Journal of the Association of Asphalt Paving Technologists **68**.
- Bautista, E. G. (2015). Experimental evaluation of the effect of coal combustion products on constructability, damage and aging resistance of asphalt mastics, The University of Wisconsin-Milwaukee.
- Bautista, E. G., et al. (2015). "Effect of coal combustion products on high temperature performance of asphalt mastics." Construction and Building Materials **94**: 572-578.
- Becker, Y., et al. (2001). "Polymer modified asphalt." Vision tecnologica **9**(1): 39-50.
- Behnood, A. (2020). "A review of the warm mix asphalt (WMA) technologies: Effects on thermo-mechanical and rheological properties." Journal of Cleaner Production **259**: 120817.
- Behnood, A. and M. M. Gharehveran (2019). "Morphology, rheology, and physical properties of polymer-modified asphalt binders." European Polymer Journal **112**: 766-791.
- Behnood, A., et al. (2015). "Effects of copper slag and recycled concrete aggregate on the properties of CIR mixes with bitumen emulsion, rice husk ash, Portland cement and fly ash." Construction and Building Materials **96**: 172-180.
- Bower, N., et al. (2016). "Evaluation of the performance of warm mix asphalt in Washington state." International Journal of Pavement Engineering **17**(5): 423-434.
- Brûlé, B. (1996). "Polymer-modified asphalt cements used in the road construction industry: basic principles." Transportation research record **1535**(1): 48-53.

Camph, D. H., et al. (1997). How to keep America moving: report on the US Department of Transportation's outreach on reauthorization of the Intermodal Surface Transportation Efficiency Act (ISTEA), US Department of Transportation.

Charoentham, N. and K. Kanitpong (2012). "Development of a performance grading system for asphalt binders used in Thailand." Asian Transport Studies **2**(2): 121-138.

Chen, J.-S., et al. (2002). "Asphalt modified by styrene-butadiene-styrene triblock copolymer: Morphology and model." Journal of Materials in Civil Engineering **14**(3): 224-229.

Chen, J.-S. and C.-J. Tsai (1999). "How good are linear viscoelastic properties of asphalt binder to predict rutting and fatigue cracking?" Journal of materials engineering and performance **8**: 443-449.

Cloutier, C., et al. (2021). The Effect of Cement Reactive Powders on the Mechanical Response of WMA Mixtures. Airfield and Highway Pavements 2021: 92-103.

Cloutier, C., Farahi, Behrouz., Sobolev, Konstantin., Faheem, Ahmed., and Kosmtaka, Steven., (2021). The Effect of Cement Reactive Powders on the Mechanical Response of WMA Mixtures. Airfield and Highway Pavements 2021, ASCE: 92-103.

D'Angelo, J. (2009). "Current status of Superpave binder specification." Road Materials and Pavement Design **10**(sup1): 13-24.

D'Angelo, J. and R. Dongr (2002). Superpave binder specifications and their performance relationship to modified binders. Proceedings of the forty-seventh annual conference of the Canadian Technical Asphalt Association (CTAA): Calgary, Alberta.

D'Angelo, J. A. (2009). "Effect of polyphosphoric acid on asphalt binder properties." Polyphosphoric Acid Modification of Asphalt Binders **27**.

Elwardany, M. D., et al. (2017). "Evaluation of asphalt mixture laboratory long-term ageing methods for performance testing and prediction." Road Materials and Pavement Design **18**(sup1): 28-61.

Faheem, A. F., et al. (2012). "Influence of filler fractional voids on mastic and mixture performance." Transportation research record **2294**(1): 74-80.

Farahi, B., et al. (2021). Effect of Using Cement Reactive Powders on Rheological Performance of Asphalt Mastics. Airfield and Highway Pavements 2021: 115-125.

Farahi, B., et al. (2019). "Experimental investigation on the behavior of reinforced concrete beams retrofitted with NSM-SMA/FRP." Amirkabir (Journal of Science and Technology) **51**(4): 685-698.

Fini, E. H., et al. (2016). "Physiochemical, rheological, and oxidative aging characteristics of asphalt binder in the presence of mesoporous silica nanoparticles." Journal of Materials in Civil Engineering **28**(2): 04015133.

Hadley, W. O., et al. (1969). An evaluation of factors affecting the tensile properties of asphalt-treated materials, Center for Highway Research, University of Texas at Austin.

Harris, B. M. and K. D. Stuart (1995). "Analysis of mineral fillers and mastics used in stone matrix asphalt." Asphalt Paving Technology **64**: 54-95.

Hasan, M. R. M., et al. (2013). "Comparative study on the properties of WMA mixture using foamed admixture and free water system." Construction and Building Materials **48**: 45-50.

Hassan, M. (2010). "Evaluation of the environmental and economic impacts of warm-mix asphalt using life-cycle assessment." International Journal of Construction Education and Research **6**(3): 238-250.

Hmoud, H. R. (2011). "Evaluation of VMA and film thickness requirements in hot-mix asphalt." Modern Applied Science **5**(4): 166.

Hoiberg, A. J. (1966). "Bituminous materials: asphalts, tars and pitches volume iii coal tars and pitches."

Jamshidi, A., et al. (2013). "Performance of warm mix asphalt containing Sasobit®: State-of-the-art." Construction and Building Materials **38**: 530-553.

Kennedy, T. W., et al. (1990). "Hypotheses and models employed in the SHRP asphalt research program." Strategic Highway Research Program, Washington DC.

Kim, H., et al. (2011). "Rheology of warm mix asphalt binders with aged binders." Construction and Building Materials **25**(1): 183-189.

Lakes, R. and R. S. Lakes (2009). Viscoelastic materials, Cambridge university press.

Lin, P., et al. (2020). "Laboratory evaluation of the effects of long-term aging on high-content polymer-modified asphalt binder." Journal of Materials in Civil Engineering **32**(7): 04020157.

Liu, J., et al. (2018). "Rheological properties of warm mix asphalt binders and warm mix asphalt binders containing polyphosphoric acid." International Journal of Pavement Research and Technology **11**(5): 481-487.

McGennis, R. B., et al. (1994). Background of Superpave asphalt binder test methods, United States. Federal Highway Administration. Office of Technology Applications.

Mohammad, L. N., et al. (2003). "Investigation of the use of recycled polymer modified asphalt binder in asphalt concrete pavements (with discussion and closure)." Journal of the Association of Asphalt Paving Technologists **72**.

Muzenski, S., et al. (2020). "Towards ultrahigh performance concrete produced with aluminum oxide nanofibers and reduced quantities of silica fume." Nanomaterials **10**(11): 2291.

Newcomb, D. (2003). "Limit the strain at the bottom of an asphalt pavement, and what do you get?: A perpetual pavement." HMAT: Hot Mix Asphalt Technology **8**(6).

Newman, J. K. (2003). Flexural beam fatigue properties of airfield asphalt mixtures containing styrene-butadiene based polymer modifiers. Proceedings of the Sixth International RILEM Symposium on Performance Testing and Evaluation of Bituminous Materials.

Pahlavan, F., et al. (2019). "Fused aromatics to restore molecular packing of aged bituminous materials." Industrial & Engineering Chemistry Research **58**(27): 11939-11953.

Pauli, A. T. (1996). "Asphalt compatibility testing using the automated Heithaus titration test." PREPRINTS OF PAPERS-AMERICAN CHEMICAL SOCIETY DIVISION FUEL CHEMISTRY **41**: 1276-1281.

Pérez-Martínez, M., et al. (2014). "Analysis of cleaner technologies based on waxes and surfactant additives in road construction." Journal of Cleaner Production **65**: 374-379.

Porter, B. W. and T. W. Kennedy (1975). Comparison of fatigue test methods for asphalt materials, University of Texas at Austin.

Presti, D. L., et al. (2017). "Improving the rheometry of rubberized bitumen: experimental and computation fluid dynamics studies." Construction and Building Materials **136**: 286-297.

Rieksts, K., et al. (2019). "The influence of filler type and gradation on the rheological performance of mastics." Road Materials and Pavement Design **20**(4): 964-978.

Rigden, P. (1947). "The use of fillers in bituminous road surfacings. A study of filler-binder systems in relation to filler characteristics." Journal of the Society of Chemical Industry **66**(9): 299-309.

Roberts, F. L., et al. (1991). "Hot mix asphalt materials, mixture design and construction."

Roque, R., et al. (2004). Guidelines for use of modifiers in superpave mixtures: executive summary and volume 1 of 3 volumes: evaluation of SBS modifier.

Sabzi, J., et al. (2020). "Effect of concrete strength and longitudinal reinforcement arrangement on the performance of reinforced concrete beams strengthened using EBR and EBROG methods." Engineering Structures **205**: 110072.

Sangiorgi, C., et al. (2017). "Alternative fillers for the production of bituminous mixtures: A screening investigation on waste powders." Coatings **7**(6): 76.

Sargand, S. and S. Kim (2001). Performance evaluation of polymer modified and unmodified Superpave mixes. Second International Symposium on Maintenance and Rehabilitation of Pavements and Technological Control. Segundo Simposio Sobre Manutencao e Rehabilitacao de Pavimentos e Controle Tecnologico Auburn University, University of Mississippi, ASCE, IRF, DOTRSPA, NAPA, FREMIX Fresagem de Pavimentos.

Sebaaly, P. E., et al. (2003). Evaluation of new pavement technologies in Nevada.

Singh, S. K., et al. (2018). "Thermal degradation of SBS in bitumen during storage: Influence of temperature, SBS concentration, polymer type and base bitumen." Polymer Degradation and Stability **147**: 64-75.

Tao, G., et al. (2019). "Characteristics of steel slag filler and its influence on rheological properties of asphalt mortar." Construction and Building Materials **201**: 439-446.

Terrel, R. L. and J. L. Walter (1986). MODIFIED ASPHALT PAVEMENT MATERIALS-THE EUROPEAN EXPERIENCE (WITH DISCUSSION). Association of Asphalt Paving Technologists Proc.

Tian, Y., et al. (2021). "Laboratory investigation on rheological, chemical and morphological evolution of high content polymer modified bitumen under long-term thermal oxidative aging." Construction and Building Materials **303**: 124565.

U.S. Energy Information Administration (2021). Asphalt and road oil production.

Vaitkus, A., et al. (2009). "Analysis and evaluation of possibilities for the use of warm mix asphalt in Lithuania." The Baltic Journal of Road and Bridge Engineering **4**(2): 80-86.

Wang, Y., et al. (2022). "Evaluation of the High-and Low-Temperature Performance of Asphalt Mortar Based on the DMA Method." Materials **15**(9): 3341.

West, R., et al. (2014). "Engineering properties and field performance of warm mix asphalt technologies." National Cooperative Highway Research Program, Washington, DC, USA, NCHRP Final Report Project(09-47A).

Wozuk, A., et al. (2017). "Effect of zeolite properties on asphalt foaming." Construction and Building Materials **139**: 247-255.

Xiao, F., et al. (2018). "A literature review on cold recycling technology of asphalt pavement." Construction and Building Materials **180**: 579-604.

Yildirim, Y. (2007). "Polymer modified asphalt binders." Construction and Building Materials **21**(1): 66-72.

Yut, I. and A. Zofka (2014). "Correlation between rheology and chemical composition of aged polymer-modified asphalts." Construction and Building Materials **62**: 109-117.

Zeida, W., et al. (2022). "Review of the Superpave performance grading system and recent developments in the performance-based test methods for asphalt binder characterization." Construction and Building Materials **319**: 126063.

Zhang, J., et al. (2015). "Viscosity-temperature characteristics of warm mix asphalt binder with Sasobit®." Construction and Building Materials **78**: 34-39.

Zhu, C. (2015). Evaluation of thermal oxidative aging effect on the rheological performance of modified asphalt binders, University of Nevada, Reno.

Zulkati, A., et al. (2012). "Effects of fillers on properties of asphalt-concrete mixture." Journal of transportation engineering **138**(7): 902-910.